COPY 1

FAA WJH Technical Center
00026834

DOT/FAA/RD-82/45-I

Systems Research &
Development Service
Washington, D.C. 20591

The Effects of Precipitation Static and Lightning on the Airborne Reception of LORAN-C

Volume I (Analysis)

FEDERAL AVIATION ADMINISTRATION
SEP 23 1982
TECHNICAL CENTER LIBRARY
ATLANTIC CITY, N.J. 08405

James D. Nickum

Avionics Engineering Center
Department of Electrical Engineering
Ohio University
Athens, Ohio 45701

April 1982

Final Report

This document is available to the U.S. public through the National Technical Information Service, Springfield, Virginia 22161.

DOT/FAA
RD-82/45,I

U.S. Department of Transportation
Federal Aviation Administration

NOTICE

This document is disseminated under the sponsorship of the Department of Transportation in the interest of information exchange. The United States Government assumes no liability for the contents or use thereof.

Technical Report Documentation Page

1. Report No. DOT/FAA/RD-82/45-I	2. Government Accession No.	3. Recipient's Catalog No.
4. Title and Subtitle THE EFFECTS OF PRECIPITATION STATIC AND LIGHTNING ON THE AIRBORNE RECEPTION OF LORAN-C VOLUME I: ANALYSIS		5. Report Date April 1982
		6. Performing Organization Code
7. Author(s) James D. Nickum		8. Performing Organization Report No. OU/AEC/EER 54-2
9. Performing Organization Name and Address Avionics Engineering Center, Department of Electrical Engineering, Ohio University, Athens, Ohio 45701		10. Work Unit No. (TRAIS)
		11. Contract or Grant No. DTFA01-81-C-10007
12. Sponsoring Agency Name and Address Federal Aviation Administration, Systems Research and Development Service, Washington, D.C. 20590		13. Type of Report and Period Covered Final Report Dec. 11, 1980 - Apr. 30, 1982
		14. Sponsoring Agency Code

15. Supplementary Notes

16. Abstract

Results of a ground p-static survey of an aircraft to determine p-static noise reduction are given. The effects of the airborne reception of Loran-C in actual thunderstorm conditions are described. Additionally, data from flight tests conducted using an airframe biased discharger producing p-static airframe charging in flight are presented. P-static noise reduction using quality static-wick dischargers to improve Loran-C reception in flight is demonstrated.

17. Key Words Loran-C, VLF, P-Static, Precipitation Static, Lightning Effects, Static-Wick Dischargers, Biased Discharger, Precipitation Static Survey, Flight Tests, Ground Tests	18. Distribution Statement Document is available to the public through the National Technical Information Service, Springfield, Virginia 22161.

19. Security Classif. (of this report)	20. Security Classif. (of this page)	21. No. of Pages	22. Price
Unclassified	Unclassified	136	

Form DOT F 1700.7 (8-72) Reproduction of completed page authorized

METRIC CONVERSION FACTORS

Approximate Conversions to Metric Measures

Symbol	When You Know	Multiply by	To Find	Symbol
		LENGTH		
in	inches	*2.5	centimeters	cm
ft	feet	30	centimeters	cm
yd	yards	0.9	meters	m
mi	miles	1.6	kilometers	km
		AREA		
in^2	square inches	6.5	square centimeters	cm^2
ft^2	square feet	0.09	square meters	m^2
yd^2	square yards	0.8	square meters	m^2
mi^2	square miles	2.6	square kilometers	km^2
	acres	0.4	hectares	ha
		MASS (weight)		
oz	ounces	28	grams	g
lb	pounds	0.45	kilograms	kg
	short tons (2000 lb)	0.9	tonnes	t
		VOLUME		
tsp	teaspoons	5	milliliters	ml
Tbsp	tablespoons	15	milliliters	ml
fl oz	fluid ounces	30	milliliters	ml
c	cups	0.24	liters	l
pt	pints	0.47	liters	l
qt	quarts	0.95	liters	l
gal	gallons	3.8	liters	l
ft^3	cubic feet	0.03	cubic meters	m^3
yd^3	cubic yards	0.76	cubic meters	m^3
		TEMPERATURE (exact)		
°F	Fahrenheit temperature	5/9 (after subtracting 32)	Celsius temperature	°C

*1 in = 2.54 (exactly). For other exact conversions and more detailed tables, see NBS Misc. Publ. 286, Units of Weights and Measures, Price $2.25, SD Catalog No. C13.10:286.

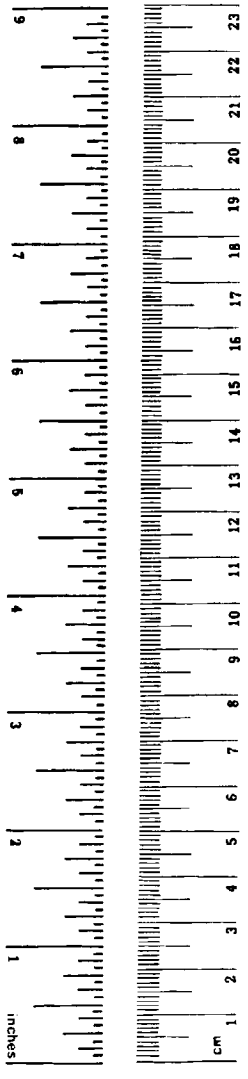

Approximate Conversions from Metric Measures

Symbol	When You Know	Multiply by	To Find	Symbol
		LENGTH		
mm	millimeters	0.04	inches	in
cm	centimeters	0.4	inches	in
m	meters	3.3	feet	ft
m	meters	1.1	yards	yd
km	kilometers	0.6	miles	mi
		AREA		
cm^2	square centimeters	0.16	square inches	in^2
m^2	square meters	1.2	square yards	yd^2
km^2	square kilometers	0.4	square miles	mi^2
ha	hectares (10,000 m^2)	2.5	acres	
		MASS (weight)		
g	grams	0.035	ounces	oz
kg	kilograms	2.2	pounds	lb
t	tonnes (1000 kg)	1.1	short tons	
		VOLUME		
ml	milliliters	0.03	fluid ounces	fl oz
l	liters	2.1	pints	pt
l	liters	1.06	quarts	qt
l	liters	0.26	gallons	gal
m^3	cubic meters	35	cubic feet	ft^3
m^3	cubic meters	1.3	cubic yards	yd^3
		TEMPERATURE (exact)		
°C	Celsius temperature	9/5 (then add 32)	Fahrenheit temperature	°F

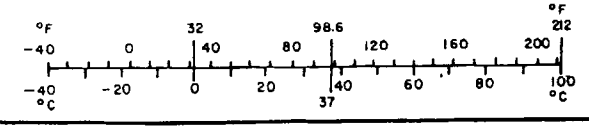

TABLE OF CONTENTS

(VOLUME I)

		PAGE
	List of Figures	v
I.	CONCLUSIONS	1
II.	INTRODUCTION	3
III.	GROUND PRECIPITATION STATIC TESTING	7
	A. Airframe Bonding Tests.	7
	1. Test Procedure.	7
	2. Airframe Bonding Test Results.	7
	3. Tires and Deicing Boot Resistivity Tests.	8
	4. Summary of Bonding Tests.	8
	B. Ground Airframe Charging Tests.	8
	1. Test Procedure and Instrumentation.	8
	2. Ground P-Static Charging Test Results.	18
	3. Summary of Ground P-Static Test Results.	35
IV.	P-STATIC FLIGHT TESTING	36
	A. Biased-Discharger Installation.	36
	B. P-Static Flight Test Procedure.	36
	C. P-Static Flight Test Results.	47
	1. Biased-Discharger Flights Using Corona Points.	47
	2. Biased-Discharger Flights Using Dayton-Granger 16375.	54
	3. Biased-Discharger Flights Using TCO Manufacturing DD1 Dischargers	60
	4. Natural Charging Flight Test.	66
	D. Summary of P-Static Flight Tests.	73
V.	GROUND LIGHTNING SIMULATION TESTING	74
	A. Lightning Simulation.	74
	1. Test Procedure.	74
	2. Ground Lightning Simulation Test Results.	81

TABLE OF CONTENTS (Continued)

		PAGE
	B. Antenna Static Field Testing.	81
	1. Test Procedure.	81
	2. Static Electric Field Test Results.	90
	C. Summary of Ground Lightning and Static Field Tests.	103
VI.	FLIGHT TESTS IN THUNDERSTORM CONDITIONS	104
	1. Test Procedure.	104
	2. Thunderstorm Flight Test Results.	104
	3. Summary of Thunderstorm Flight Test Results.	123
VII.	RECOMMENDATIONS	124
VIII.	REFERENCES	125
IX.	ACKNOWLEDGEMENTS	126
X.	PROJECT TEAM MEMBERS AT OHIO UNIVERSITY	127

LIST OF FIGURES

		PAGE
Figure 2-1.	N7AP Ohio University DC-3 Flying Laboratory.	4
Figure 2-2.	Interior View N7AP - Looking Toward Tail.	5
Figure 2-3.	Heath H-89 Computer at Operator Console.	6
Figure 3-1.	N7AP Instrumented Static-Wick Discharger Placement.	9
Figure 3-2.	Acrylic Sheets Under Main Landing Gear.	10
Figure 3-3.	Acrylic Sheet Under Tail Wheel.	11
Figure 3-4.	Ion Flood Fixture on Leading Edge of Wing.	13
Figure 3-5.	Ion Collection Fixtures Behind Control Surfaces.	14
Figure 3-6.	Close-Up of Ion Collection Fixture and Dayton-Granger Dischargers.	15
Figure 3-7.	Ion Flood and Ion Collection Fixtures on Right Wing.	16
Figure 3-8.	Block Diagram of Ground P-Static Instrumentation.	17
Figure 3-9.	Noise Receiver Antenna on Bottom of Aircraft.	19
Figure 3-10.	Noise13 29-May-81 Noise vs. Microamps Discharger-Corona Point Detector-Carr. Negative-Point Corona.	20
Figure 3-11.	Noise3 28-May-81 Noise vs. Microamps Discharger-Dayton Omega Detector-Carr. Negative-Point Corona.	21
Figure 3-12.	Noise4 28-May-81 Noise vs. Microamps Discharger-TCO ESD3 Detector-Carr. Negative-Point Corona.	22
Figure 3-13.	Noise13 29-May-1981 Airframe KV vs. Microamps Discharger-Corona Point Detector-Carr. Negative-Point Corona.	24
Figure 3-14.	Noise3 28-May-1981 Airframe KV vs. Microamps Discharger-Dayton Omega Detector-Carr. Negative-Point Corona.	25

LIST OF FIGURES (Continued)

		PAGE
Figure 3-15.	Noise4 26-May-1981 Airframe KV vs. Microamps Discharger-TCO ESD-3 Detector-Carr. Negative-Point Corona.	26
Figure 3-16.	Calibration Curve of Airframe Potential Negative-Point Corona.	27
Figure 3-17.	Airframe Potential Calibration Fixture.	28
Figure 3-18.	Noise9 29-May-1981 Noise vs. Microamps. Discharger-Corona Point Detector-Carr. Positive-Point Corona.	29
Figure 3-19.	Noise11 29-May-1981 Noise vs. Microamps. Discharger-Dayton Omega Detector-Carr. Positive-Point Corona.	30
Figure 3-20.	Noise7 29-May-1981 Noise vs. Microamps. Discharger-TCO ESD-3 Detector-Carr. Positive-Point Corona.	31
Figure 3-21.	Noise9 29-May-1981 Airframe KV vs. Microamps. Discharger-Corona Point Detector-Carr. Positive-Point Corona.	32
Figure 3-22.	Noise11 29-May-1981 Airframe KV vs. Microamps. Discharger-Dayton Omega Detector-Carr. Positive-Point Corona.	33
Figure 3-23.	Noise7 29-May-1981 Airframe KV vs. Microamps. Discharger-TCO ESD-3 Detector-Carr. Positive-Point Corona.	34
Figure 4-1.	Biased Discharger on Tail of N7AP.	37
Figure 4-2.	Block Diagram of Instrumentation for P-Static Flight Testing.	38
Figure 4-3.	Power Lines in Test Area.	39
Figure 4-4.	Corona Points on Right Elevator of N7AP.	41
Figure 4-5.	Biased-Discharger Flight TCO DD1, March 2, 1982.	42
Figure 4-6.	Biased-Dscharger Flight Corona Points.	43
Figure 4-7.	Biased-Discharger Flight Dayton-Granger.	44
Figure 4-8.	Biased-Discharger Flight TCO DD1, March 19,1982.	45

LIST OF FIGURES (Continued)

		PAGE
Figure 4-9.	Biased-Discharger Flight TCO DD1, March 29, 1982.	46
Figure 4-10.	Flight 10 March, 1982, Biased-Discharger, Dayton-Granger, Noise vs. Microamps.	48
Figure 4-11.	Flight 10 March, 1982, Biased-Discharger, Dayton-Granger, Airframe KV vs. Microamps.	49
Figure 4-12.	Flight 10 March, 1982, Biased-Discharger, Dayton-Granger, Noise vs. Time.	50
Figure 4-13.	Flight 10 March, 1982, Biased-Discharger, Dayton-Granger, Microamps vs. Time.	51
Figure 4-14.	Flight 10 March, 1982, Biased-Discharger, Dayton-Granger, Airframe KV vs. Time.	52
Figure 4-15.	Biased-Discharger Power Supply vs. Time.	53
Figure 4-16.	Flight 18 March, 1982, Biased-Discharger, Dayton-Granger, Noise vs. Microamps.	55
Figure 4-17.	Flight 18 March, 1982, Biased-Discharger, Dayton-Granger, Airframe KV vs. Microamps.	56
Figure 4-18.	Flight 18 March, 1982, Biased-Discharger, Dayton-Granger, Noise vs. Time.	57
Figure 4-19.	Flight 18 March, 1982, Biased-Discharger, Dayton-Granger, Microamps vs. Time.	58
Figure 4-20.	Flight 18 March, 1982, Biased-Discharger, Dayton-Granger, Airframe KV vs. Time.	59
Figure 4-21.	Flight 29 March, 1982, Biased-Discharger, Dayton-Granger, Noise vs. Microamps.	61
Figure 4-22.	Flight 29 March, 1982, Biased-Discharger, Dayton-Granger, Airframe KV vs. Microamps.	62
Figure 4-23.	Flight 29 March, 1982, Biased-Discharger, Dayton-Granger, Noise vs. Time.	63
Figure 4-24.	Flight 29 March, 1982, Biased-Discharger, Dayton-Granger, Microamps vs. Time.	64
Figure 4-25.	Flight 29 March, 1982, Biased-Discharger, Dayton-Granger, Airframe KV vs. Time.	65

LIST OF FIGURES (Continued)

		PAGE
Figure 4-26.	Discharger Flight Test Granger, March 11, 1982.	67
Figure 4-27.	Flight 11 March, 1982, Natural Charging, Dayton-Granger, Noise vs. Microamps.	68
Figure 4-28.	Flight 11 March, 1982, Natural Charging, Dayton-Granger, Airframe KV vs. Microamps.	69
Figure 4-29.	Flight 11 March, 1982, Natural Charging, Dayton-Granger, Noise vs. Time.	70
Figure 4-30.	Flight 11 March, 1982, Natural Charging, Dayton-Granger, Microamps vs. Time.	71
Figure 4-31.	Flight 11 March, 1982, Natural Charging, Dayton-Granger, Airframe KV vs. Time.	72
Figure 5-1.	Typical Lightning Simulator Position Around N7AP.	75
Figure 5-2.	T/SSI Test Log.	76
Figure 5-3.	Computer Generated Plot of Current Pulse of Simulator.	77
Figure 5-4.	Typical Position of Lightning Simulator Around Aircraft.	78
Figure 5-5.	Close-Up View of Spark Gap of Lightning Simulator.	79
Figure 5-6.	Display of StormScope for 240° Azimuth Testing.	80
Figure 5-7.	TI-9900 Receiver Test, WPAFB Dayton, Ohio .1 NM squares, Azimuth = 000.	82
Figure 5-8.	Trimble Receiver Test, WPAFB Dayton, Ohio .1 NM squares, Azimuth = 000.	83
Figure 5-9.	TI9900 Receiver Test, WPAFB Dayton, Ohio .1 NM squares, Azimuth = 090.	84
Figure 5-10.	Trimble Receiver Test, WPAFB Dayton, Ohio .1 NM squares, Azimuth = 090.	85
Figure 5-11.	TI9900 Receiver Test, WPAFB Dayton, Ohio .1 NM squares, Azimuth = 180.	86
Figure 5-12.	Trimble Receiver Test, WPAFB Dayton, Ohio .1 NM squares, Azimuth = 180.	87

LIST OF FIGURES (Continued)

		PAGE
Figure 5-13.	TI9900 Receiver Test, WPAFB Dayton, Ohio .1 NM squares, Azimuth = 270.	88
Figure 5-14.	Trimble Receiver Test, WPAFB Dayton, Ohio .1 NM squares, Azimuth = 270.	89
Figure 5-15.	Trimble Loran-C Antenna and StormScope Antenna.	91
Figure 5-16.	TI-9900 Loran-C Antenna.	92
Figure 5-17.	Static Field Fixture Around Trimble Loran-C Antenna.	93
Figure 5-18.	TI9900 Receiver Applied Static Field Test, WPAFB Dayton, Ohio, .1 NM squares, 10 KV/Meter.	94
Figure 5-19.	Trimble Receiver Applied Static Field Test, WPAFB Dayton, Ohio, .1 NM squares, 10 KV/Meter.	95
Figure 5-20.	TI9900 Receiver Applied Static Field Test, WPAFB Dayton, Ohio, .1 NM squares, 20 KV/Meter.	96
Figure 5-21.	Trimble Receiver Applied Static Field Test, WPAFB Dayton, Ohio, .1 NM squares, 20 KV/Meter.	97
Figure 5-22.	TI9900 Receiver Applied Static Field Test, WPAFB Dayton, Ohio, .1 NM squares, 50 KV/Meter.	98
Figure 5-23.	Trimble Receiver Applied Static Field Test, WPAFB Dayton, Ohio, .1 NM squares, 50 KV/Meter.	99
Figure 5-24.	TI9900 Receiver Applied Static Field Test, WPAFB Dayton, Ohio, .1 NM squares, 100 KV/Meter.	100
Figure 5-25.	Trimble Receiver Applied Static Field Test, WPAFB Dayton, Ohio, .1 NM squares, 100 KV/Meter.	101
Figure 5-26.	Static Field Testing.	102
Figure 6-1.	Flight Plan Route, August 29, 1981. UNI toward SGH VOR to APE VOR then approach to Port Columbus, thunderstorm activity.	105
Figure 6-2.	Flight Plan Route, August 29, 1981. Port Columbus to ZZV VOR to UNI NDB to UNI, thunderstorm activity.	106

LIST OF FIGURES (Continued)

		PAGE
Figure 6-3.	Flight Test TI9900 Receiver, August 29, 1981. UNI towards SGH VOR to APE to Port Columbus, thunderstorm activity.	107
Figure 6-4.	Flight Test Trimble Receiver, August 29, 1981. UNI to MXO divert to SGH to APE landing at Port Columbus, thunderstorm activity.	108
Figure 6-5.	Flight Test TI9900 Receiver, August 29, 1981. Port Columbus to ZZV VOR to UNI NDB to UNI, thunderstorm activity.	109
Figure 6-6.	Flight Test Trimble Receiver, August 29, 1981. Port Columbus to ZZV to UNI NDB to UNI, thunderstorm activity.	110
Figure 6-7.	Radar Overlay for Flight of August 29, 1981.	112
Figure 6-8.	Fight Plan Route, August 31, 1981. UNI to MXQ to APE to UNI NDB to UNI, thunderstorm activity.	113
Figure 6-9.	Radar Overlay August 31, 1981 - 15:08 P.M.	114
Figure 6-10.	Radar Overlay August 31, 1981 - 16:15 P.M.	115
Figure 6-11.	Radar Overlay August 31, 1981 - 17:15 P.M.	116
Figure 6-12.	Flight Test of the Trimble Receiver August 31, 1981. UNI to MXQ to APE to UNI NDB to UNI, thunderstorm activity.	117
Figure 6-13.	Flight Test TI9900 Receiver, August 31, 1981. UNI to MXQ to APE to UNI NDB to UNI, thunderstorm activity.	118
Figure 6-14a.	Copy of the Printout of the FAA/Mitre Weather Radar Uplink Receiver Output.	120
Figure 6-14b.	A Plot of the Ground Track.	120
Figure 6-15.	Flight Test Trimble Receiver, August 12, 1981. HNN to PKB to ZZV to HNN, no thunderstorm activity.	121
Figure 6-16.	Flight Test of the TI9900 Receiver, September 24, 1981, WPAFB to UNI NDB to UNI, no thunderstorm activity.	122

(Photographs used in the report are by courtesy of the author)

I. CONCLUSIONS

This report details the results of ground and flight tests to evaluate the effects of precipitation, static and lightning on the airborne reception of Loran-C signals. These tests have indicated methods by which the noise produced by p-static can be reduced on the aircraft and thus allow for increased signal-to-noise ratios in the installed Loran-C equipment. The demonstrated p-static noise reduction using a ground-based precipitation static survey is in the range of 20 to 50db in the 100Khz Loran-C frequency spectrum. This noise reduction is achieved by installation of properly placed modern, static-wick dischargers on the airframe. It is recommended that the placement and quantity of dischargers be determined by the airframe manufacturer using ground, p-static tests on a specific airframe.

During an 8-month period, a total of 26.1 hours of DC-3 time was consumed to determine the noise reduction achievable by using quality static-wick dischargers. Six hours of this time was conducted under actual thunderstorm conditions. The aircraft is equipped with 12 instrumented static-wick dischargers, two Loran-C receivers and data collection equipment to measure the dischargers current, noise produced, airframe voltage and Loran-C position outputs. All of the raw data are available and documented in Volume II of the report.

Artificial p-static airframe charging using a biased-discharger with up to 70Kv potential is a method which yields useful in-flight data on effectiveness of static-wick dischargers for low charging currents.

The effects of lightning on the reception of Loran C in aircraft have been found to be of minimal significance. Based on the flight tests performed, the inclusion of effective static-wick dischargers has provided good results. The commercial Loran-C receivers selected for this work have yielded very accurate positional information when used in the vicinity of lightning activity. On all of the plots obtained from these flights, the cross-track errors were less than 0.5 nm and typically 0.1 nm. Along track errors also appeared typically in this range. All of the results were obtained using the 9960 GRI Northeast Loran-C chain, Seneca, N.Y.-Carolina Beach, N.C. (M-Y) and Seneca, N.Y.-Dana, In.(M-Z) station pairs which provide good station geometry in the Southeastern Ohio area. It was only on two occasions the Loran C could not provide navigation signals due to lightning or p-static interference, but as will be pointed out in the report, there are other factors involved in these two instances.

The ground-based lightning simulation testing performed at WPAFB also indicated that, the Loran-C receivers produced on the average, well under 0.1 nautical-mile error in the receiver position information. This corresponds well with the information recorded during flights in thunderstorm areas, even though the ground simulation was not a highly accurate model of actual thunderstorm electrical activity.

The results of placing a static electric field around the Loran-C receiver antenna has indicated very minimal errors in the computed Loran-C

position. The static electric field tests also performed at WPAFB indicated that errors of less than 0.05 nm are produced by DC static fields up to 100 KV/Meter.

In general, the results presented in this report should encourage the further investigation of the use of Loran-C as a viable navigation system for aircraft in the enroute and terminal areas.

II. INTRODUCTION

Over the last six years the Avionics Engineering Center at Ohio University has been actively involved in studying the application of Loran-C to the navigation of aircraft. The preceding contract, DOT-FA79WA-4320 [1], involved reviewing the literature and making recommendations related to the problems of reducing precipitation static in aircraft. The work documented here logically follows that work. This report will describe a ground test procedure that can be used to determine, for a specific static-wick installation, the amount of p-static noise produced by airframe charging. This testing was performed using a DC-3 aircraft, N7AP, that is instrumented to measure the individual discharger currents and the noise produced by this corona discharge, Figure 2-1. Mr. Robert Truax, owner of TCO Manufacturing, traveled to Ohio University to consult on conducting the ground p-static survey from May 18, 1981 to May 29, 1981. Mr. Truax brought with him all the necessary p-static test fixtures described in the text to conduct the p-static survey of the aircraft. To document the data, a computer-operated data collection system was installed in the aircraft to provide rapid and accurate recording of many parameters. This data collection system is very versatile and can be reconfigured for many different data collection tasks relating to measuring p-static noise. The aircraft is also equipped with two Loran-C receivers that are used in the testing to determine if any position output errors are encountered while the receivers operate in the flight environment during thunderstorms and p-static charge-forming conditions. Figures 2-2 and 2-3 are photographs of equipment installed in the aircraft.

This report deals with making real measurements of the p-static performance of the aircraft and Loran-C receivers to determine if Loran C can provide the necessary navigation performance in an all-weather situation. This report is intended to give the reader a general impression for the kinds of benefits achievable by providing good static-wick dischargers on an aircraft which uses Loran-C as an all-weather navigation aid.

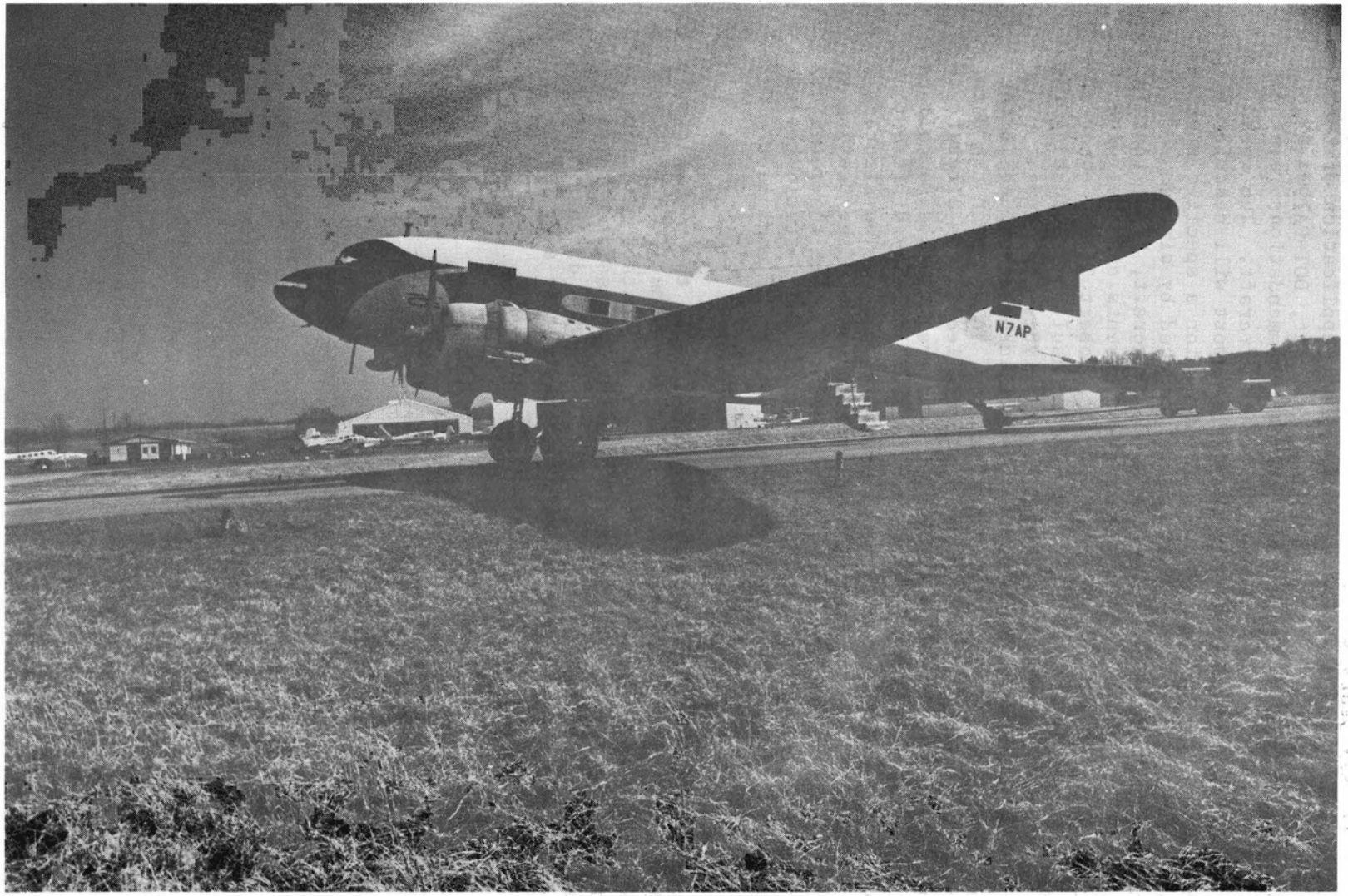

Figure 2-1. N7AP Ohio University DC-3 Flying Laboratory.

Figure 2-2. Interior View N7AP - Looking Toward Tail.

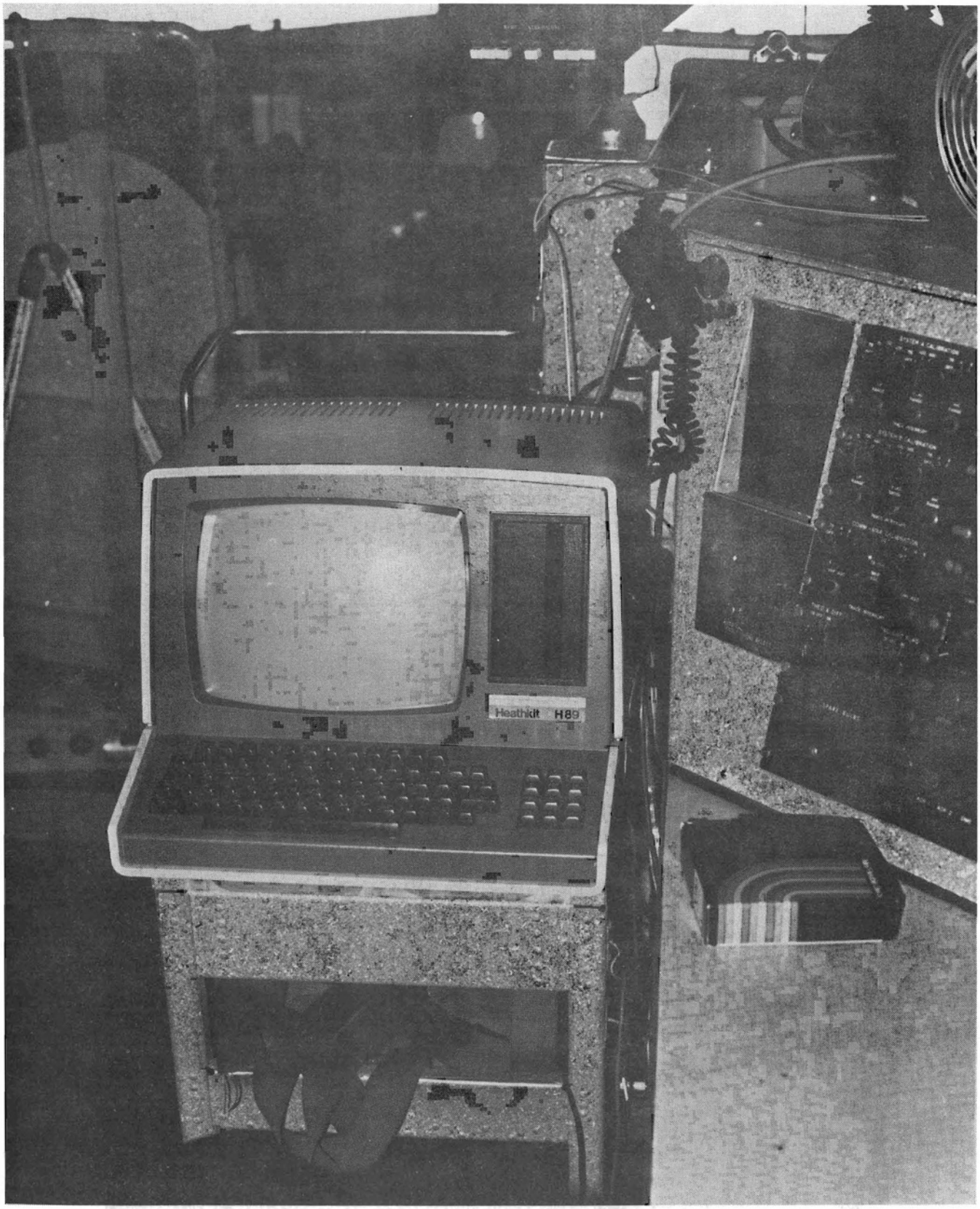

Figure 2-3. Heath H-89 Computer at Operator Console.

III. GROUND PRECIPITATION STATIC TESTING

A. Airframe Bonding Tests.

1. Test Procedure. The airframe bonding testing was done to determine the conducting state of the entire aircraft skin, control surfaces, engine cowling and landing gear. This was necessary because any electrically isolated aircraft skin panels can cause arc noise which contributes to the total noise generated in p-static charging conditions.

The method used was to examine the entire aircraft using an ohmmeter capable of measuring resistances to at least 0.1 ohm. Areas of particular interest are junctions of metal panels which are secured using screws and not rivets. Occasionally, an insulating oxide can form under the edge of the metal causing a high resistance bond. In general, for p-static conditions, these are not serious. Also, if the rate of charging is high, the possibility for arc noise is greater. Of particular interest in arc noise are the propellers. If good bonding is not provided, a good possibility for arcing noise exists because the high velocity propellers allow them to acquire charge at high rates. If this charge cannot be conducted to the airframe, arcing noise will be generated as the charge arcs to the airframe at the propeller hubs.

N7AP is equipped with pneumatic deicing boots on the leading edges of wings, ailerons, and rudder. These frontal areas, if not electrically conductive, will not transfer charge to the metal airframe in a noiseless manner. Therefore, it is advantageous for this equipment to be electrically conductive. Since these leading edge areas account for much of the frontal wetted area, they are the interface for accumulating the charge on the airframe. If these areas are of high insulating value, the charge that accumulates there will become bound, and, when the voltage increases high enough, the charge will streamer along the surface to the metal aircraft skin. This causes significantly higher noise than p-static as arcing is an energetic process. A value of conductivity of several megohm per square is sufficient to eliminate the streamering noise problem on the leading edge deicing boots [2].

Tires and landing gear also need to be conductive so that if the airframe should become charged in flight, upon landing, this charge can bleed off before ground personnel touch the aircraft. The high voltage that can accumulate on the aircraft, combined with the capacitance of the airframe, could in rare instances, cause a serious electric shock if the airframe is discharged by ground personnel touching the aircraft.

2. Airframe Bonding Test Results. The aircraft used for these tests is a DC-3, N7AP, the flying laboratory for the Avionics Engineering Center at Ohio University. There were 204 individual bonding measurements made on this aircraft. Nearly all points tested indicated resistances of 1.0 ohm or less (most were 0.2 to 0.4 ohm)[1] which is

---

[1]Conversation with Robert Truax regarding Adequate Bonding Resistivity, May, 1981.

adequate for good bonding. There was one small metal panel on the rudder that was isolated from the rest of the airframe and one of the grounding jacks used for grounding the airframe during refueling was not bonded. All of the control surfaces were also bonded adequately to the rest of the airframe. In general, the aircraft bonding was very good despite the airframe age of nearly 40 years.

3. Tires and Deicing Boot Resistivity Tests. The resistivity tests on the deicing boots and tires were made using a megohm meter with a probe that would provide resistivity measurements in ohms per square. The measurements on the deicing boots showed a 6.6 megohm per square resistivity. The tires indicated approximately 100 megohm per square. These values were determined to be adequate to provide enough resistivity to permit the currents likely to be encountered.

4. Summary of Bonding Tests. The tests are a good point to begin in characterizing the state of p-static noise susceptibility that an airframe will have. Finding any improper bonding at this point can eliminate wasted time when performing the airframe charging tests. Improper bonding can lead to significant arcing noise especially at high airframe charge rates due to p-static.

The equipment necessary to perform these tests are very basic and simple to use and the airframe does not have to be flown to get this information. Airframe bonding is therefore a logical place to start in an aircraft p-static survey.

B. Ground Airframe Charging Tests.

1. Test Procedure and Instrumentation. Figure 3-1 is a diagram of the current placement of instrumented static-wick dischargers on the DC-3. These dischargers are mounted on insulating material and a wire is returned to the operator console in the aircraft to measure the discharging currents.

In order to artificially charge the aircraft on the ground, it was necessary to place the entire aircraft on insulators. Sheets of 1/4-inch thick acrylic plastic, 4 ft. by 8 ft., were placed under each wheel, Figures 3-2 and 3-3. This plastic forms a very good insulator if the surface is kept clean. To determine leakage currents flowing across the surface of the plastic, a metalic foil (guard ring) was placed around the perimeter of the plastic on the top edge. These were all connected together through a sensitive ammeter capable of measuring microamps of current. Any current flow across the plastic can then be monitored through a guard ring on the plastic sheets.

During the p-static ground testing, two types of corona were produced at the tips of the static-wick dischargers, negative-point and positive-point. Negative-point corona results when the discharger tips are at a more negative potential than the surrounding areas. Positive-point corona results when the discharger tips are more positive than the surrounding areas.

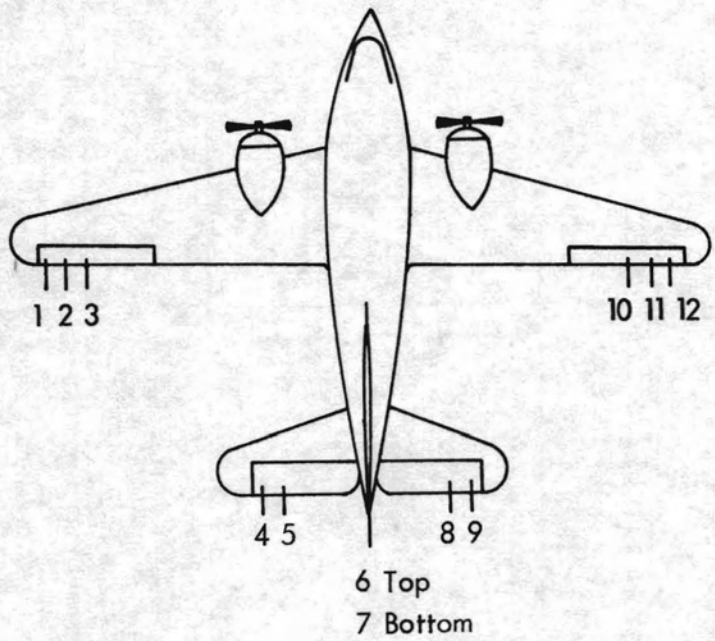

Figure 3-1. N7AP Instrumented Static-Wick Discharger Placement.

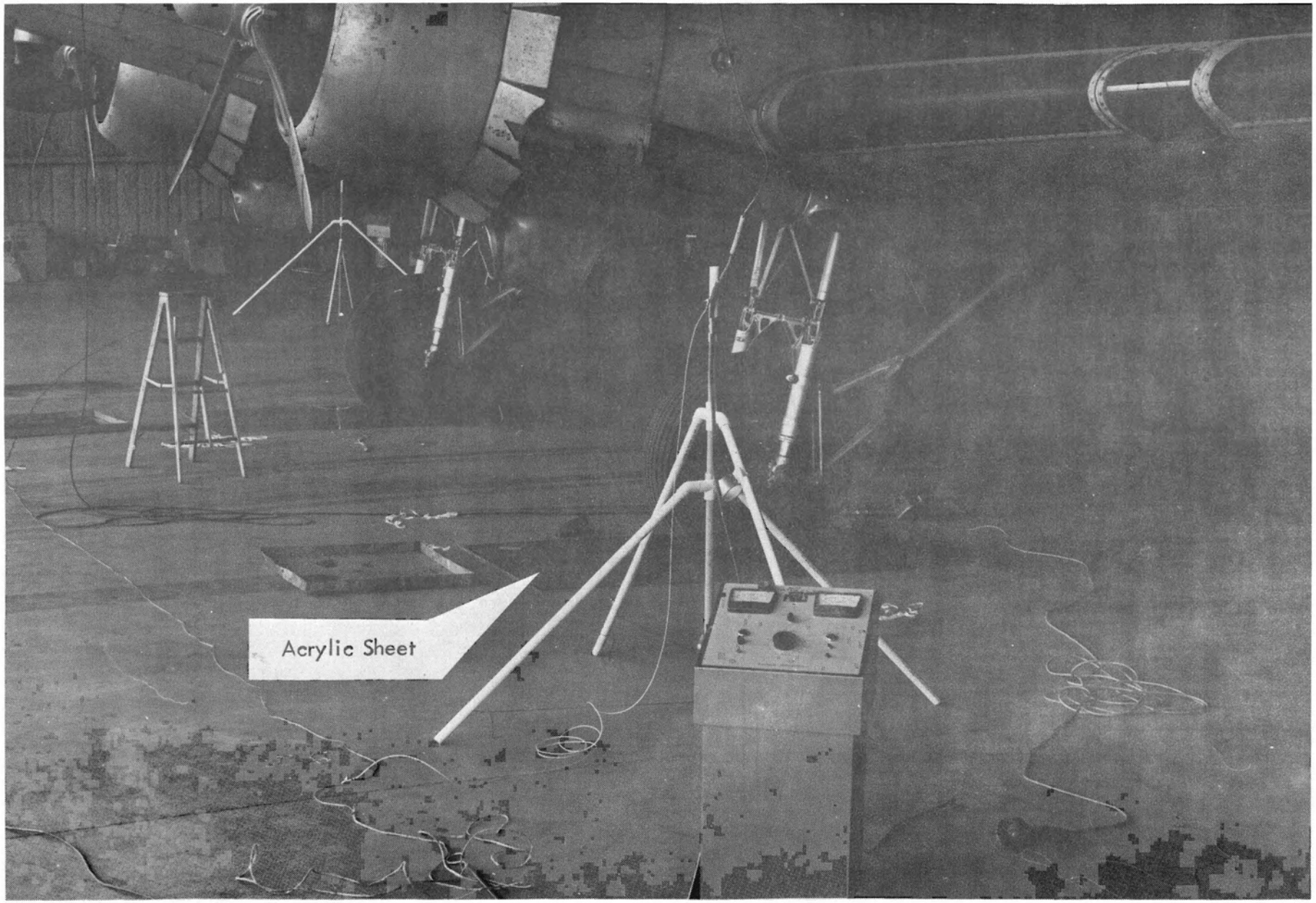

Figure 3-2. Acrylic Sheets Under Main Landing Gear.

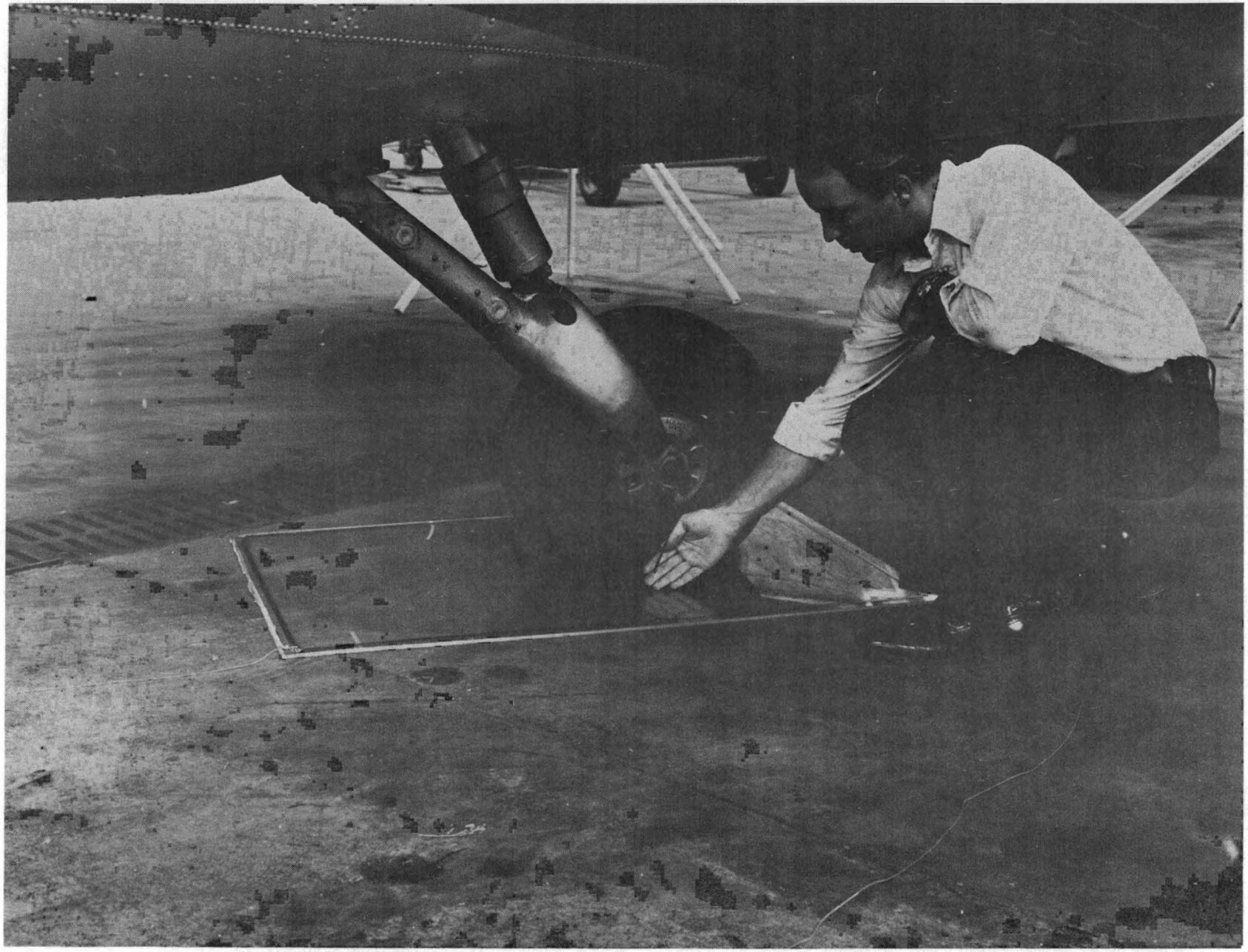

Figure 3-3. Acrylic Sheet Under Tail Wheel. Note guard ring around edge.

To produce negative-point corona at the tips of the static dischargers, it is necessary to deposit negative charge on the aircraft. This can be done by flooding the leading edge of the wings with negative ions created by a high voltage corona. Figure 3-4 is a photo of the ion flood fixture used to produce the flood of ions to charge the aircraft. The ion flood fixtures were connected to the negative lead of the high voltage power supply. Once the airframe was flooded with the negative ions, a return path was necessary for the current flow or else a space charge will inhibit depositing further charge on the airframe. Also, since it was intended to simulate the aircraft discharging current in flight, the current was to be conducted off the aircraft on the static dischargers. To facilitate this, ion collection fixtures were placed at the rear of control surfaces where dischargers are mounted. These ion collection fixtures were then connected to the return lead of the high voltage power supply, in this case, the positive lead. Therefore, when the airframe was flooded with negative ions the airframe was charged negatively. This charge was removed from the airframe by the positive electric field induced at the dischargers by the ion collection fixtures. Note that there were no hard connections made to the aircraft so that it always remained isolated from ground and the power supply. Figures 3-5 and 3-6 are photos of the ion collection fixture placed behind the control surface. The inside of the fixture was coated with high resistivity paint and, therefore, provided a simulated equipotential field at the discharger location. In the return lead of the ion collection fixture was a string of 1 meg resistors which decoupled the electric field from the high voltage power supply. Figure 3-7 is a photo of the ion flood and ion collection fixtures on the right wing.

To monitor the high voltage power supply so that all of the current flowing from the supply returns to the supply, sensitive ammeters were placed in the ion flood fixture circuit and the ion collection fixture circuits. This allows accountability such that all the current flowing to the aircraft returned from the aircraft. This was also observed by measurements made by the guard ring currents of the insulating plastic sheets under the tires.

All of this instrumentation, including the HV power supply, were operated external to the aircraft. This information was monitored during the tests and was not included in the data collection information directly.

The data-collection equipment contained in the aircraft for the ground p-static tests includes the following: Heath H-89 digital microcomputer, Serial Lab Products remote I/O unit, Monroe model 225K electrostatic field meter, Electrometrics EMC-25 interference analyzer and the discharger instrumentation panel. Figure 3-8 is a block diagram of the entire ground test instrumentation setup. A detailed description of the data-collection instrumentation is contained in Volume II. Some general information about the setup is described here. The H-89 computer was the controller for the data collection. It, under software control, commands the Serial I/O unit to read the analog voltages relating to the discharger current, airframe potential and noise levels at 100Khz and records them on the internal

Figure 3-4. Ion Flood Fixture on Leading Edge of Wing.

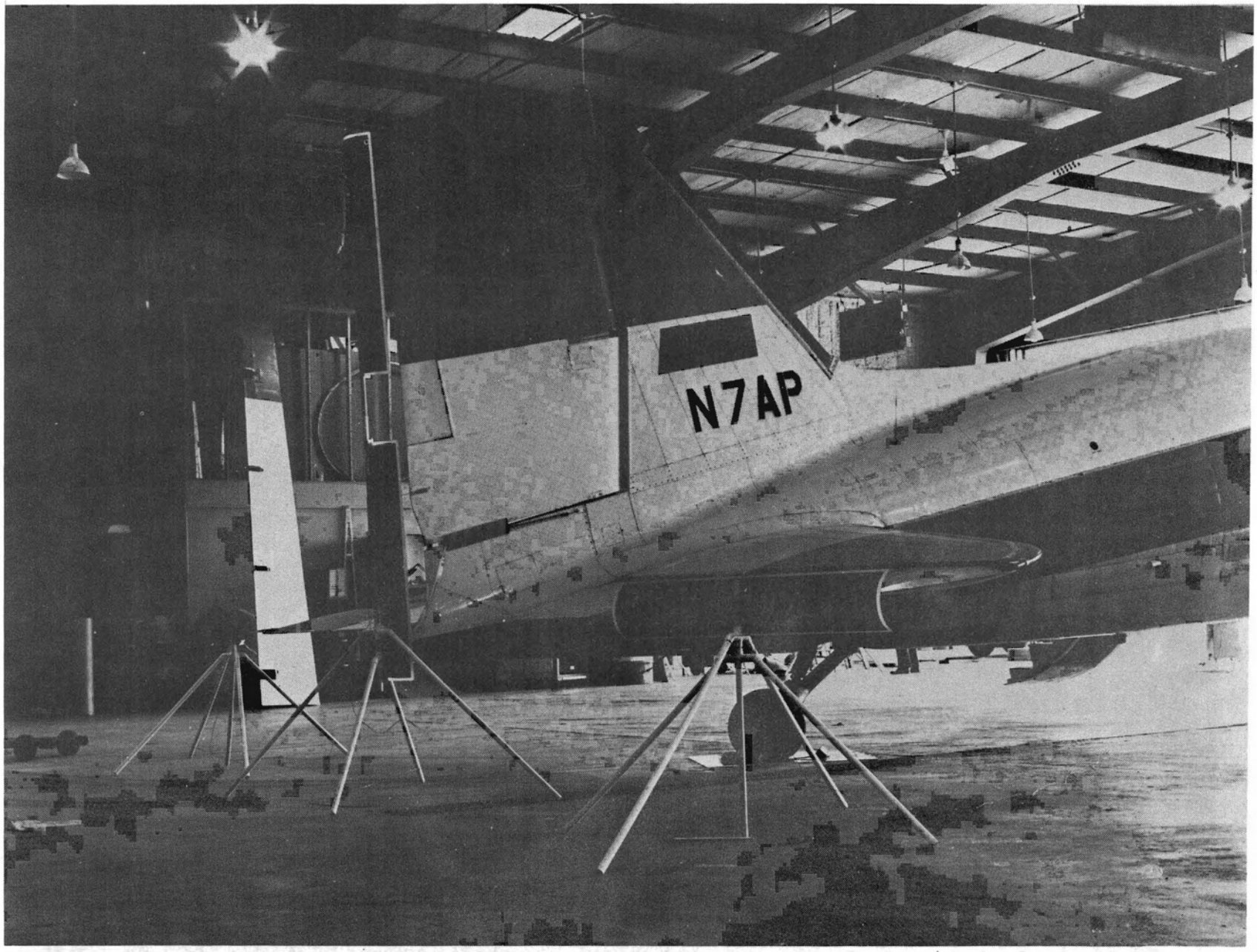

Figure 3-5. Ion Collection Fixtures Behind Control Surfaces.

Figure 3-6. Close-Up of Ion Collection Fixture and Dayton-Granger Dischargers.

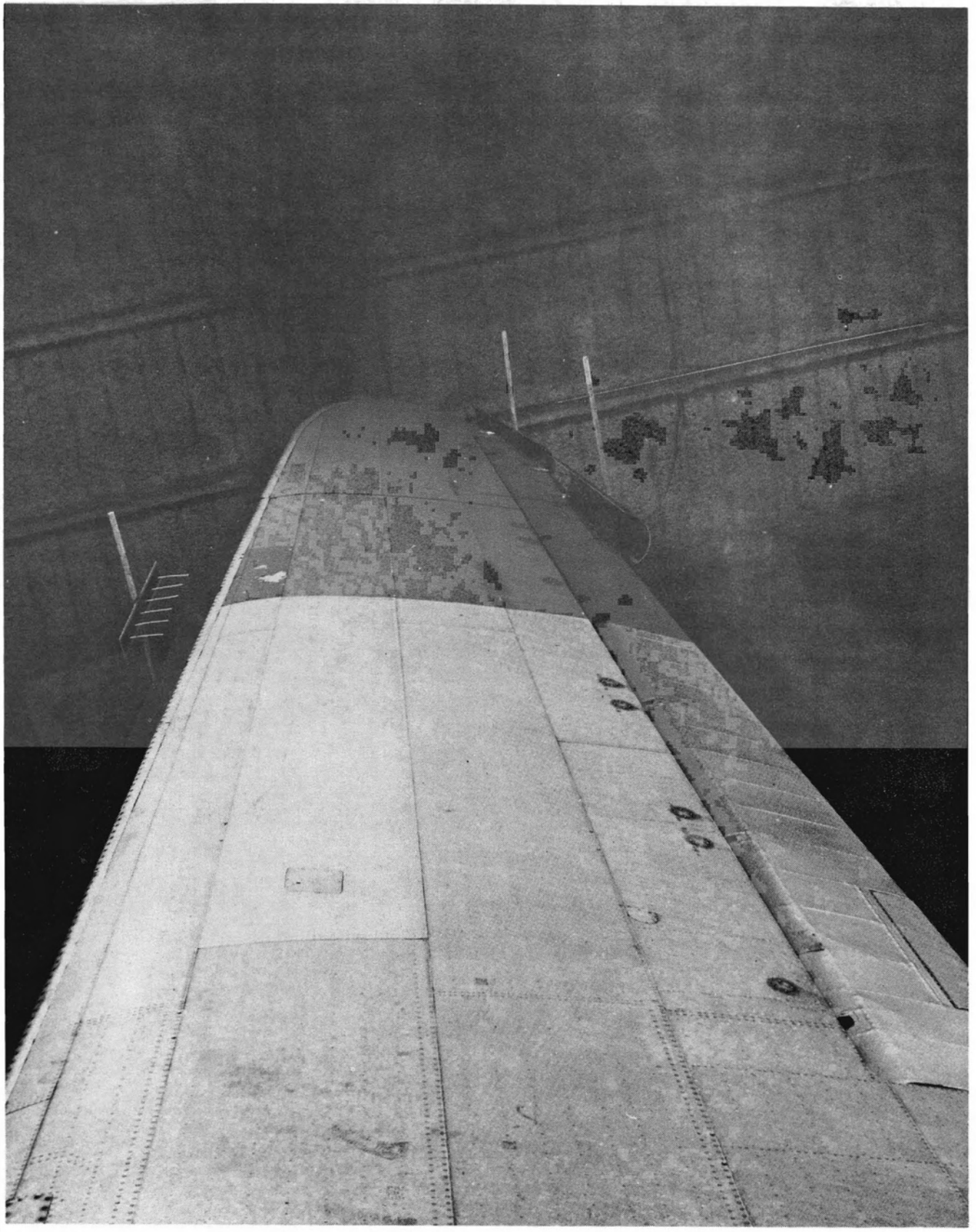

Figure 3-7. Ion Flood and Ion Collection Fixtures on Right Wing.

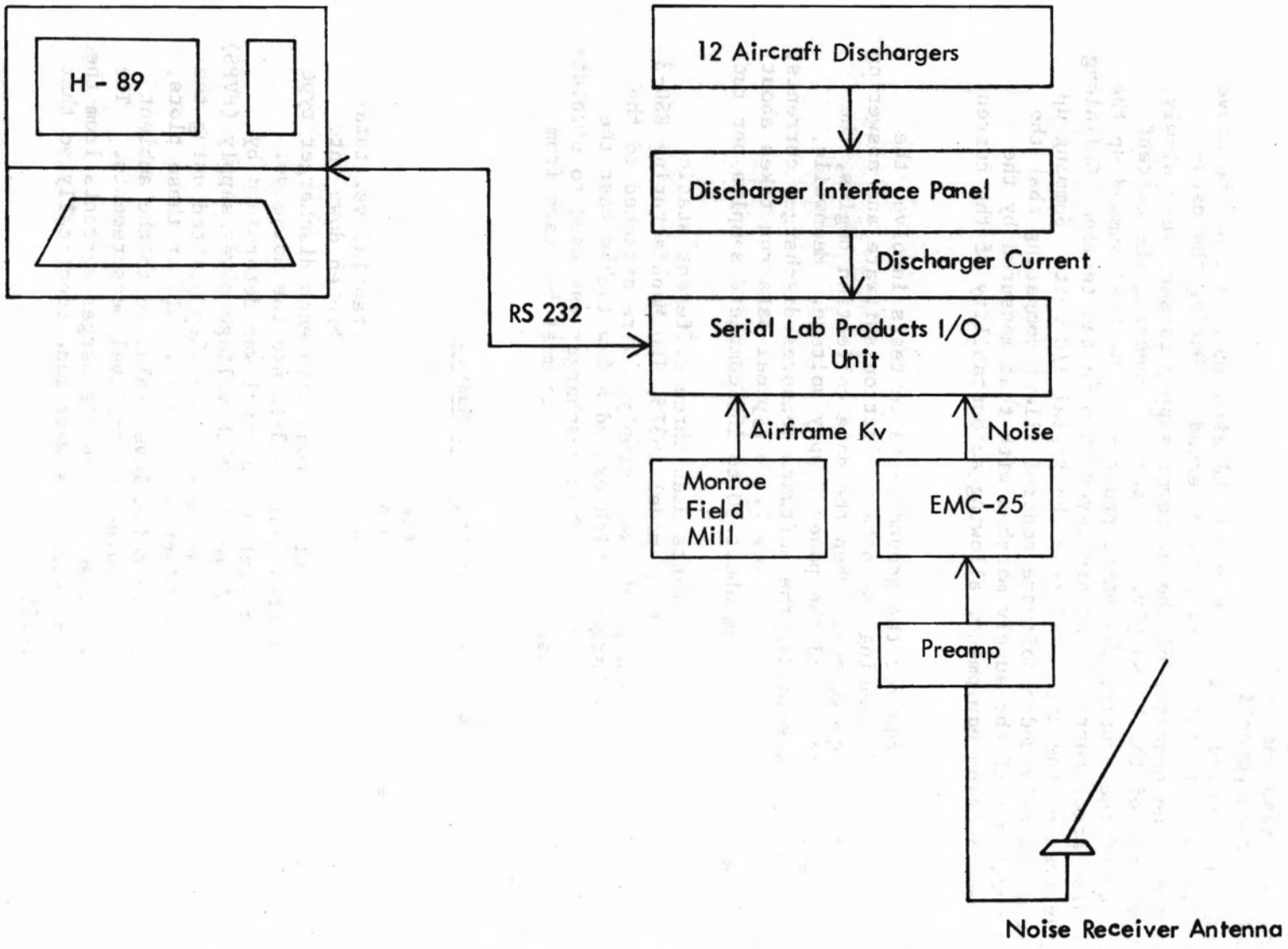

Figure 3-8. Block Diagram of Ground P-Static Instrumentation.

floppy disk. The Serial I/O unit can therefore be commanded to read any of the data at any time. In the ground p-static noise tests, all 12 of the dischargers were read individually along with the noise level of the EMC-25, and airframe potential. Figure 3-9 is a photo of the noise receiver antenna mounted on the bottom of the airplane. All of the above data were read approximately every 6 to 8 seconds. During the data-collection time, the operator of the HV power supply raises, very slowly, the output voltage of the HV supply. For ease of checking the current accountability of the supply, the BASIC program in the H-89 summed up the individual discharger currents and displayed them on the terminal CRT along with all the rest of the data read from the Serial I/O unit. Summing up these currents quickly under software control allows comparing that the current measured out of the supply matches with that measured by the onboard data-collection equipment, allowing accountability of the current flow.

An example data run for the ground p-static tests involved the operator in the aircraft running the data-collection software and answering the file documentation questions. When the data collection begins, the power supply operator increased the power supply voltage. Meanwhile, approximately every six seconds, the software measures discharger currents, field mill output and 100 KHz noise level. A typical data run takes about 5 to 10 minutes to run, providing about 50 to 100 complete samples per run.

The p-static ground survey tests used three different static dischargers, the Dayton-Granger Omega model 16375, TCO Manufacturing ESD-3 and corona points. The corona points were simply a wire attached to the base attachment for the dischargers which extend a few inches past the trailing edge of the control surface. This discharger was used to simulate the aircraft without any dischargers as the corona must be drawn from a specific point in order that the current be instrumented.

2. Ground P-Static Charging Test Results.

The test data results are presented in two forms, the first set of plots indicates noise level vs. total discharger micro-amps. The second set of plots indicates the relationship of airframe potential vs. total discharger micro-amps. Each set of plots is further broken down into positive-point corona and negative-point corona with each discharger type tested in each corona type. Figures 3-10 to 3-12 are the noise vs. discharger current plots. The ambient noise level was determined by averaging the EMC-25 noise level while the high voltage power supply (HVPS) is set to 0 volts. The measured noise levels were then plotted using the previously determined reference ambient noise level. All of these plots, therefore, indicate the increase in noise level relative to the ambient noise level and do not represent absolute noise level measurements. The total discharger currents were the sum of the discharger currents from the instrumented dischargers. All measurements were made identically so that results could be compared directly.

Figures 3-10, 3-11 and 3-12 are the negative-point corona plots for the corona points, Dayton-Granger 16375 and TCO ESD-3 dischargers,

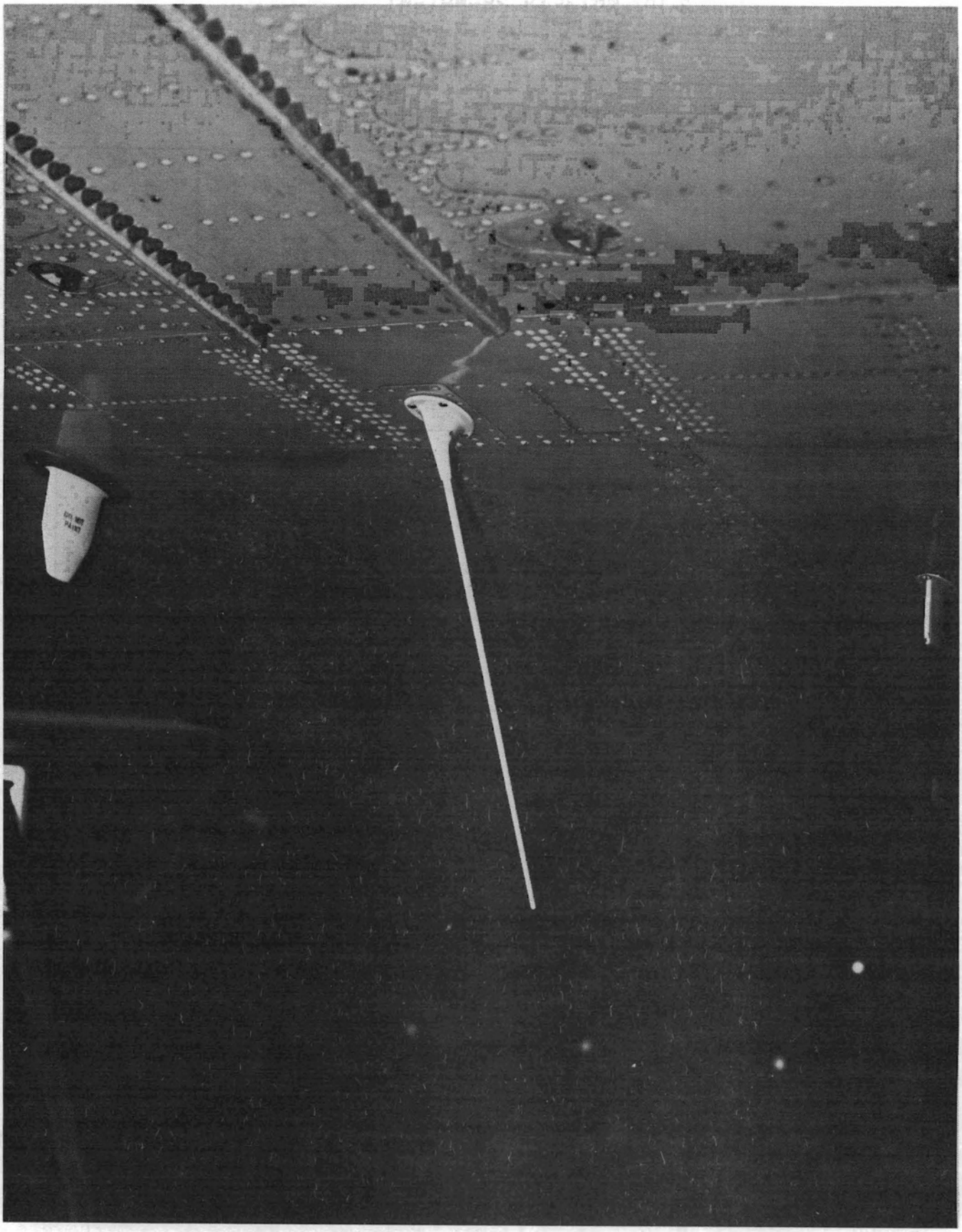

Figure 3-9. Noise Receiver Antenna on Bottom of Aircraft.

Figure 3-10. NOISE13 29-MAY-81
DISCHARGER=CORONA POINT
DETECTOR=CARR.,BANDWIDTH=WIDE
NEGATIVE POINT CORONA

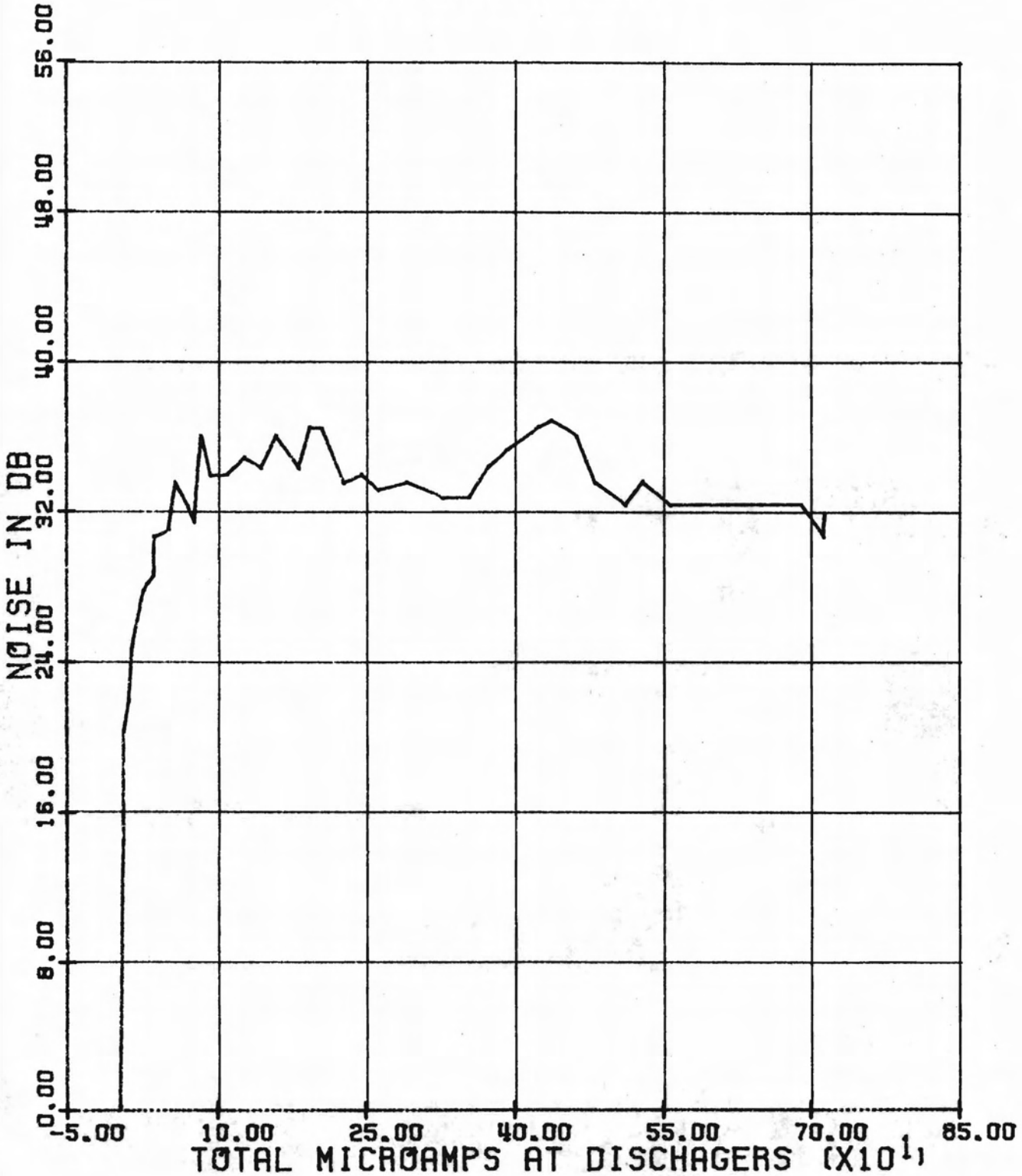

Figure 3-11. NOISE3 28-MAY-81
DISCHARGER=DAYTON OMEGA
DETECTOR=CARR.,BANDWIDTH=WIDE
NEGATIVE POINT CORONA

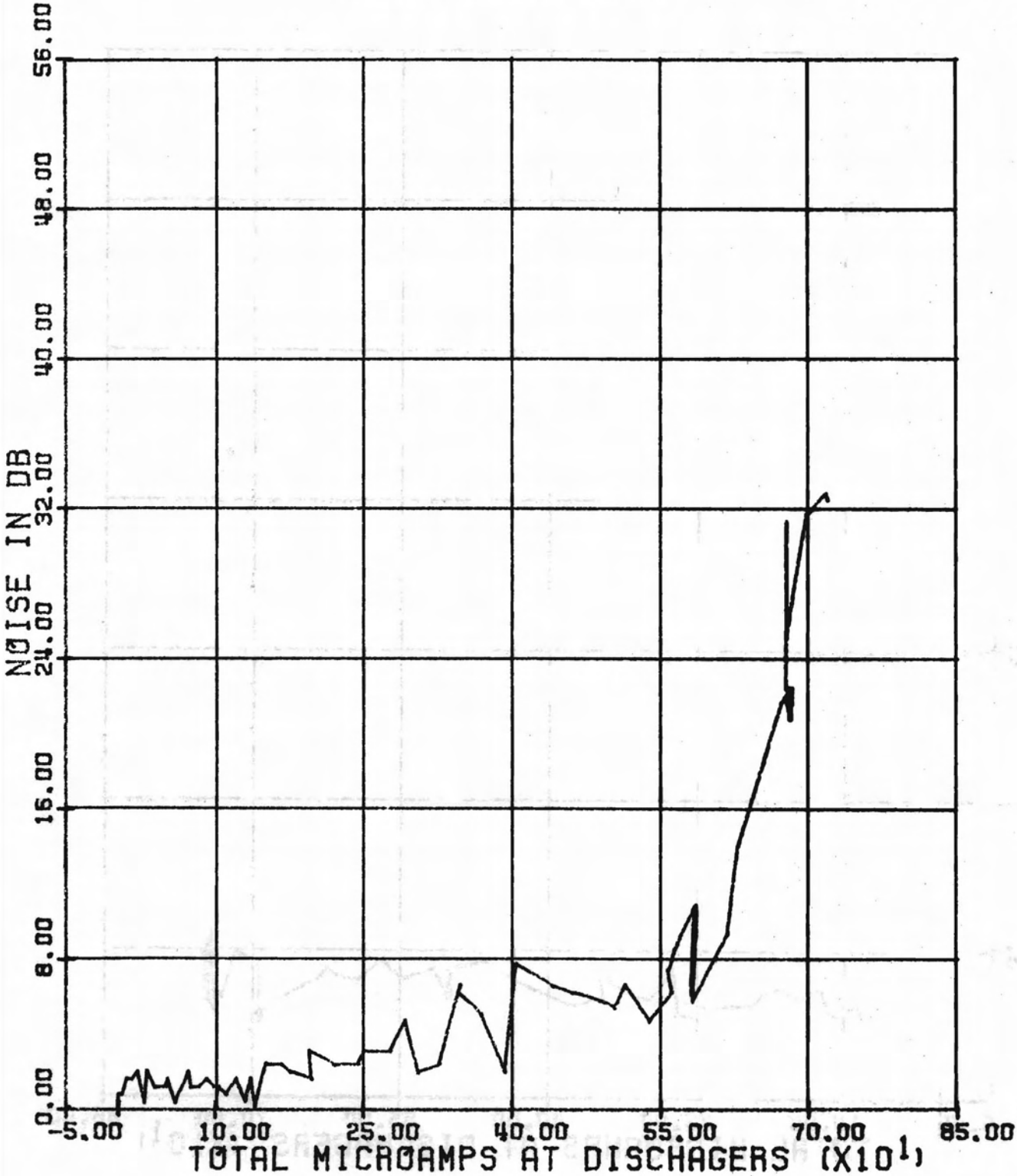

Figure 3-12. NOISE4 28-MAY-1981
DISCHARGER=TCO ESD-3
DETECTOR=CARR..BANDWIDTH=WIDE
NEGATIVE POINT CORONA

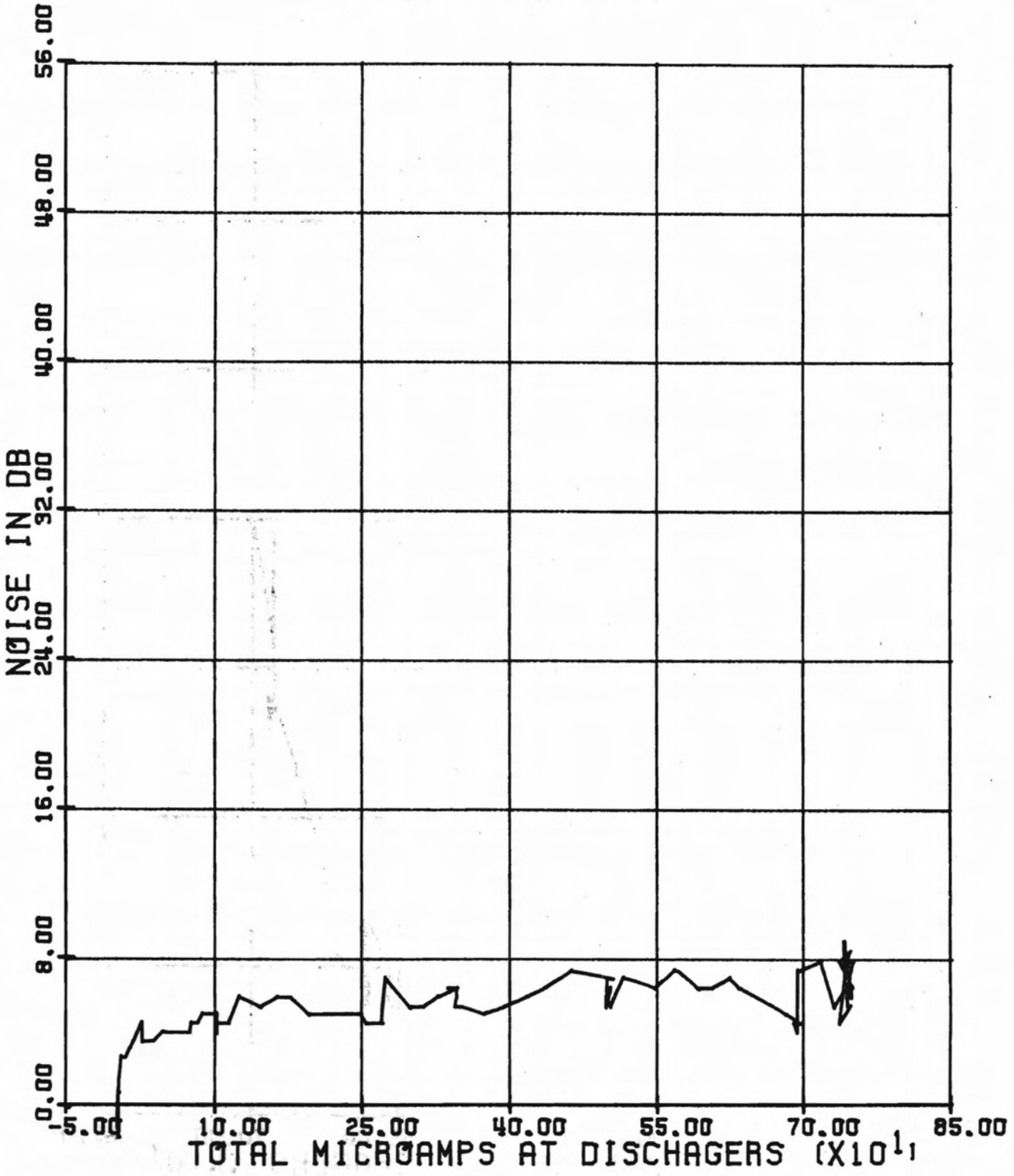

respectively. From these plots it can be seen that a noise reduction of greater than 30 db can be gained by using a well-designed static-wick discharger placed properly on the airframe. All of these measurements were made using the EMC-25 with the carrier detector at 100 Khz center frequency and the 400 hz bandwidth filter. Volume II contains detailed information on the instrumentation.

Figures 3-13 to 3-15 are the plots of the airframe voltage vs. the discharger current for the case of negative-point corona using the corona points, Dayton-Granger 16375 and TCO ESD-3 dischargers respectively. These data are a measure of the dynamic impedance of the airframe and charging system. These plots also indicate the average power levels in the corona. For quiet discharger operation, the airframe voltage should be kept as low as possible for any given discharger current which corresponds to a relatively low impedance level. The dischargers should act like a high voltage zener to provide more change in current for a small change in airframe potential.

The airframe potential for the plots was derived for the particular installation on the aircraft by plotting field mill output vs. power supply voltage with the power supply connected directly to the airframe. A conducting sheet was placed at a specific distance from the field mill with the opposite power supply terminal connected directly to this plate. Figure 3-16 is the plot of the results which produces a linear curve to calculate the airframe potential. Figure 3-17 is a photo of the calibration fixture used with the field mill.

The plots of positive-point corona for noise vs. current are shown in Figures 3-18 through 3-20. Comparing these figures also indicates a reduction of corona noise, but the reduction was less with positive-point corona. From the tests performed so far, there has always been a requirement for more high voltage potential to produce a positive-point corona threshold. This was believed to be due to the polarity of the field and its intensity at the tips of the dischargers. With negative-point corona, ionized oxygen was believed to be produced at the discharger tips. With positive-point corona, ionized nitrogen was believed to be produced. Since the ionization potential of nitrogen is higher (14.534ev) than oxygen (13.618ev), it indicates that a higher electrostatic field would be required to produce ionized nitrogen than ionized oxygen.

Generally, natural p-static charging produces negative-point corona, but in the vicinity of thunderstorm activity the strong crossed fields encountered can produce very high positive-point corona also. The data shown here indicates that noise due to positive-point corona was greater than noise due to negative-point corona. This may relate to the decreased efficiency of the static-wick dischargers for positive-point corona. This problem should be investigated in more detail, with possible modification of the dischargers to make them more efficent in discharging positive-point corona.

Referring to Figures 3-21 to 3-23 which are potential vs. current plots for corona points, Dayton-Granger and TCO ESD-3 dischargers,

Figure 3-13. NOISE13 29-MAY-1981
DISCHARGER=CORONA POINT
DETECTOR=CARR..BANDWIDTH=WIDE
NEGATIVE POINT CORONA

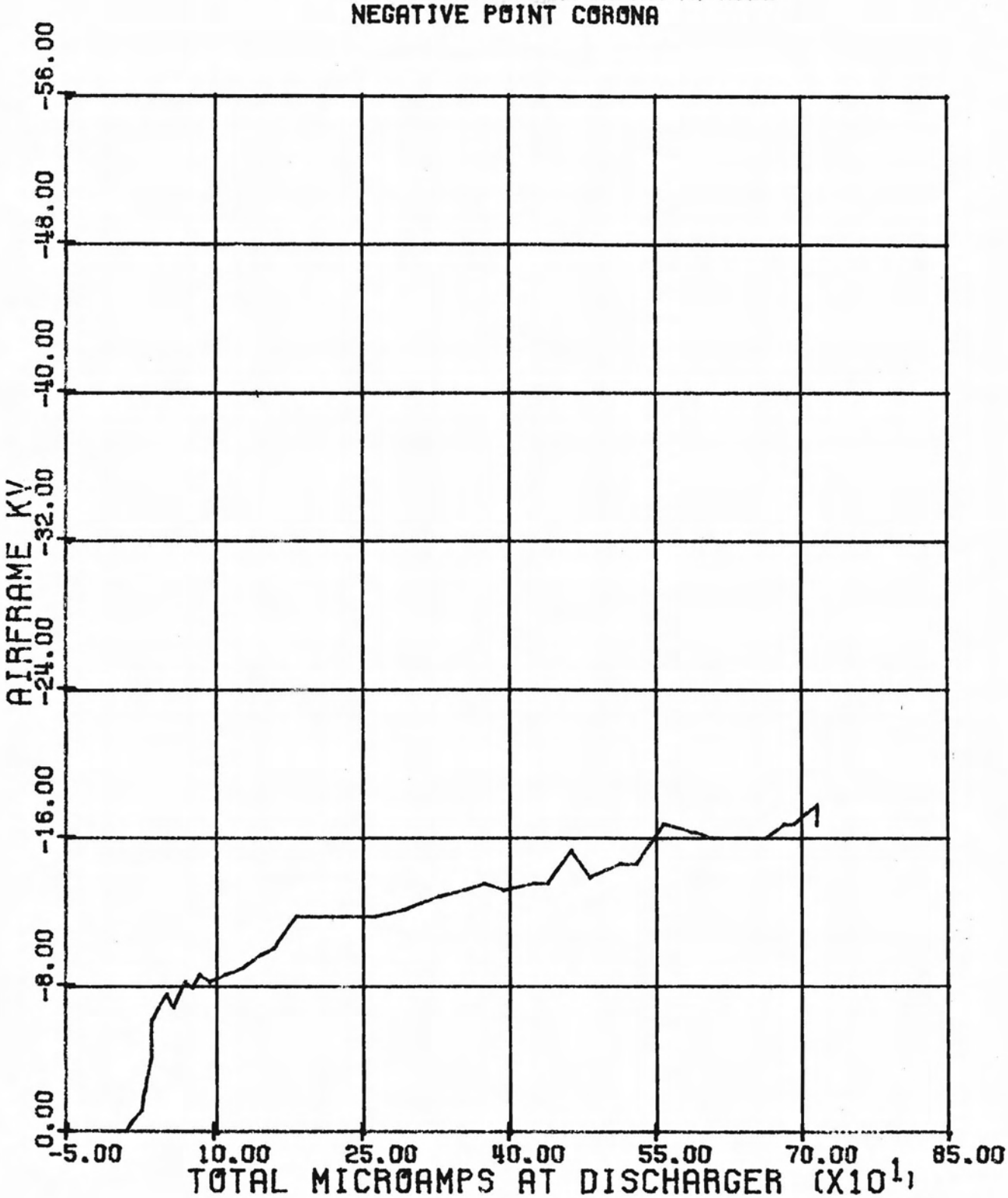

Figure 3-14. NOISE3 28-MAY-1981
DISCHARGER= DAYTON OMEGA
DETECTOR=CARR.,BANDWIDTH=WIDE
NEGATIVE POINT CORONA

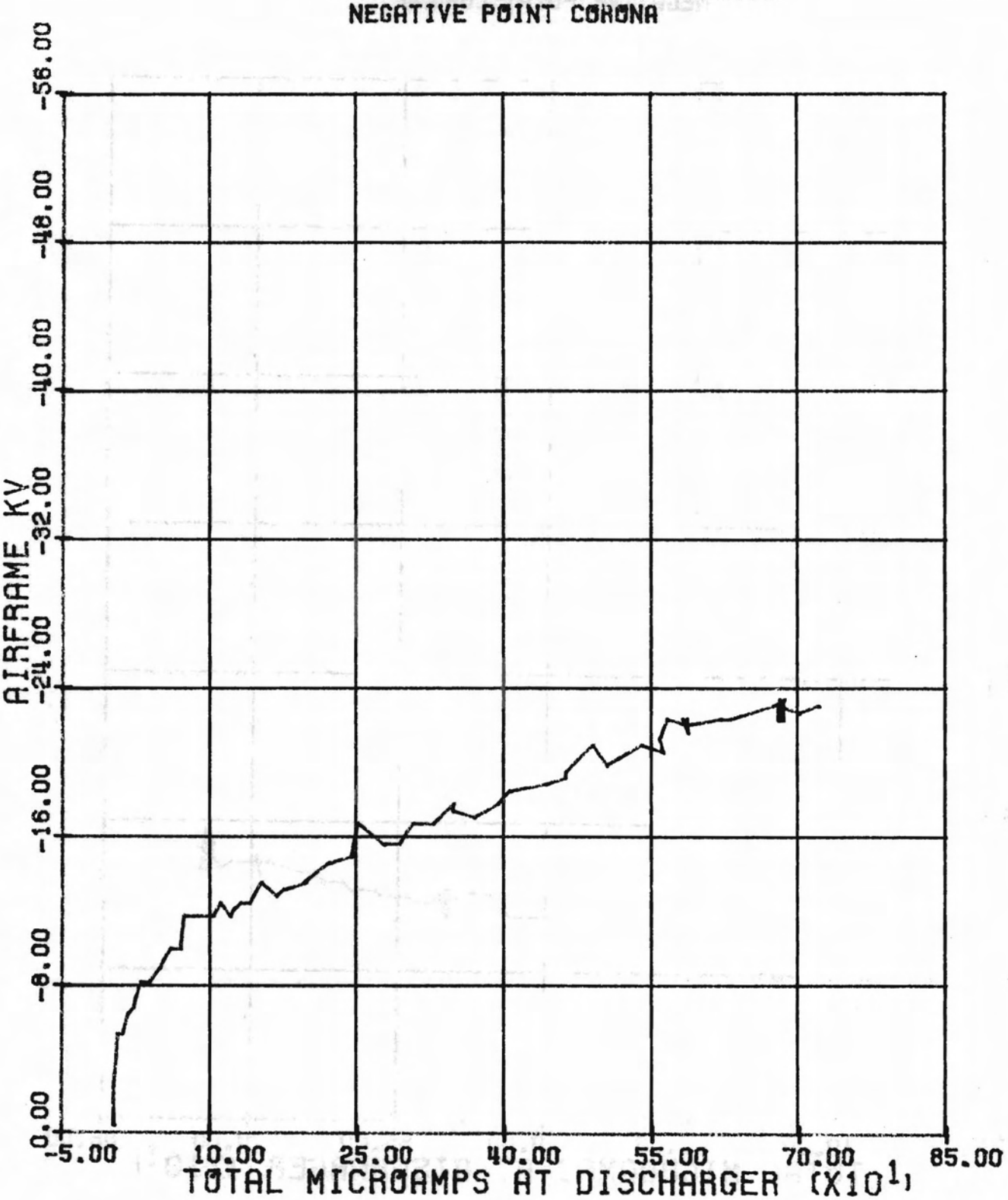

Figure 3-15.

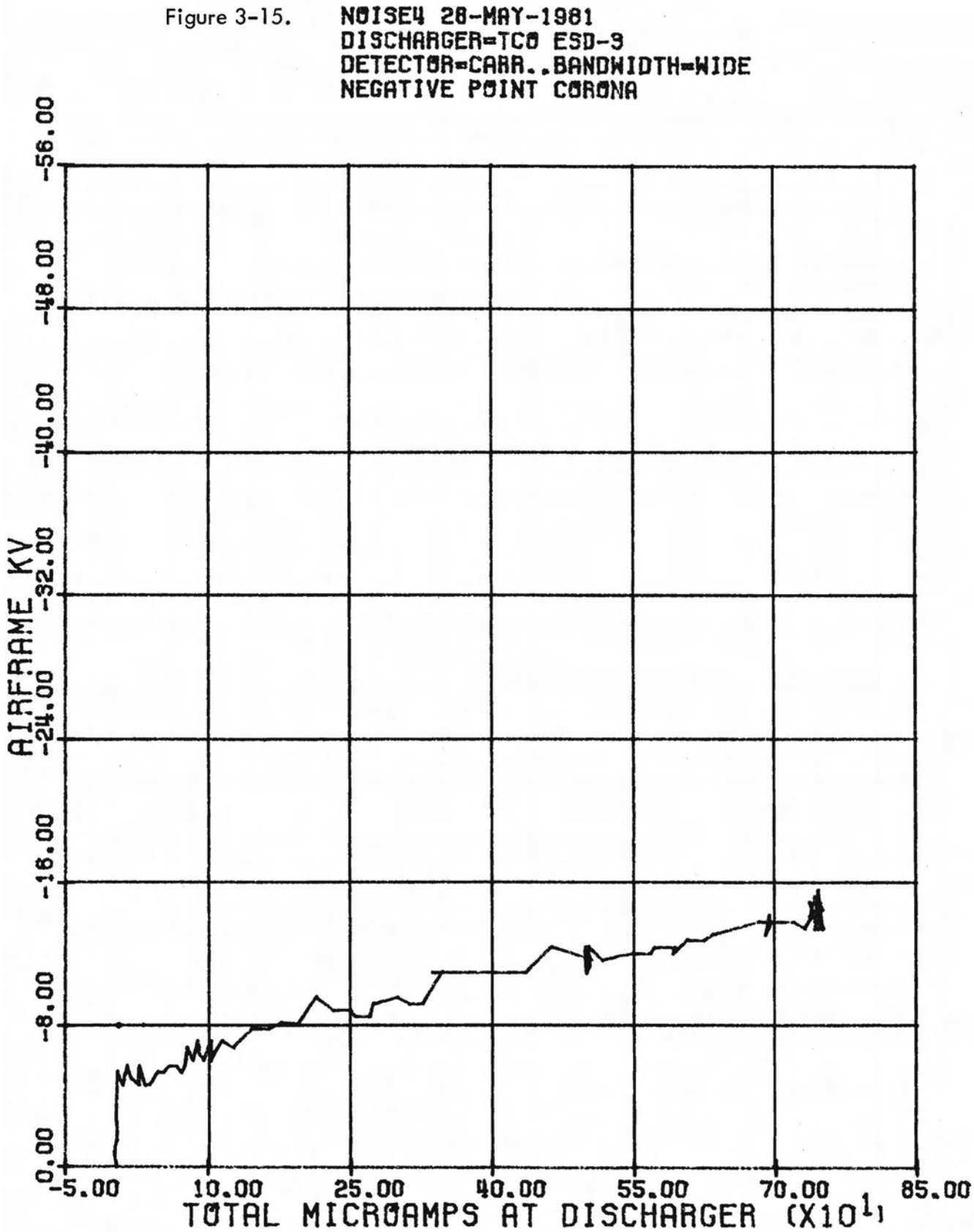
NOISE4 28-MAY-1981
DISCHARGER=TCO ESD-9
DETECTOR=CARR..BANDWIDTH=WIDE
NEGATIVE POINT CORONA
AIRFRAME KV
-56.00
-48.00
-40.00
-32.00
-24.00
-16.00
-8.00
0.00
-5.00
10.00
25.00
40.00
55.00
70.00
85.00
TOTAL MICROAMPS AT DISCHARGER (X10¹)

Figure 3-16. CALIBRATION CURVE OF AIRFRAME POTENTIAL NEG. POINT CORONA

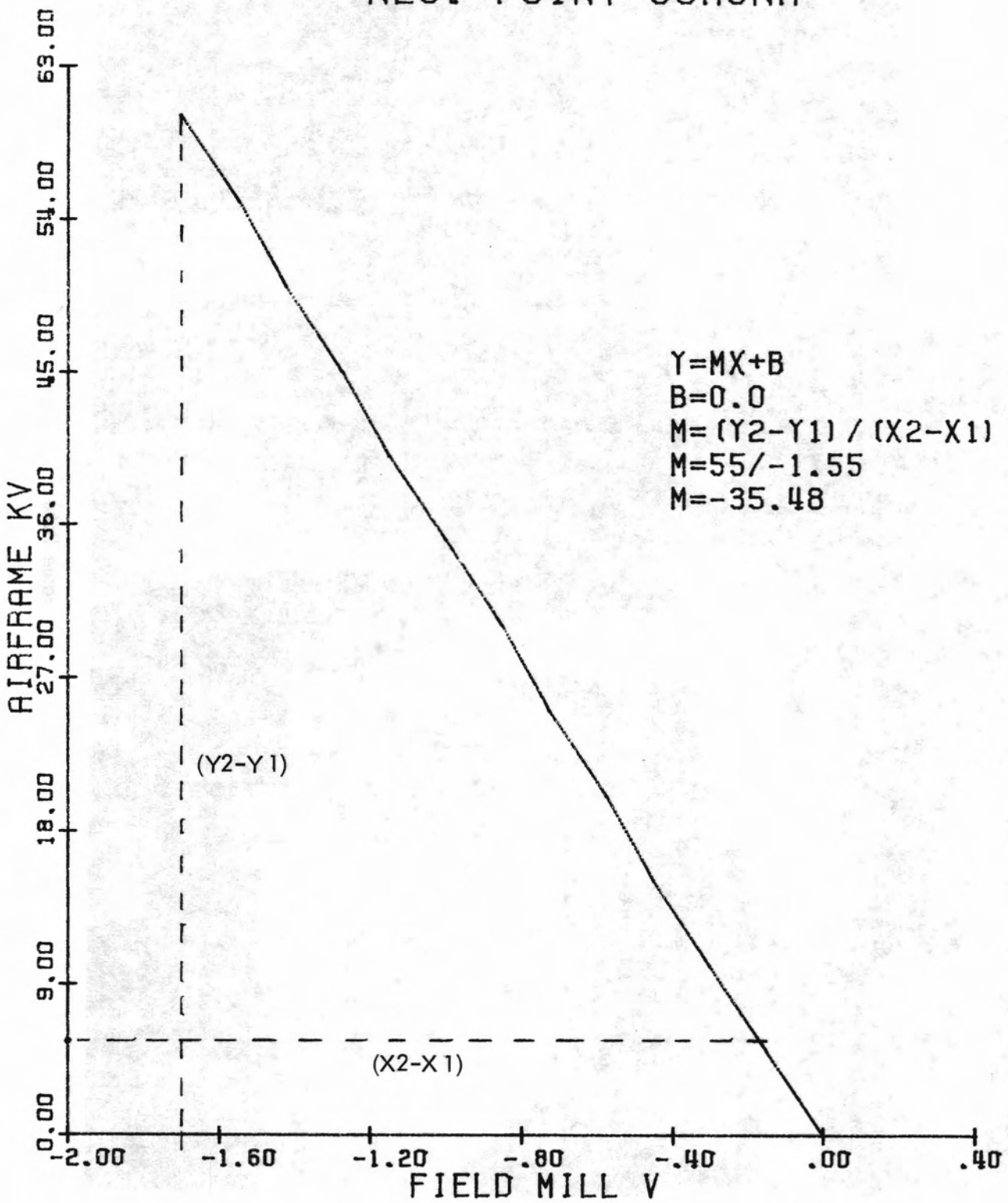

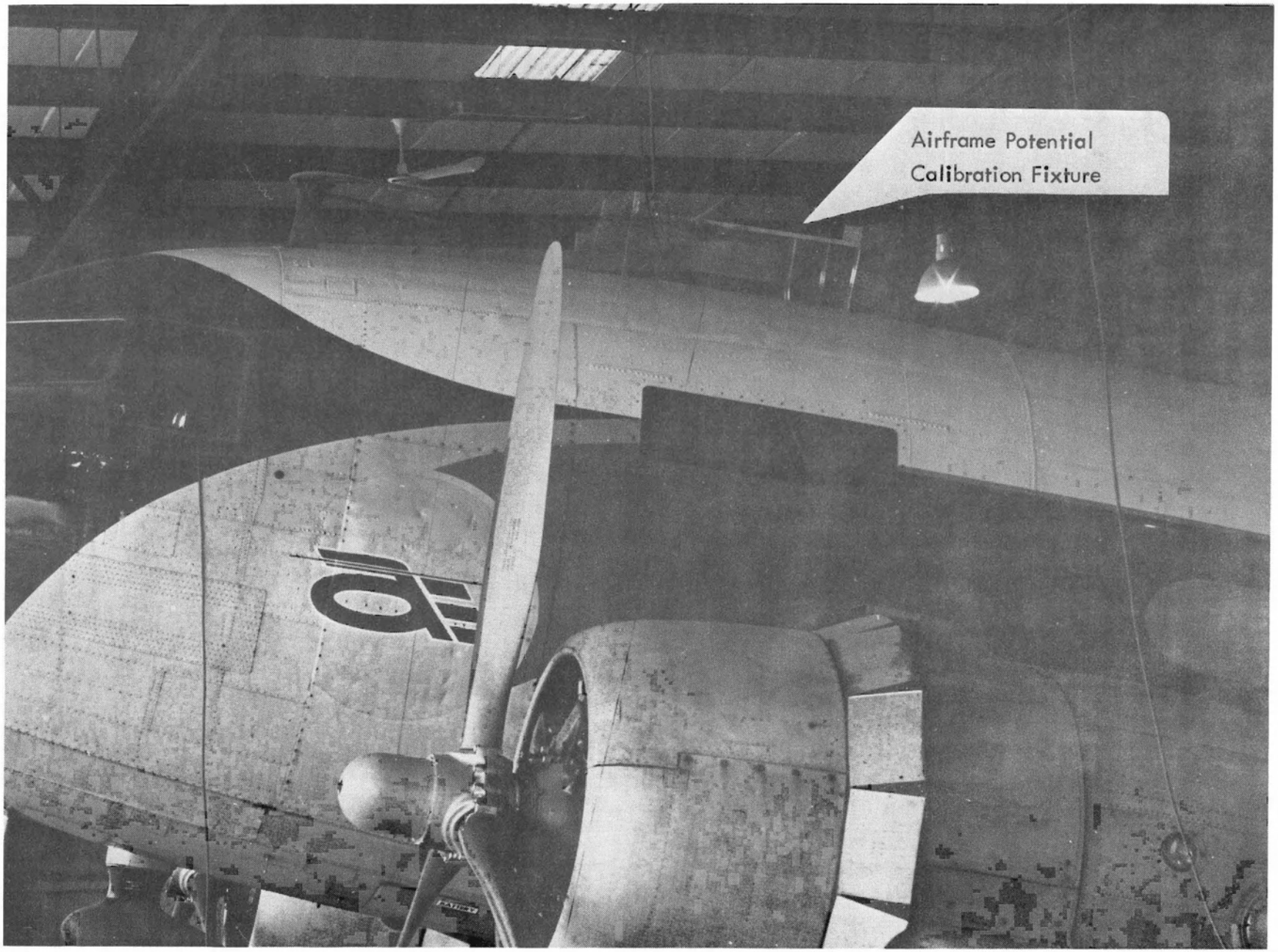

Figure 3-17. Airframe Potential Calibration Fixture.

Figure 3-18. NOISE9 29-MAY-1981
DISCHARGER= CORONA POINT
DETECTOR=CARR.,BANDWIDTH=WIDE
POSITIVE POINT CORONA

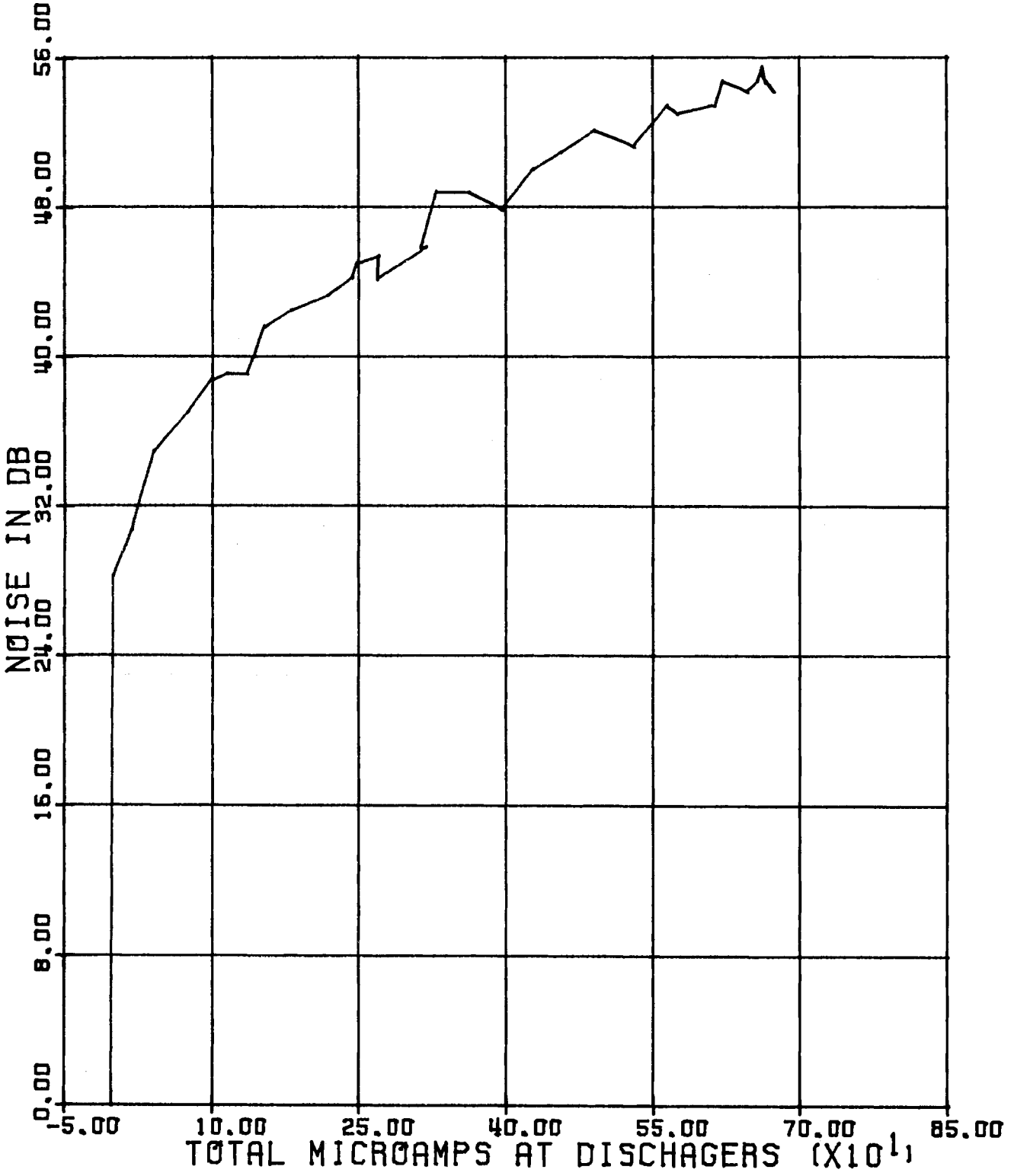

Figure 3-19. NOISE11 29-MAY-1981
DISCHARGER= DAYTON OMEGA
DETECTOR=CARR..BANDWIDTH=WIDE
POSITIVE POINT CORONA

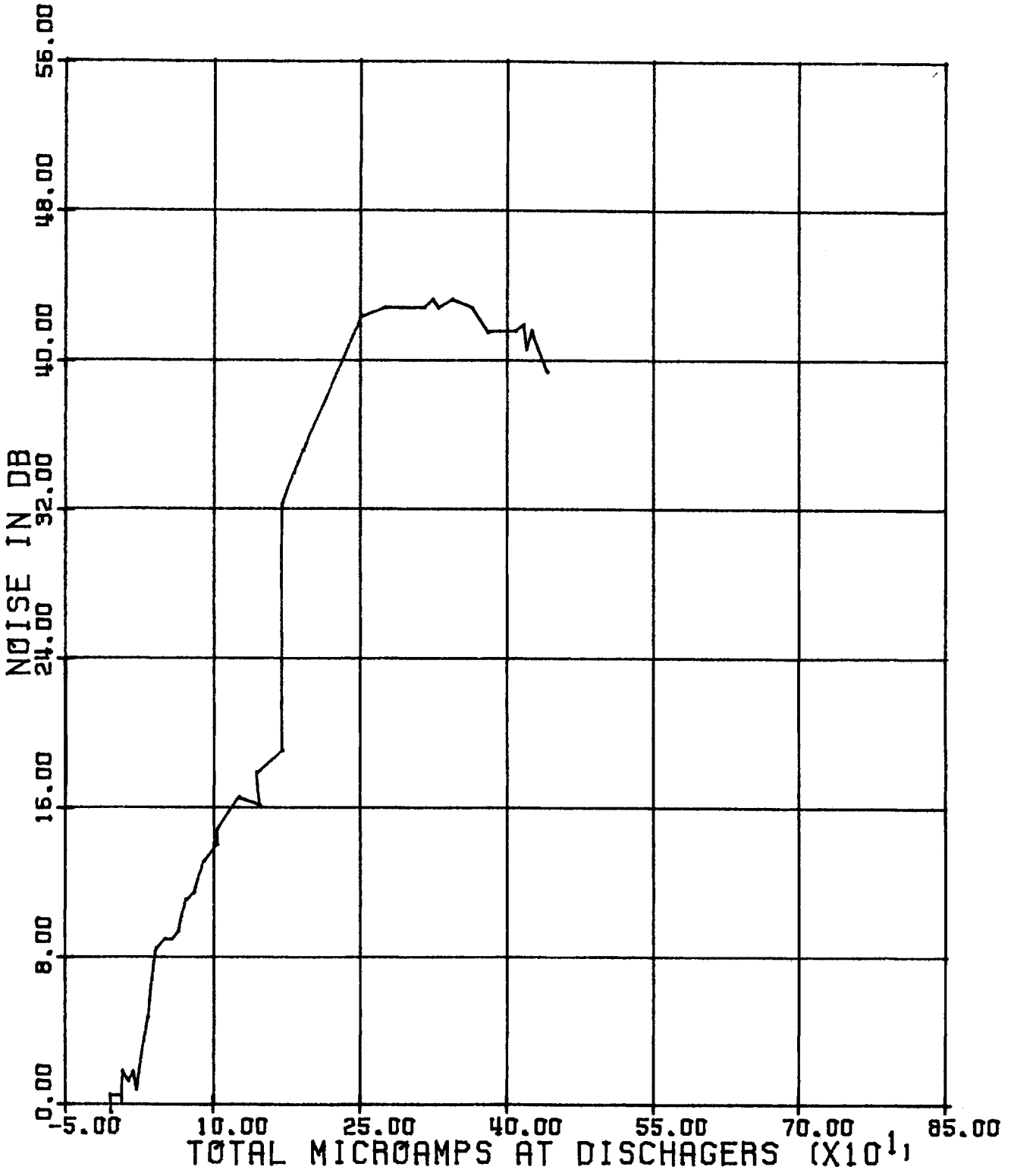

Figure 3-20. NOISE7 28-MAY-1981
DISCHARGER=TCO ESD-3
DETECTOR=CARR..BANDWIDTH=WIDE
POSITIVE POINT CORONA

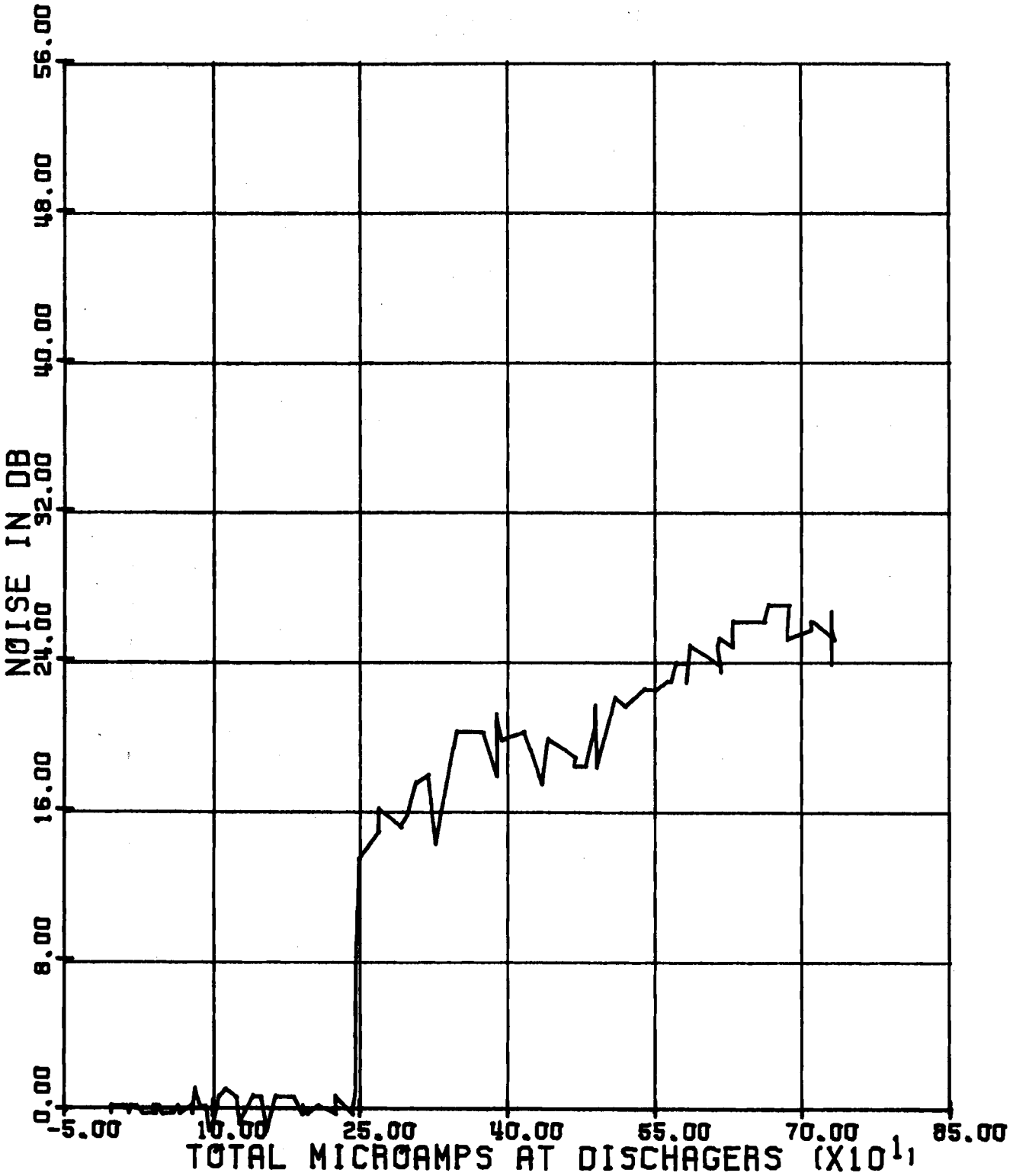

Figure 3-21. NOISE9 29-MAY-1981
DISCHARGER=CORONA POINT
DETECTOR=CARR..BANDWIDTH=WIDE
POSITIVE POINT CORONA

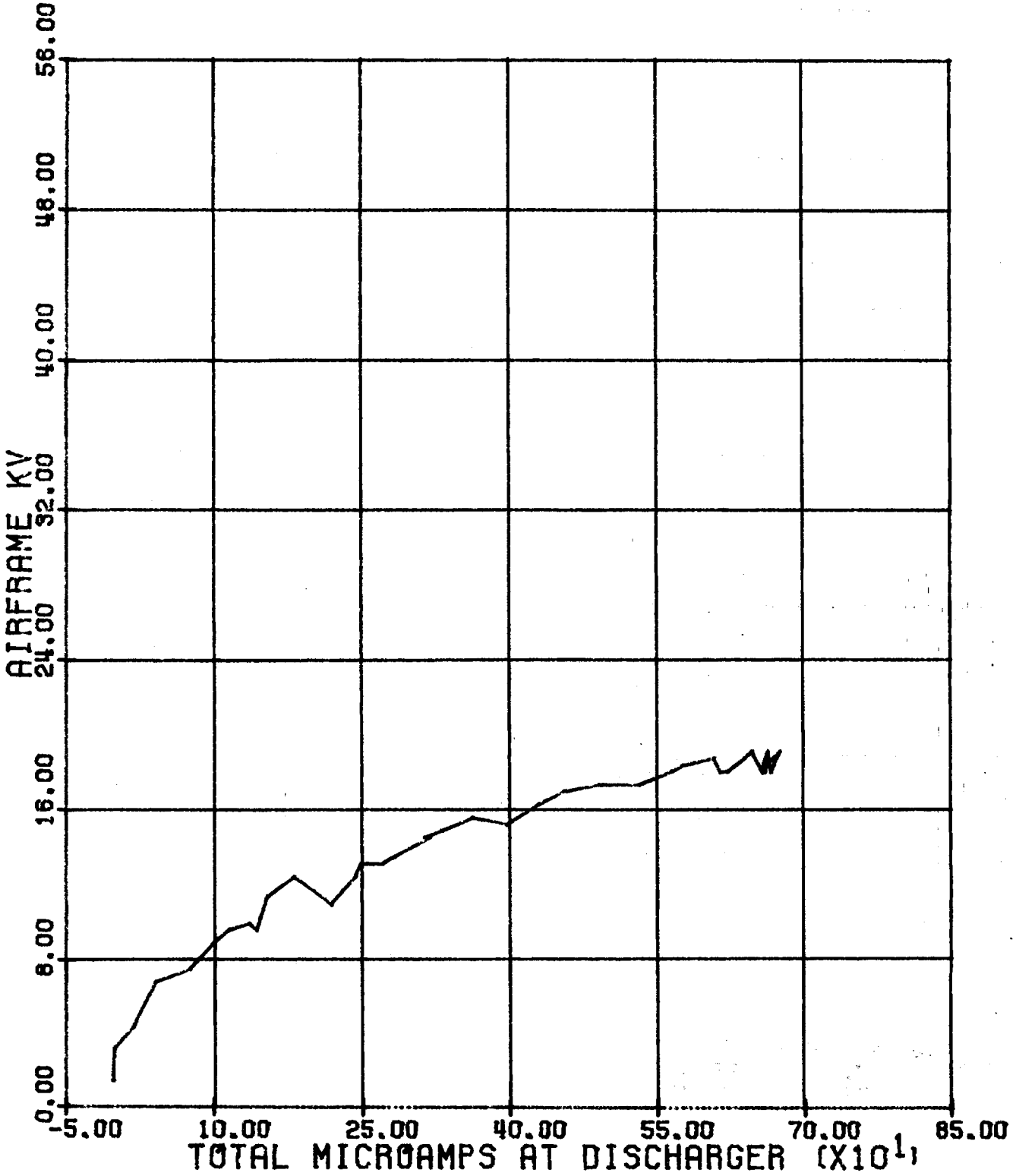

Figure 3-22. NOISE11 29-MAY-81
DISCHARGER=DAYTON OMEGA
DETECTOR=CARR.,BANDWIDTH=WIDE
POSITIVE POINT CORONA

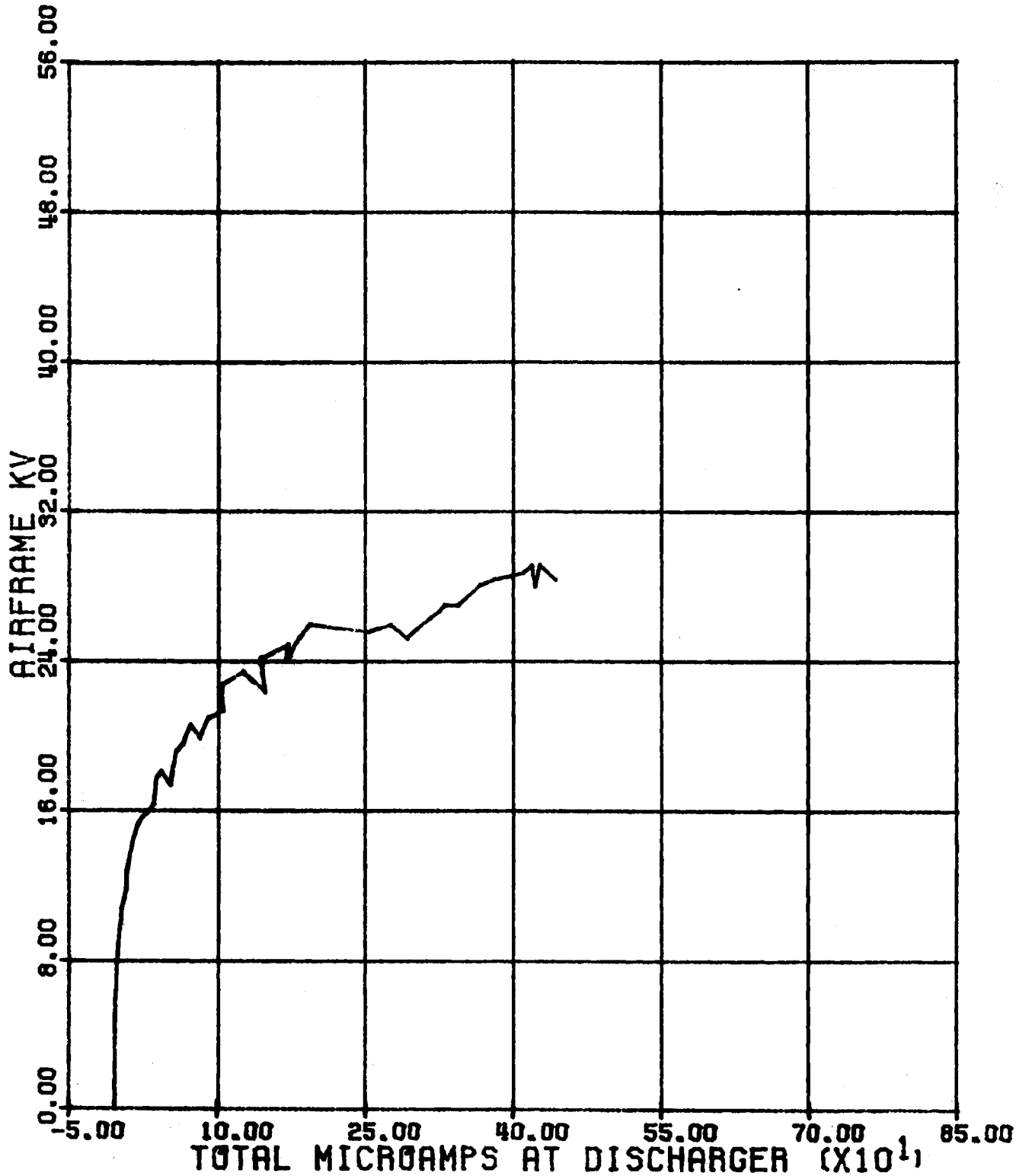

Figure 3-23. NOISE7 29-MAY-1981
DISCHARGER=TCO ESD-3
DETECTOR=CARR.,BANDWIDTH=WIDE
POSITIVE POINT CORONA

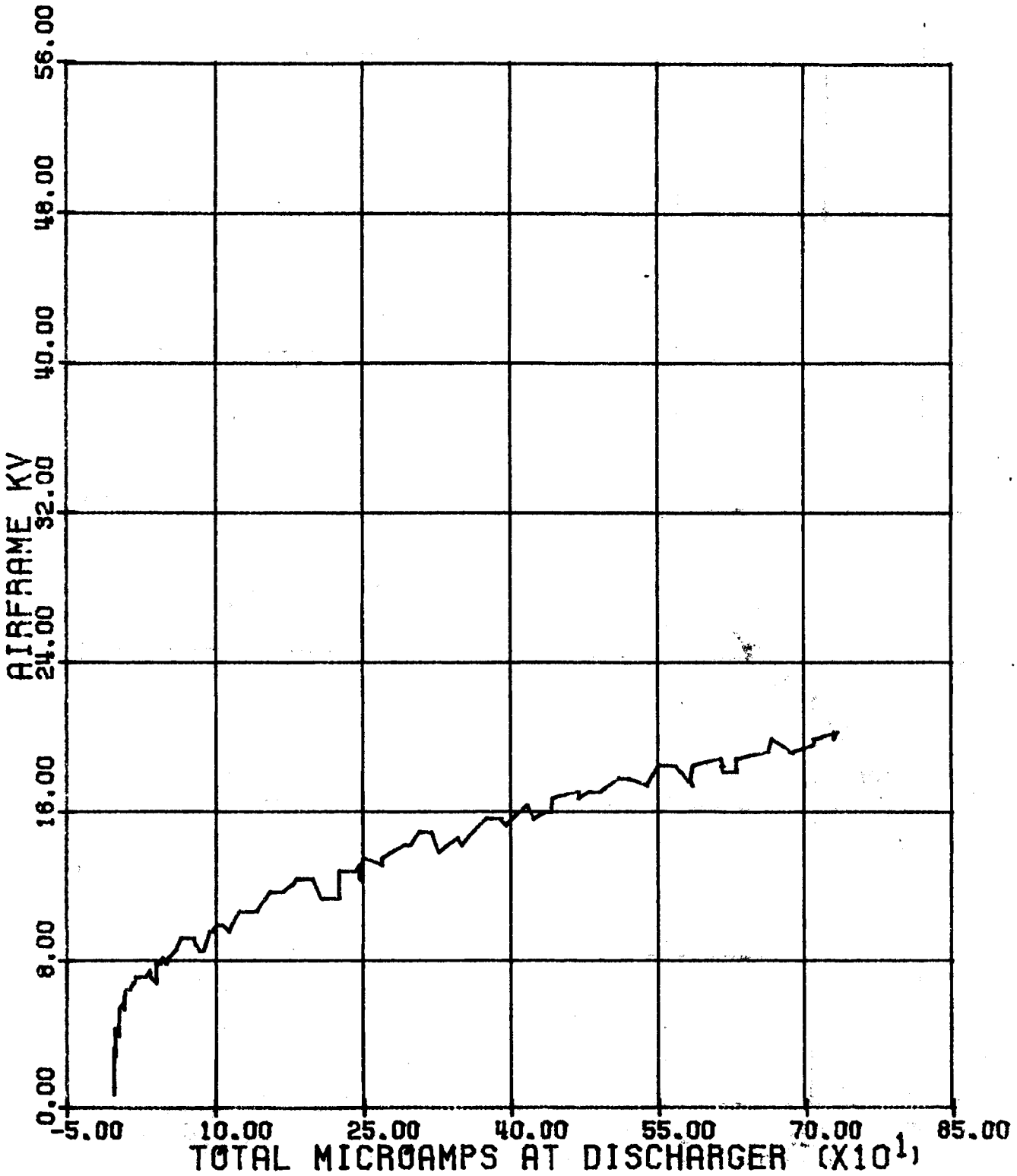

respectively, the Dayton-Granger discharger allows the airframe to charge to a higher voltage before significant discharging occurs. Actually, the corona points begin discharging at a lower airframe potential than the Dayton-Granger dischargers. The Dayton-Granger discharger does appear to be quieter in positive-point corona than the corona points for currents less than about 200 microamps, but at that point the noise level approaches that of the corona points. This indicates that the Dayton-Granger dischargers do not discharge positive-point corona as easily as negative-point corona. The TCO ESD-3 discharger also indicated this trend but not to the same degree as noted by the data plots.

3. Summary of Ground P-Static Test Results. The ground p-static testing has shown that a correlation does exist between the use of good quality static-wick dischargers and their ability to reduce the corona noise generated by p-static in the 100 Khz Loran-C frequency range. Based on the data presented here, noise reductions of more than 30 db can be effected at discharge current levels of more than 600 microamps. The ability of the dischargers to reduce the positive-point corona noise is an area where more information is needed relating to discharger design.

The test methods described in the bonding and ground p-static survey tests are extracted from test methods developed by Robert Truax of TCO Manufacturing Company, Ft. Meyers, Florida for which a patent is pending.

IV. P-STATIC FLIGHT TESTING

A. Biased Discharger Installation.

Figure 4-1 is a photograph of the biased-discharger installation on the tail of the DC-3 aircraft used in the flight tests. The biased-discharger used consists of 4 TCO ESD-3 static-wick dischargers mounted on the end of an acrylic tube approximately 30 cm. long. A high voltage cable extends from the mounting plate for the 4 ESD-3 dischargers through the tail cone up to the operators console in the aircraft. This high voltage cable was connected to a 0-80KV power supply that was used to bias the dischargers on the tail.

The instrumentation was set up to sum the currents from each of the control surfaces individually. This provided five currents to monitor from the airframe. These five included both wings, both elevators and the rudder. Other inputs for the instrumentation were the output current from the high voltage power supply driving the biased discharger, the EMC-25 noise level output and the output of the field mill on the top of the airframe. This provided eight inputs to be recorded on the data collection equipment pertaining to the noise performance of the airframe. All of the data pertaining to the airframe noise and charging measurements were recorded on the floppy disk in the Heath H-89 computer using a BASIC language program in the H-89 that digitizes through the Serial Lab Products Serial I/O unit. This equipment is described in detail in Volume II. The position information out of the TI-9900 Loran-C receiver was recorded directly on the Byte Bucket cassette tape unit. Figure 4-2 is a diagram of the instrumentation used to collect the p-static noise data in flight.

B. P-Static Flight Test Procedure.

A total of six flights were conducted making measurements using this data collection setup. Four of the flights were made around a closed course of total length of 129 nm beginning at Ohio University airport, directly to the York VOR, continuing on to the Henderson VOR then to the UNI NDB and returning to the Ohio University airport. The other two flights consisted of a roundtrip to Port Columbus Airport, a trip of 56 nm on each leg; the other trip went from UNI, directly to York VOR, directly to Henderson VOR, directly to Parkersburg Airport. This final trip length was 168 nm. These flights were conducted over a standard flight route to eliminate possible outside noise variables. The flights were conducted over high voltage power lines, and Figure 4-3 notes the most prominent lines along the routes.

In the cockpit, the pilots had access to a CDI that presents steering information from the TI-9900 Loran-C receiver. The CDI has selectable sensitivities of 0.5 nm either side to 1.25 nm either side of course. This information was constantly cross-checked using Collins 51RV4 VOR/ILS receivers and Foster 511 RNAV and was also cross-checked with TACAN, and, in all cases, the Loran C provided very accurate and consistant results during the flights.

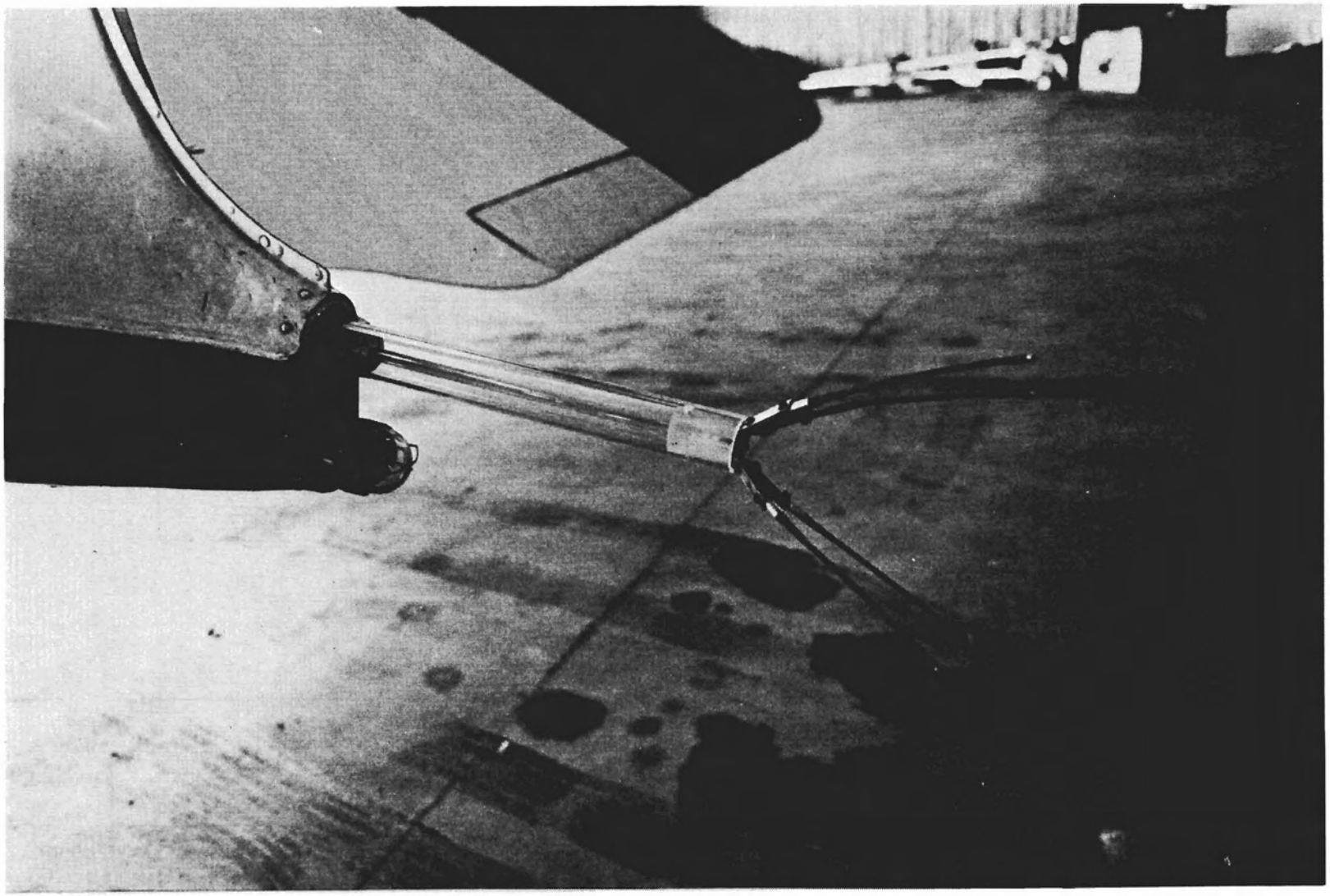

Figure 4-1. Biased Discharger on Tail of N7AP.

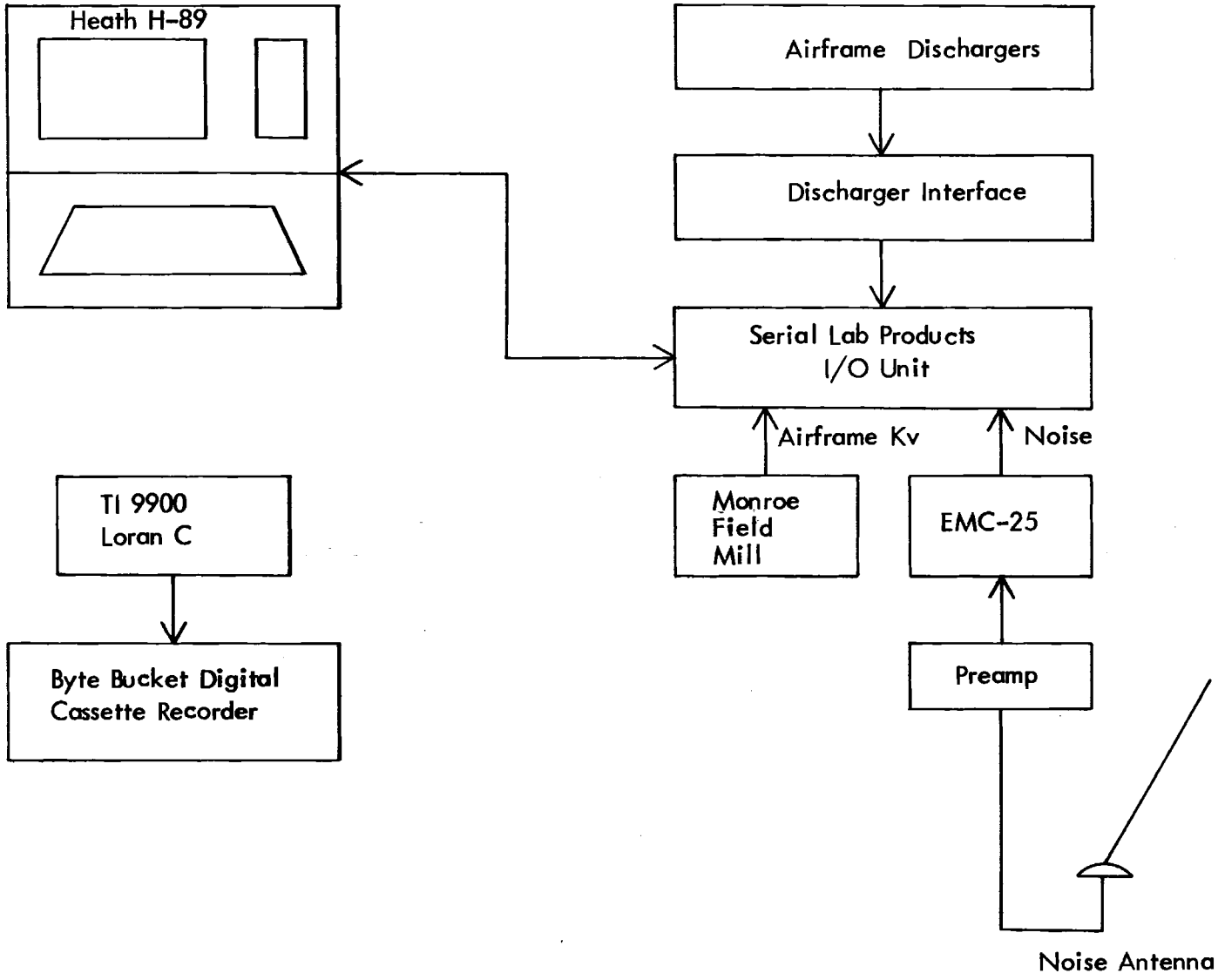

Figure 4-2. Block Diagram of Instrumentation for P-Static Flight Testing.

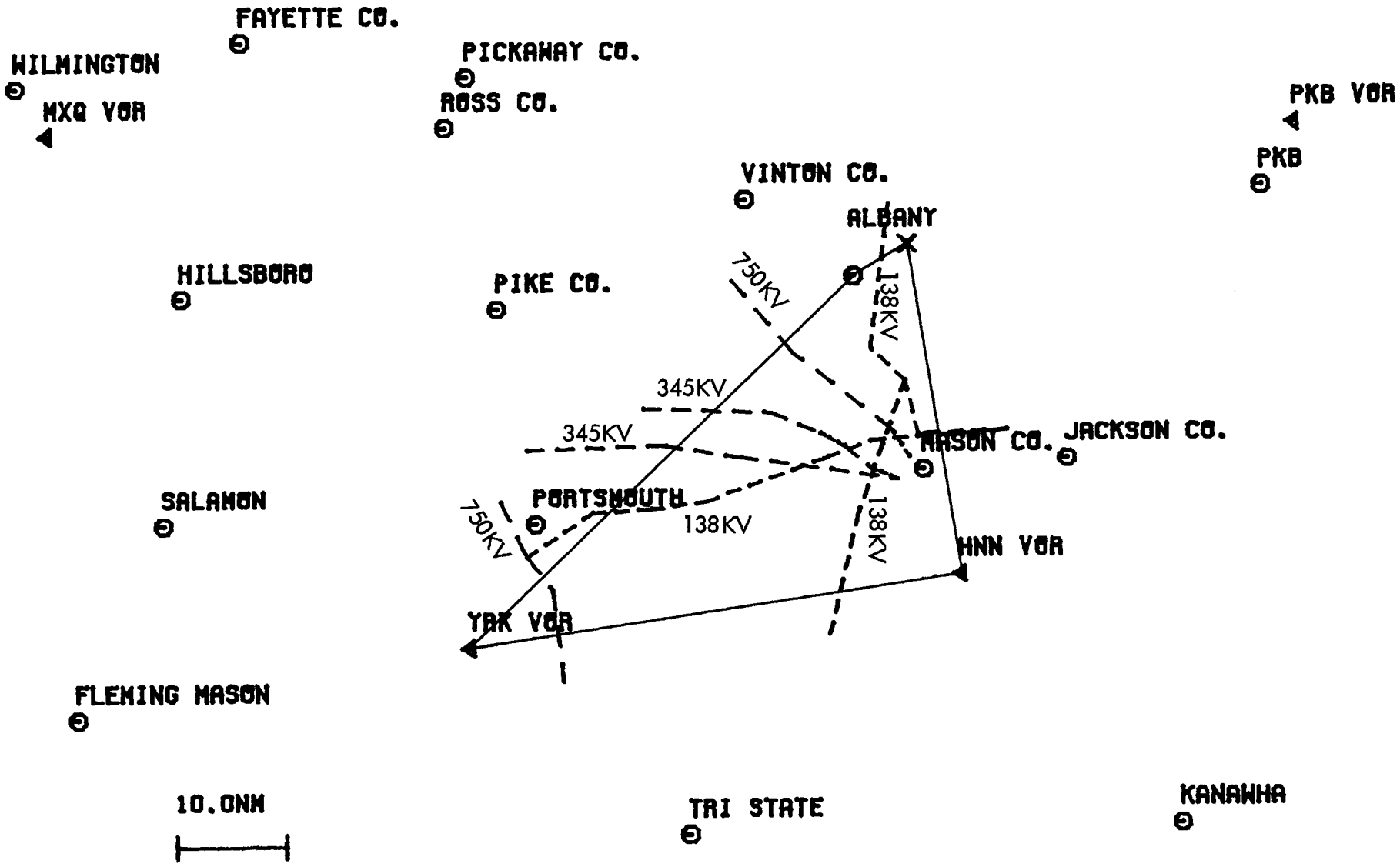

Figure 4-3.
POWER LINES IN TEST AREA

One of the flights, conducted March 11, 1982, consisted of a flight in an area of thunderstorm activity and heavy rain showers. This flight was conducted along the closed route and will be described in detail later.

There were basically five flights used to evaluate the flight noise characteristics of the three discharger types tested in the ground p-static survey, the corona points, Dayton-Granger 16375 and TCO ESD-3. Figure 4-4 is a photograph of the corona points mounted on the right elevator trailing edge. All of these flights were made using the biased-discharger to charge the airframe. Figures 4-5 to 4-8 are the recorded Loran-C ground tracks of the flights around the closed routes. Figure 4-9 is the recorded Loran-C ground track of the portion of the final flight test along the closed route. These figures are for flights conducted using the biased-discharger to charge the airframe artifically in flight. All of these flights were conducted in clear air with no spheric activity in the area. During all of these flights, the TI-9900 had no trouble with signal-to-noise problems due to the airframe charging.

The data from the dischargers and noise produced is plotted in several different forms to try to gain a picture of the total effects of the discharging current, the noise produced and any airframe charging effects. This data was also plotted to try to determine if any location-related noise effects were producing any masking results.

Before the flight data results can be described, a few words about the procedure followed during the flights is in order. For all of the flights, during takeoff only the TI-9900 Loran-C receiver and the Byte Bucket digital cassette recorder were operating. After takeoff, the remaining equipment was powered up and the data collection was begun. The biased-discharger data was taken during the flight while using the displayed data on the H-89 computer as a reference. Each time a line of data was taken it was displayed on the computer along with a count of the line number. Using this line number, the power supply was increased 5 kv every 10 lines starting at 0 kv and going to 65 kv. At the end of the ten lines at 65 kv, the supply was turned off and another ten lines were taken, then the software data collection was stopped. This data collection method was performed three times during the closed course flights. Volume II provides more detail on the specifics of the data recorded during each flight. In order to correlate the data from the dischargers and the TI-9900, the discharger data collection software prompted the operator to enter the time which was available as an output on the TI-9900 display as well as recorded with each data point recorded on the digital cassette tape. This time information provided correlation to an accuracy of 15 seconds or better. The discharger data collection software produced a record of data every 6.5 seconds. The TI-9900 produced a recorded data position every 14.7 seconds.

The Loran-C plots were obtained with the TI-9900 using the 9960 GRI northeast Loran-C chain tracking Seneca, N.Y. - Carolina Beach, N.C. (M-Y) and Seneca, N.Y. - Dana, In. (M-Z) pairs with no TD corrections made.

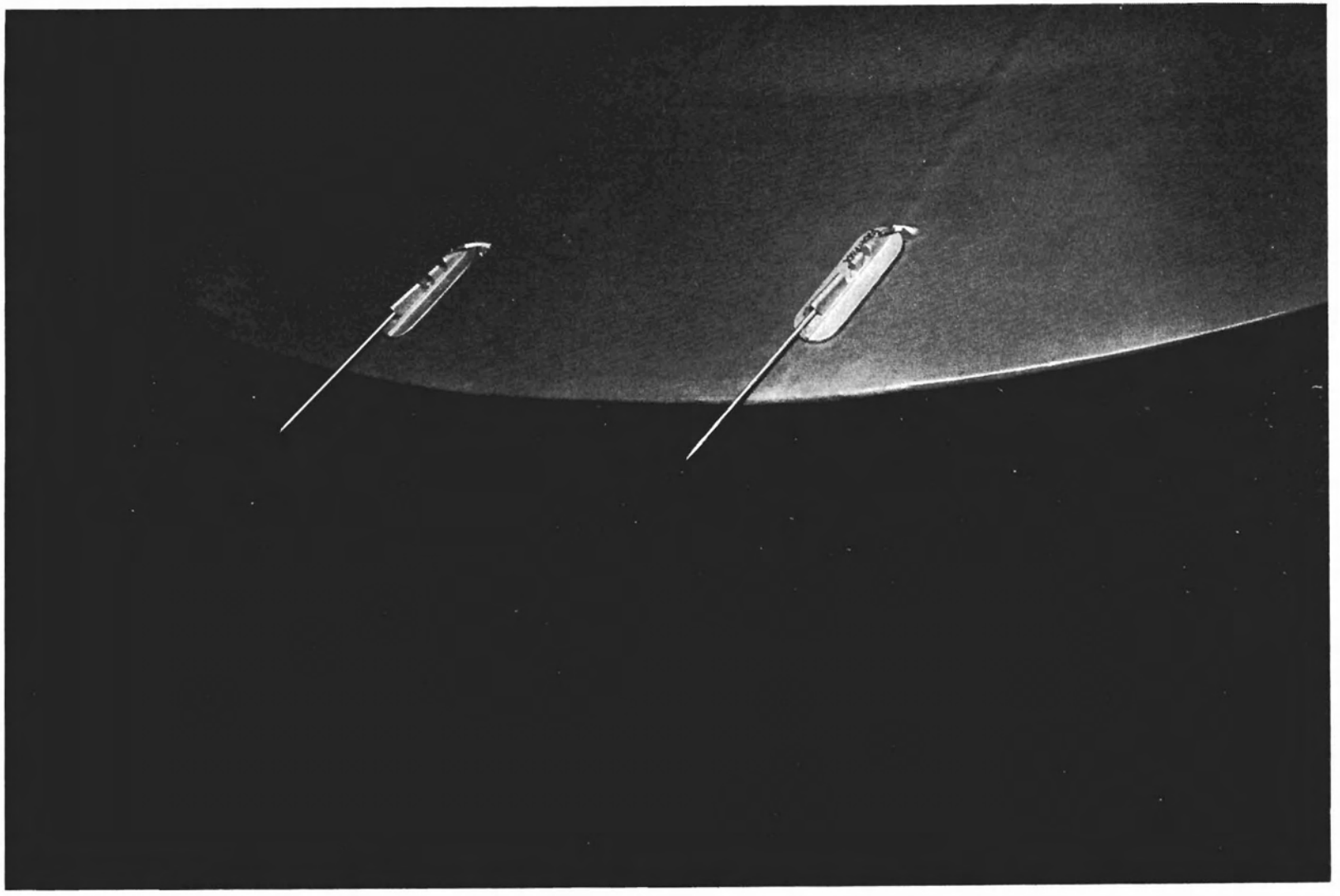

Figure 4-4. Corona Points on Right Elevator of N7AP.

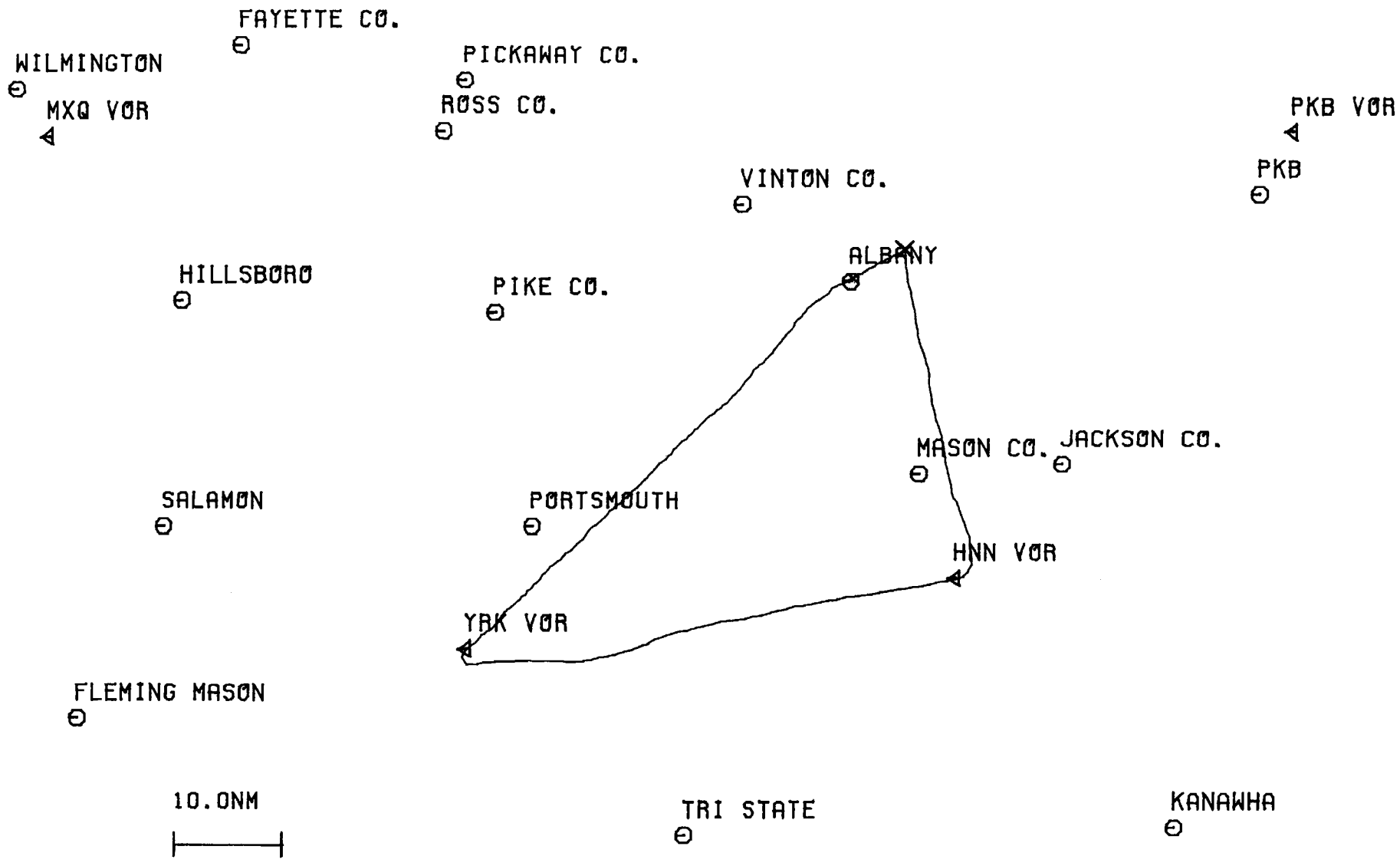

Figure 4-5. Biased Discharger Flight, TCO DD1, March 2, 1982, UNI to YRK to HNN to UNI NDB.

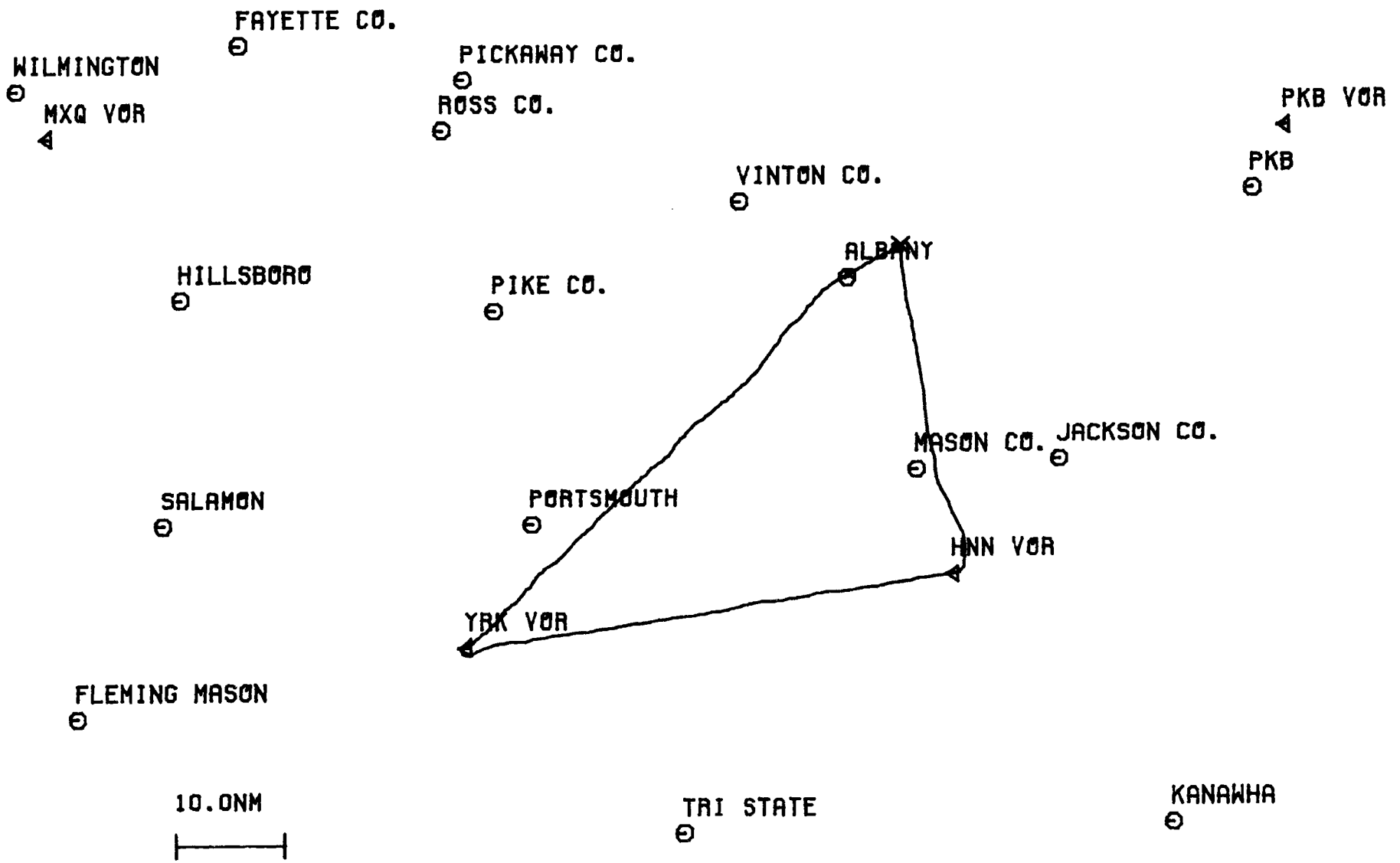

Figure 4-6. Bias Discharger Flight, Corona Points, March 10, 1982, UNI to YRK to HNN to UNI NDB.

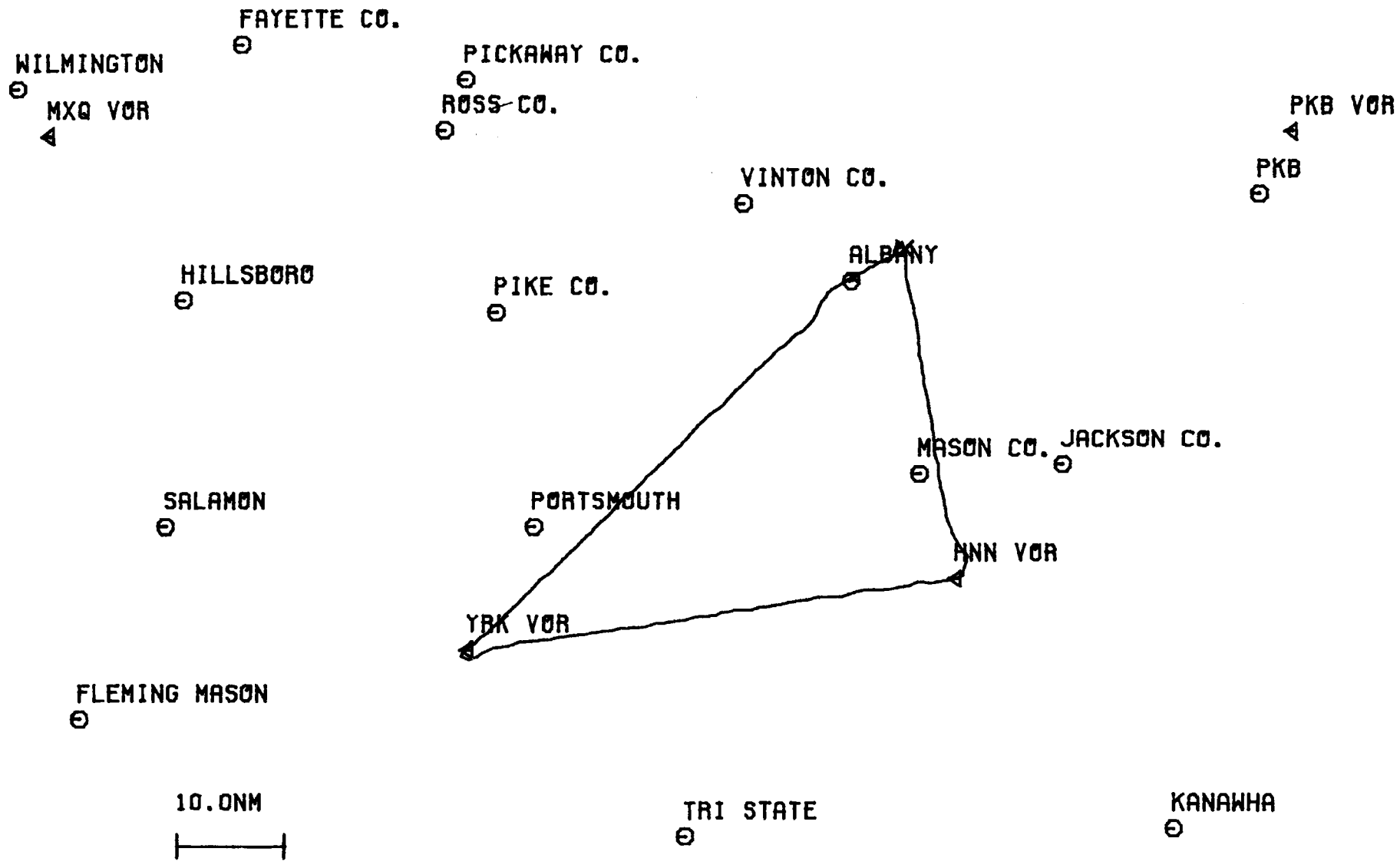

Figure 4-7. Bias Discharger Flight, Dayton Granger, March 18, 1982
UNI to YRK to HNN to UNI NDB.

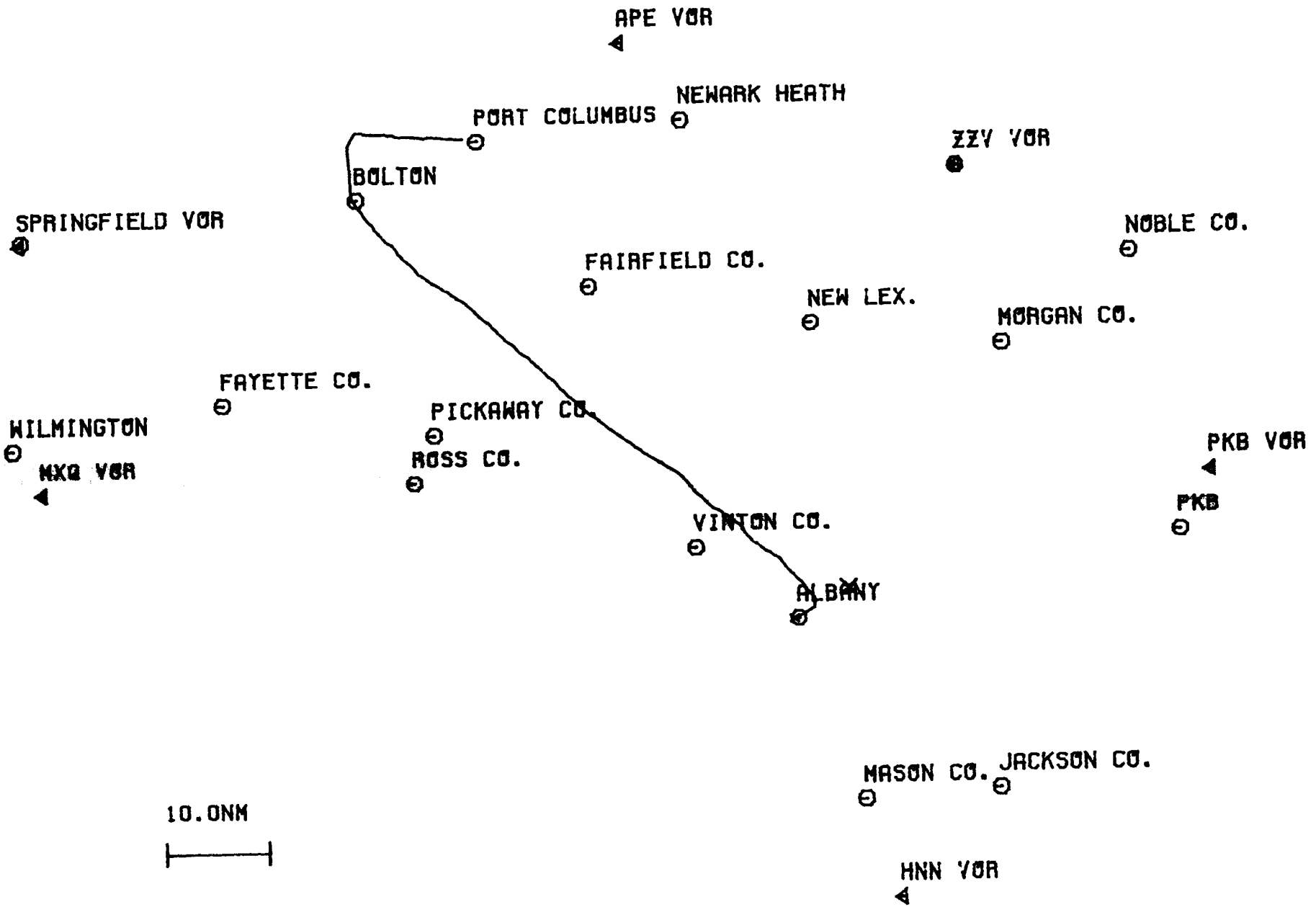

Figure 4-8. Biased Discharger Flight, TCO DD1, March 19, 1982, UNI to CMH.

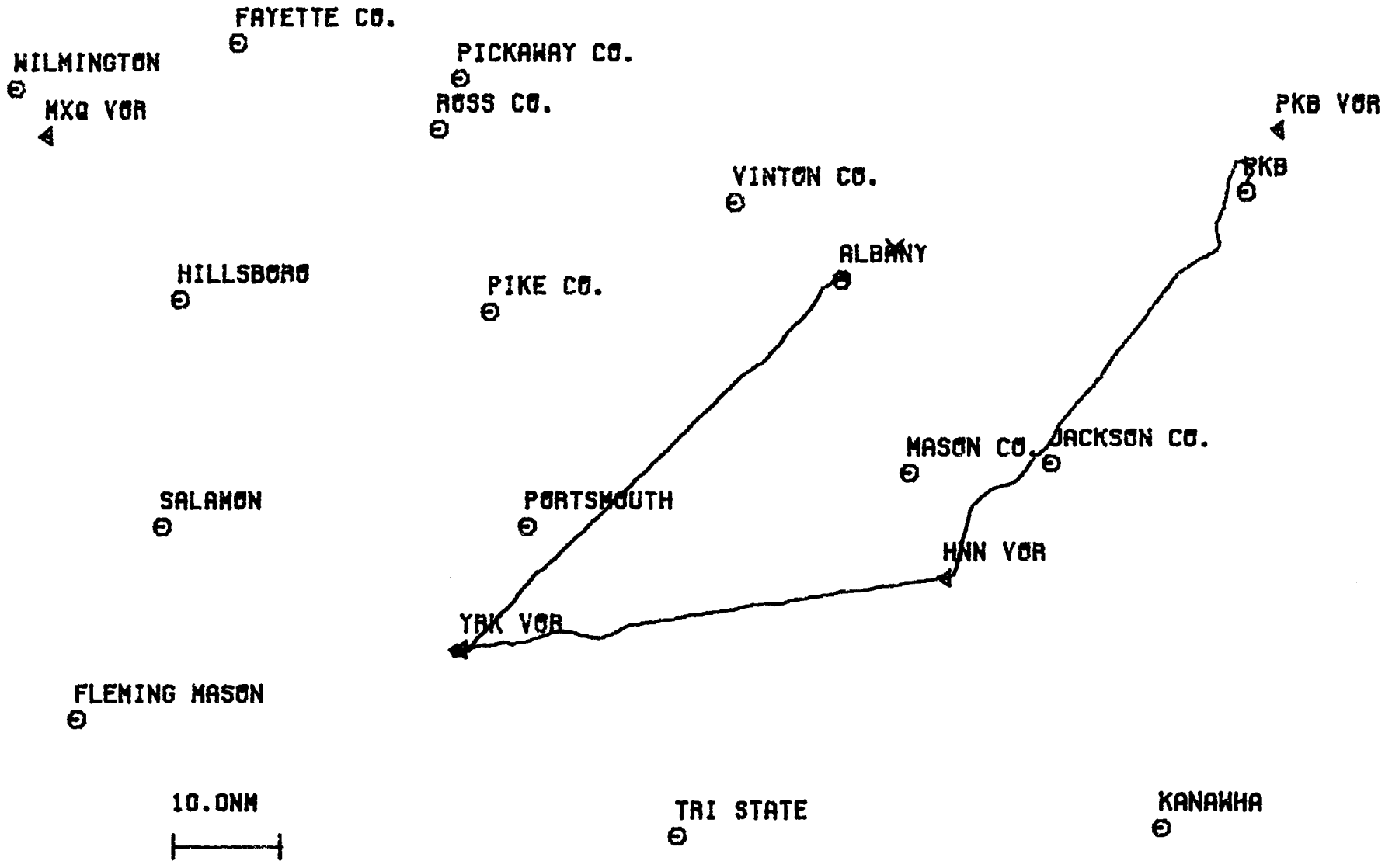

Figure 4-9. Biased Discharge Flight, TCO DD1, March 29, 1982, UNI to PKB.

C. P-Static Flight Test Results.

The graphic output data of the biased discharger airframe charging in flight is described in the following manner. The results will be discussed first by describing the plots of the corona points as dischargers. Each of the individual flight tests is plotted five different ways as follows.

1. Noise vs. Total Discharger Current
2. Airframe KV vs. Total Discharger Current
3. Noise vs. Time of Flight
4. Airframe KV vs. Time of Flight
5. Total Discharger Current vs. Time of Flight

The first two plots named above were similar to the plots produced for the ground p-static survey except that in the plots presented here the data points were plotted individually and not connected as in a time sequence plot. This was done so that the density of point plotting is easily discernable without the clutter of the connecting lines between plot points. Since the recorded data were collected in time sequence fashion, the last three plots named above provide useful information to relate the discharger current, airframe KV and noise to each other without undue complications.

1. Biased Discharger Flights Using Corona Points. Figure 4-10 is the plot of noise vs. current, and Figure 4-11 is the plot for airframe KV vs. current for the biased-discharger airframe charging with the corona points. Since there are three sets of plots for each of these graphs, for the ease of readability, only one of the three sets will be presented in the text. All of the plots will be included in Volume II. Note that in Figure 4-10 there is a definite trend toward increased noise for an increase in discharger current, but due to the limitation on the high voltage power supply the discharge current is limited. Relating this to the ground p-static testing, Figure 4-10 only represents a small portion of Figure 3-18 described earlier in the ground p-static test data. The noise rise indicated in Figure 4-10 is approximately 8 db for a maximum discharger current of about 50 microamps. This does indicate that, based on the data plotted in the ground p-static tests, the noise with corona points does build up quickly. This initial slope, as observed in the ground p-static testing, is not linear and begins to decrease with increasing noise.

Figures 4-12 to 4-14 are the plots of the variables; discharger current, noise, and airframe KV vs. time for the corona points using the biased-discharger to charge the airframe. The effect of the biased-discharger is shown in Figure 4-12, the noise vs. time plot. It can be seen that there indeed is a correlation between noise and discharger wick currents as was expected based on the ground p-static testing. Figure 4-13 is the current vs. time plot for the corona point which indicates that about 390 seconds into the plot, the airframe began to discharge current. Relating this to Figure 4-15 this corresponds to a biased-discharger voltage of 30 KV. Also note that the discharge current off of the airframe

Figure 4-10.

FILE NAME BIAS FLMAR10B
DATE 10-MAR-82 BIASED DISCHARGER
RUN 2 CORONA PTS
DETECTOR CARR BANDWIDTH WB
TIME 09:55

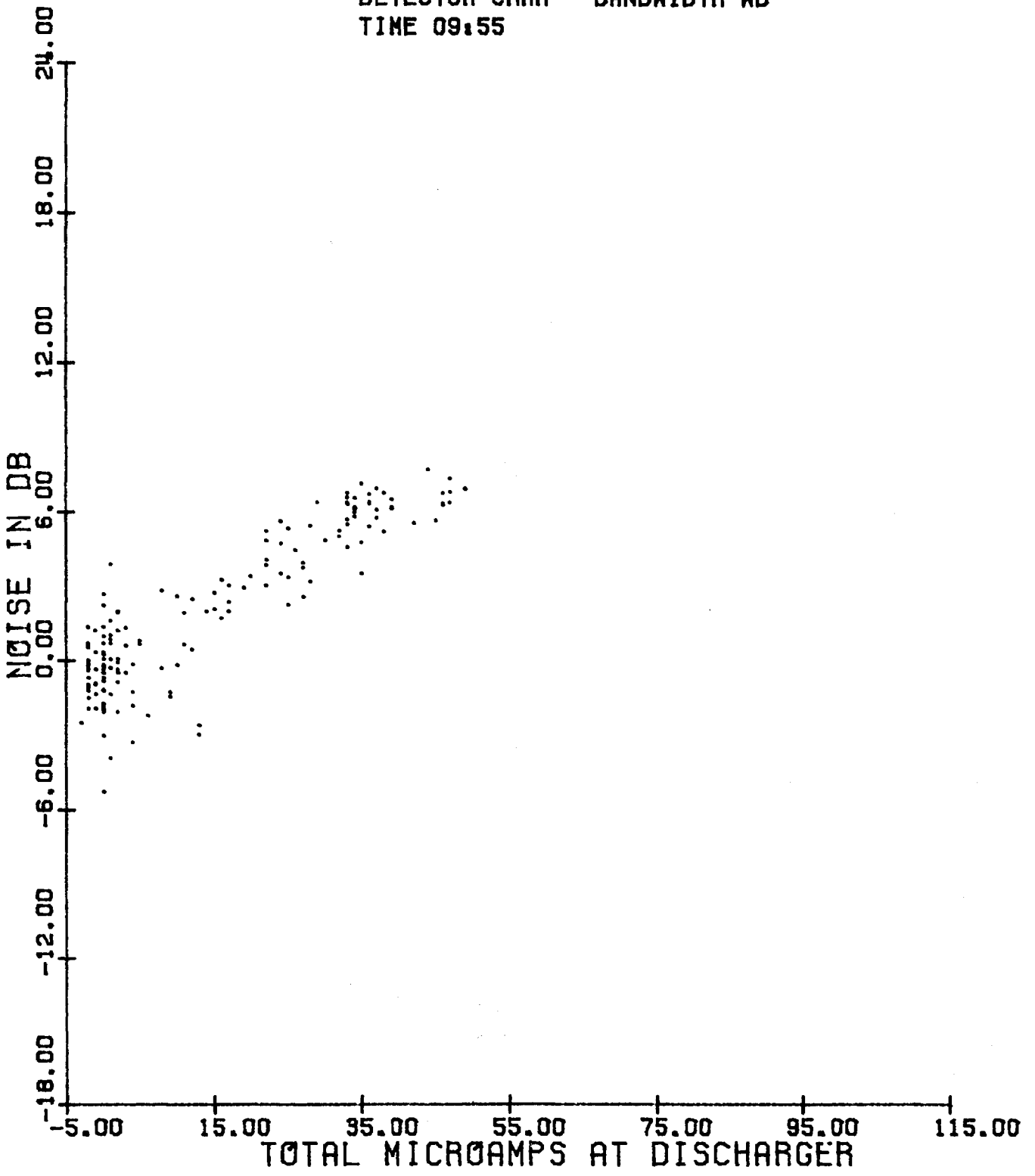

Figure 4-11.

FILE NAME BIAS FLMAR10B
DATE 10-MAR-82 BIASED DISCHARGER
RUN 2 CORONA PTS
DETECTOR CARR BANDWIDTH WB
TIME 09:55

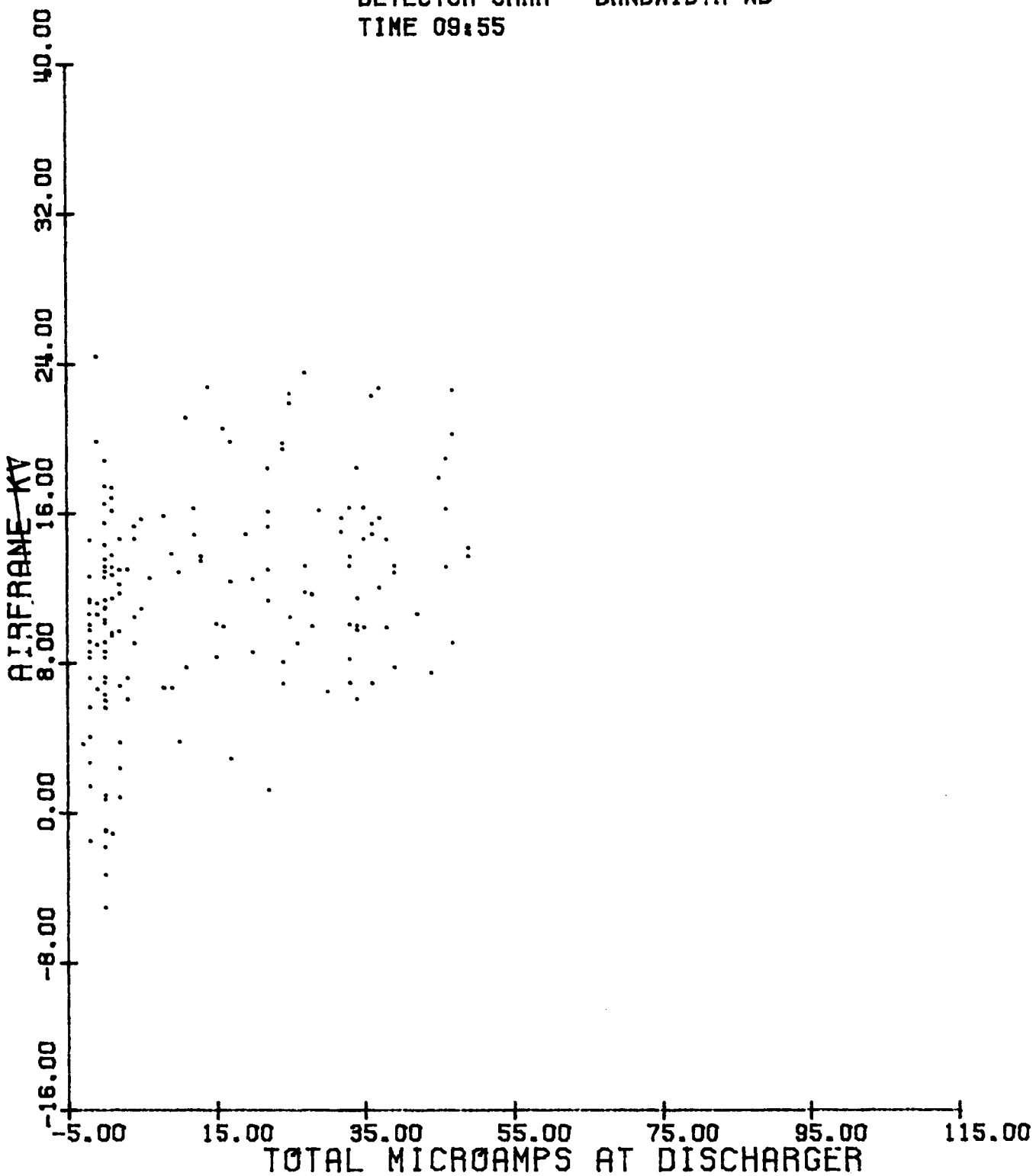

Figure 4-12.

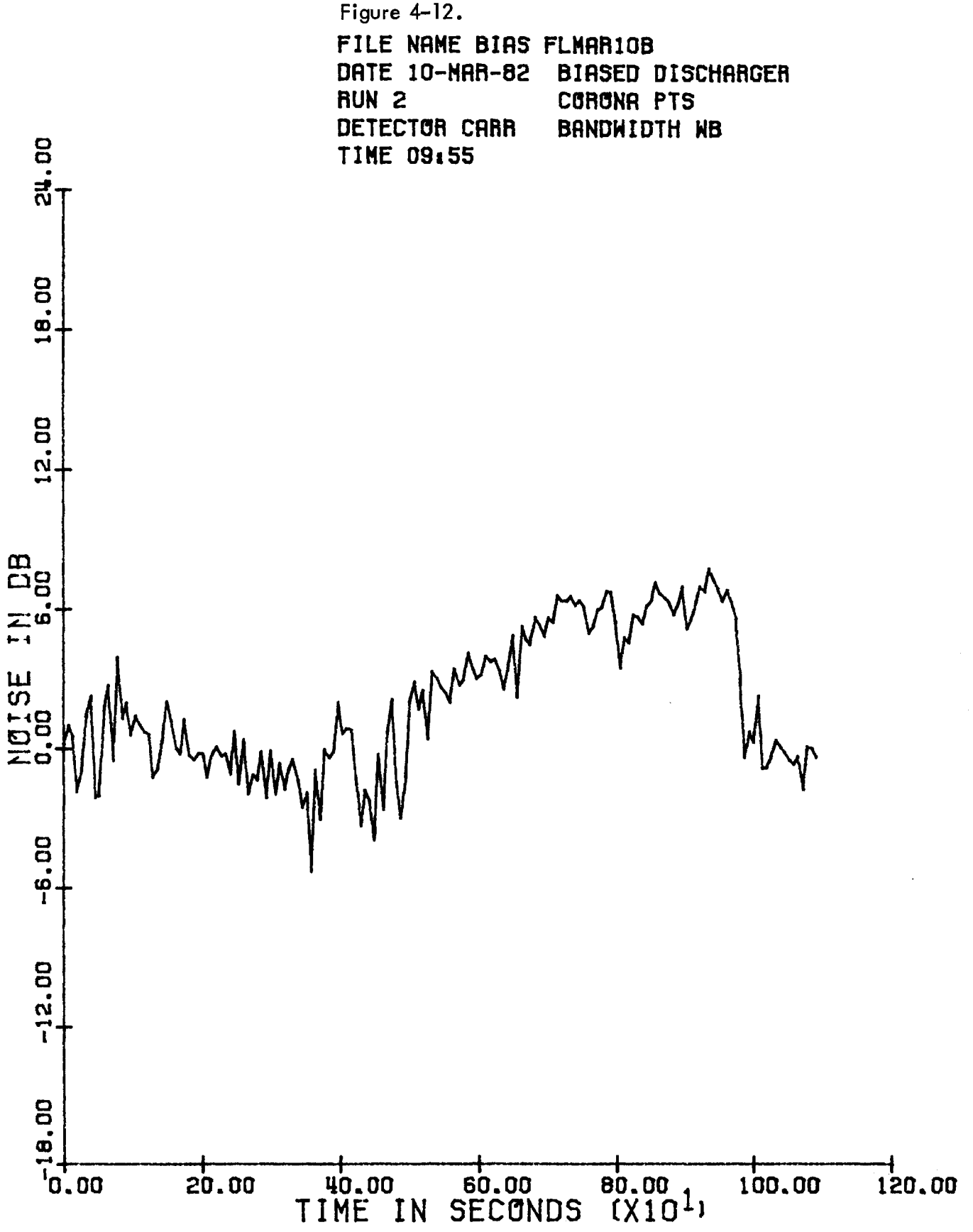
FILE NAME BIAS FLMAR10B
DATE 10-MAR-82 BIASED DISCHARGER
RUN 2 CORONA PTS
DETECTOR CARR BANDWIDTH WB
TIME 09:55
NOISE IN DB
24.00
18.00
12.00
6.00
0.00
-6.00
-12.00
-18.00
0.00
20.00
40.00
60.00
80.00
100.00
120.00
TIME IN SECONDS (X10^1)

Figure 4-13.

FILE NAME BIAS FLMAR10B
DATE 10-MAR-82 BIASED DISCHARGER
RUN 2 CORONA PTS
DETECTOR CARR BANDWIDTH WB
TIME 09:55

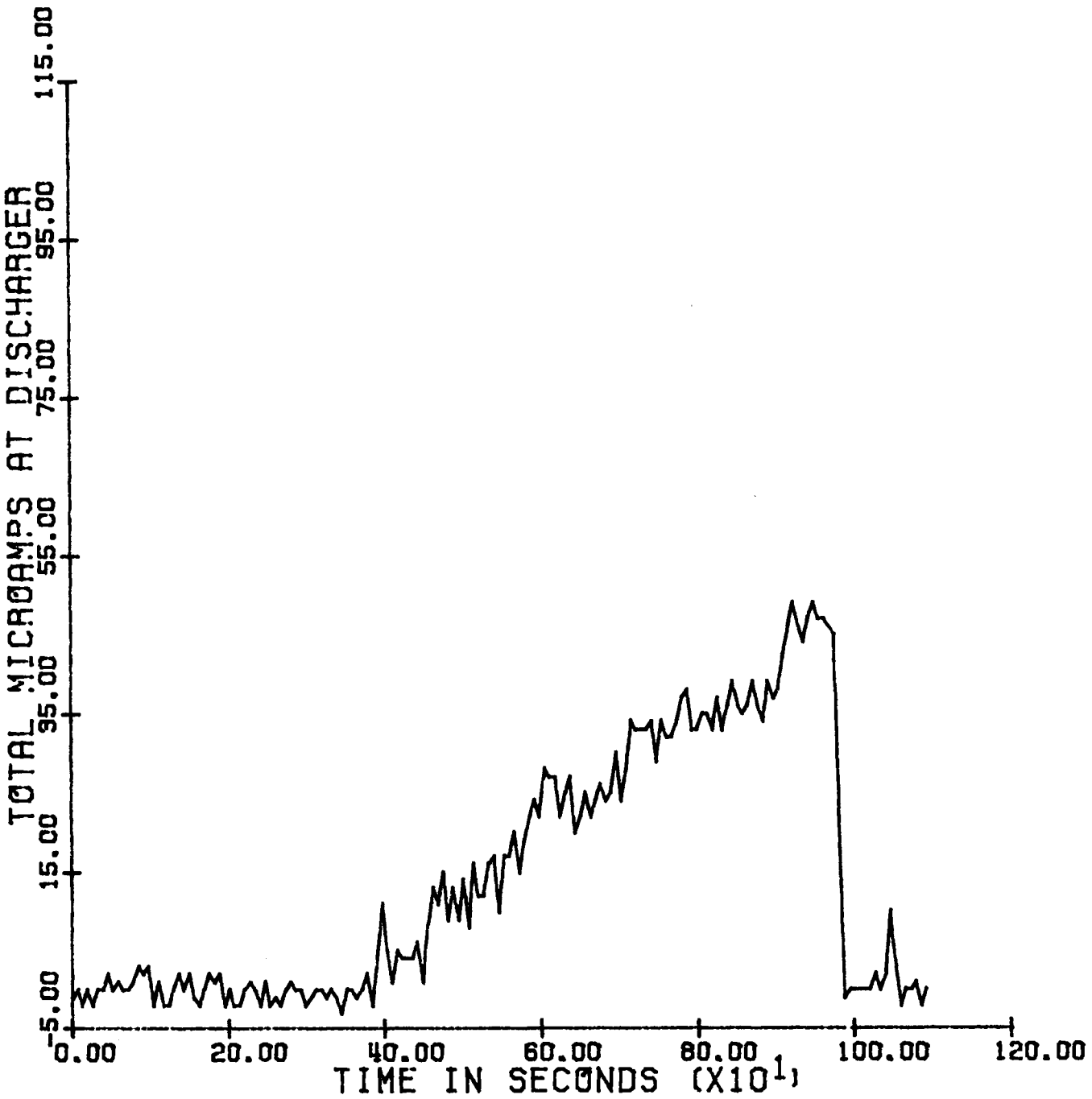

Figure 4-14.

FILE NAME BIAS FLMAR10B
DATE 10-MAR-82 BIASED DISCHARGER
RUN 2 CORONA PTS
DETECTOR CARR BANDWIDTH WB
TIME 09:55

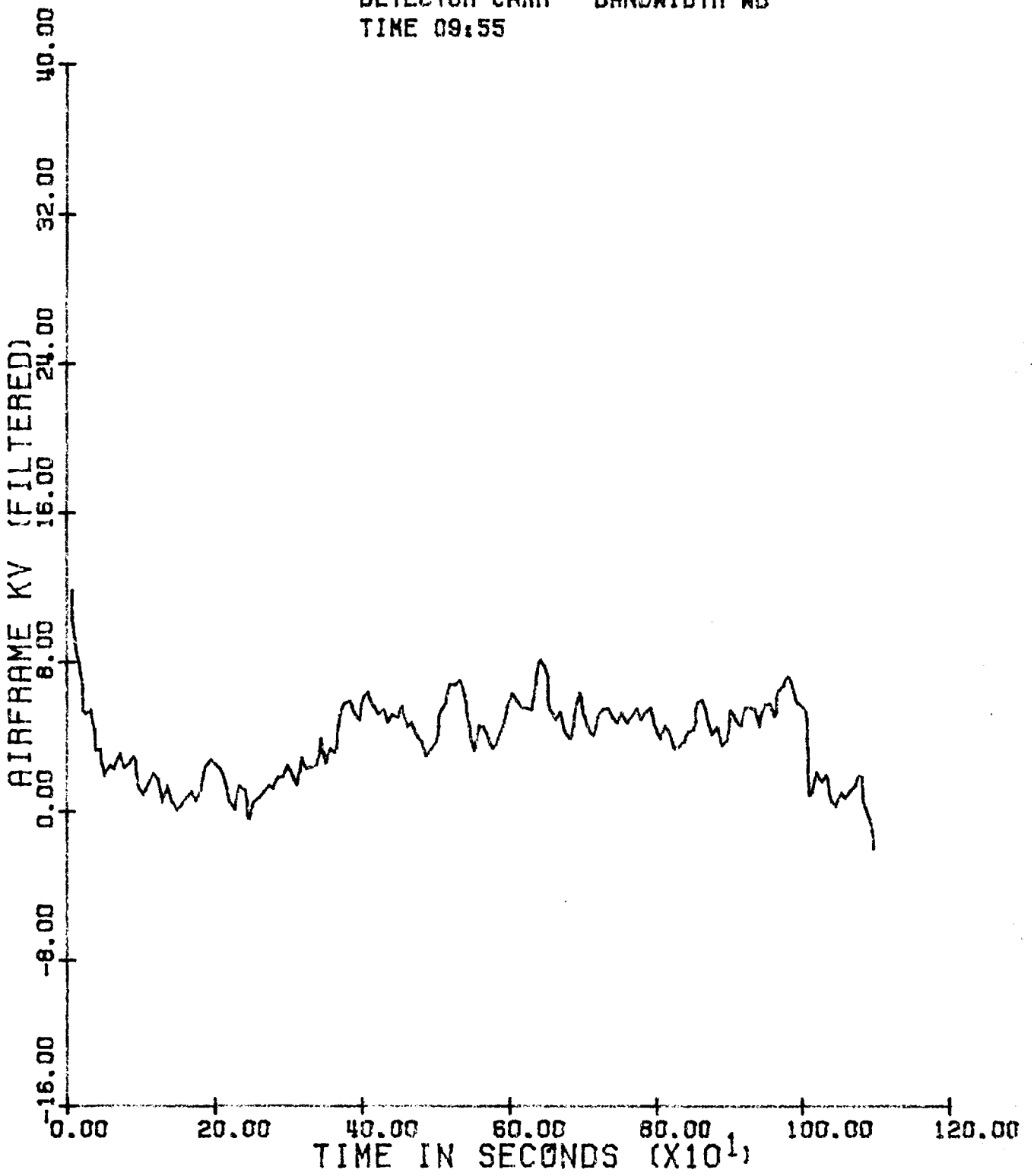

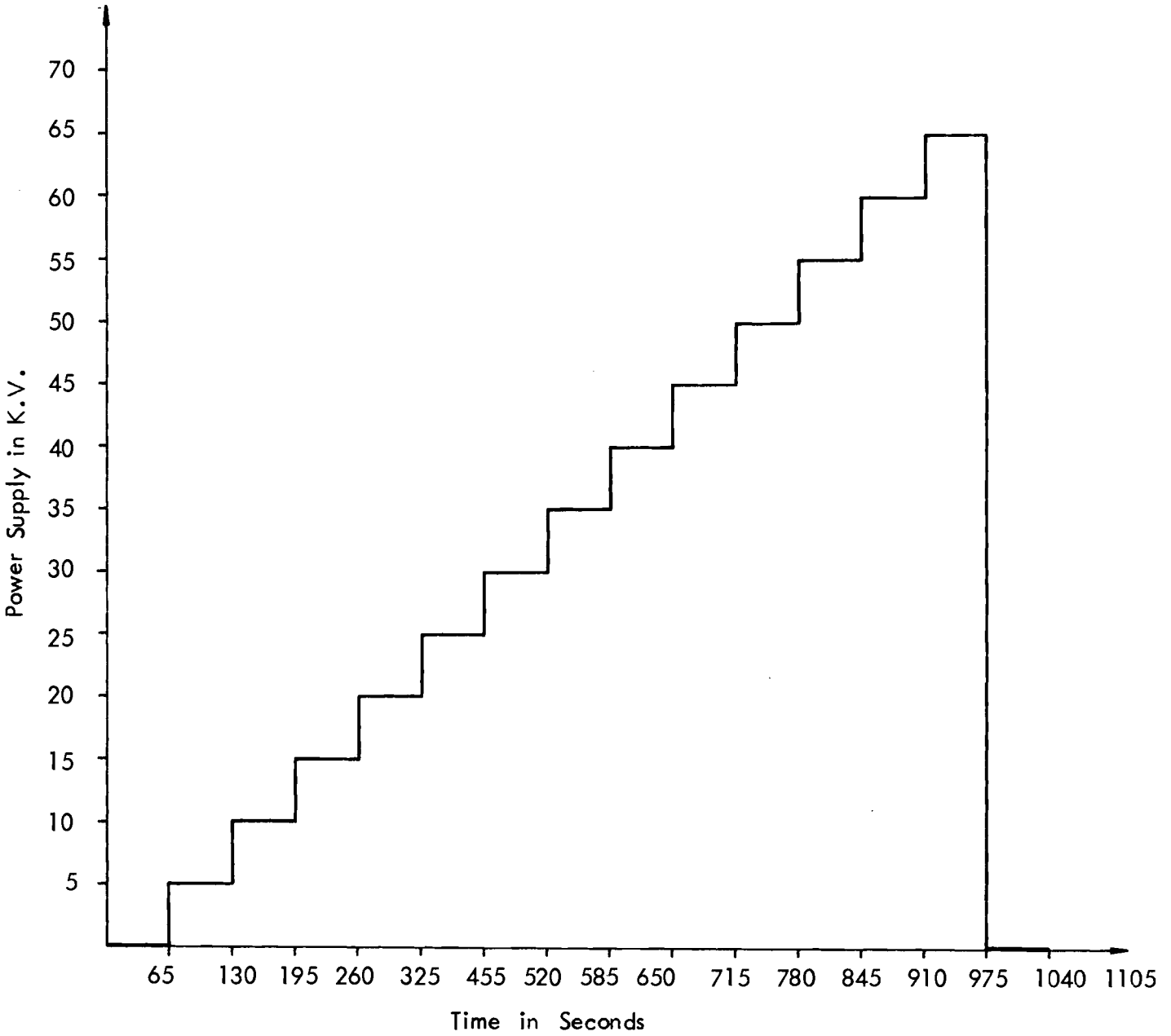

Figure 4-15. Biased Discharger Power Supply vs. Time.

appears to be linear as a function of biased-discharger voltage at least for this range. The sudden drop in the plot of Figure 4-13 at 980 seconds is due to turning the biased-discharger supply off which corresponds to the step to 0 KV shown at 975 seconds in Figure 4-15. Figure 4-14, which is a plot of the high voltage vs. time for the biased-discharger, indicates the transfer function between the input and the output response of the airframe to the biased discharger stimulus. Note in Figure 4-14 that the airframe potential begins to increase about the 300 second-point which corresponds to a biased-discharger voltage of approximately 25 KV. The roughness of the airframe KV measurements is believed due to the type of transducer used for the field mill measurements. This field mill sensor uses a vibrating diaphram behind an aperture looking through the aircraft skin on the top of the airframe. Some of the rough output data are thought due to the airstream as it flowed past the aperture causing dynamic pressures on the diaphram which tends to cause errors in the readings. Even with this condition the increased trend in potential can be observed in the plot of this data. For the KV plots indicated here, the data was smoothed analytically.

The data presented above are for the corona points which were used to represent the worst case data for the evaluation. Only one set of the three sets of data is presented here with the text, the other two sets of plots are presented in Volume II for completeness. This is done for the sake of readability.

2. Biased-Discharger Flights Using Dayton-Granger 16375. Figures 4-16 to 4-20 are the plots of the biased-discharger data for the flights using the Dayton-Granger model 16375 static-wick dischargers. These plots are of the same scale as the plots made using the corona points so that comparisons can easily be made. Figures 4-16 and 4-17 are the plots of noise vs. current and airframe KV vs. current, respectively. Comparing Figure 4-13 with Figure 4-18 the noise has stayed fairly level as compared with the noise increase using the corona points. This is what is expected since the Dayton-Granger dischargers are fairly quiet. Also note that the total discharger current is not as high as the current levels obtainable using the corona points. This would indicate a higher discharger threshold for these dischargers but the noise levels are still low. A reduction of 5 db is indicated using the Dayton-Granger dischargers at equivalent current levels compared to the noise output of the corona points. Therefore, it can be seen that even for the small charging currents represented here, almost a 2:1 reduction of noise level was achieved by using a good static-wick discharger. As will be seen later, a similar reduction in noise can be achieved using the TCO manufacturing ESD-3 or DD1 static-wick dischargers.

Figures 4-18 to 4-20 are the plots of the noise, current and airframe KV vs. time. These plots again indicate the performance of the dischargers as a function of the biased-discharger potential. It can be seen that the average noise level was fairly constant as compared with the same plots for the corona points. Also, note that the airframe potential was higher with the Dayton dischargers than with the corona points as dischargers. The corona points indicated by Figure 4-14 show that a

Figure 4-16.

FILE NAME BIAS FLMAR18C
DATE 18-MAR-82 BIASED DISCHARGER
RUN 3 DAYTON GRANGER
DETECTOR CARR BANDWIDTH WB
TIME 14:51

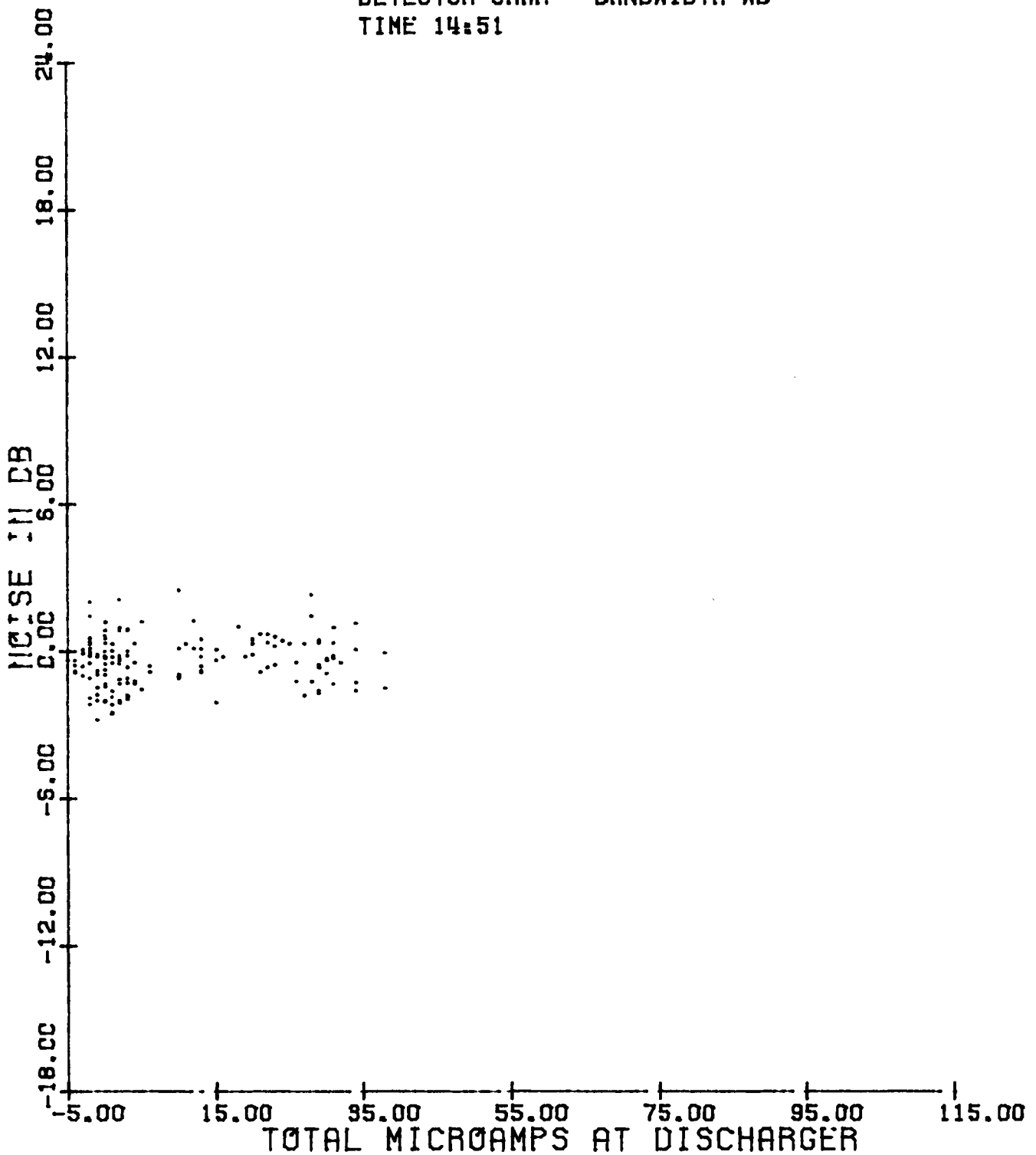

Figure 4-17.

FILE NAME BIAS FLMAR18C
DATE 18-MAR-82 BIASED DISCHARGER
RUN 3 DAYTON GRANGER
DETECTOR CARR BANDWIDTH WB
TIME 14:51

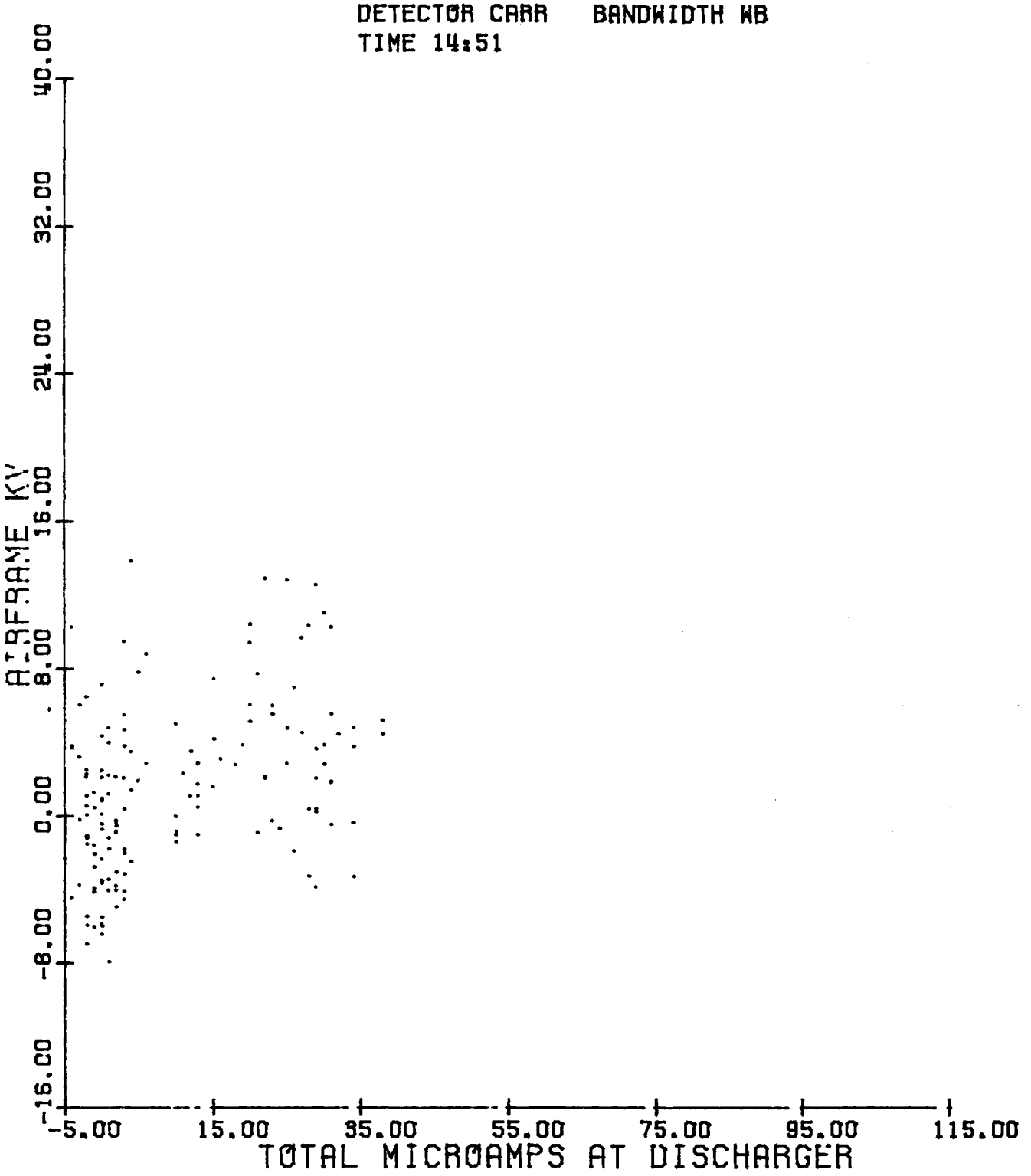

Figure 4-18.

FILE NAME BIAS FLMAR18C
DATE 18-MAR-82 BIASED DISCHARGER
RUN 3 DAYTON GRANGER
DETECTOR CARR BANDWIDTH WB
TIME 14:51

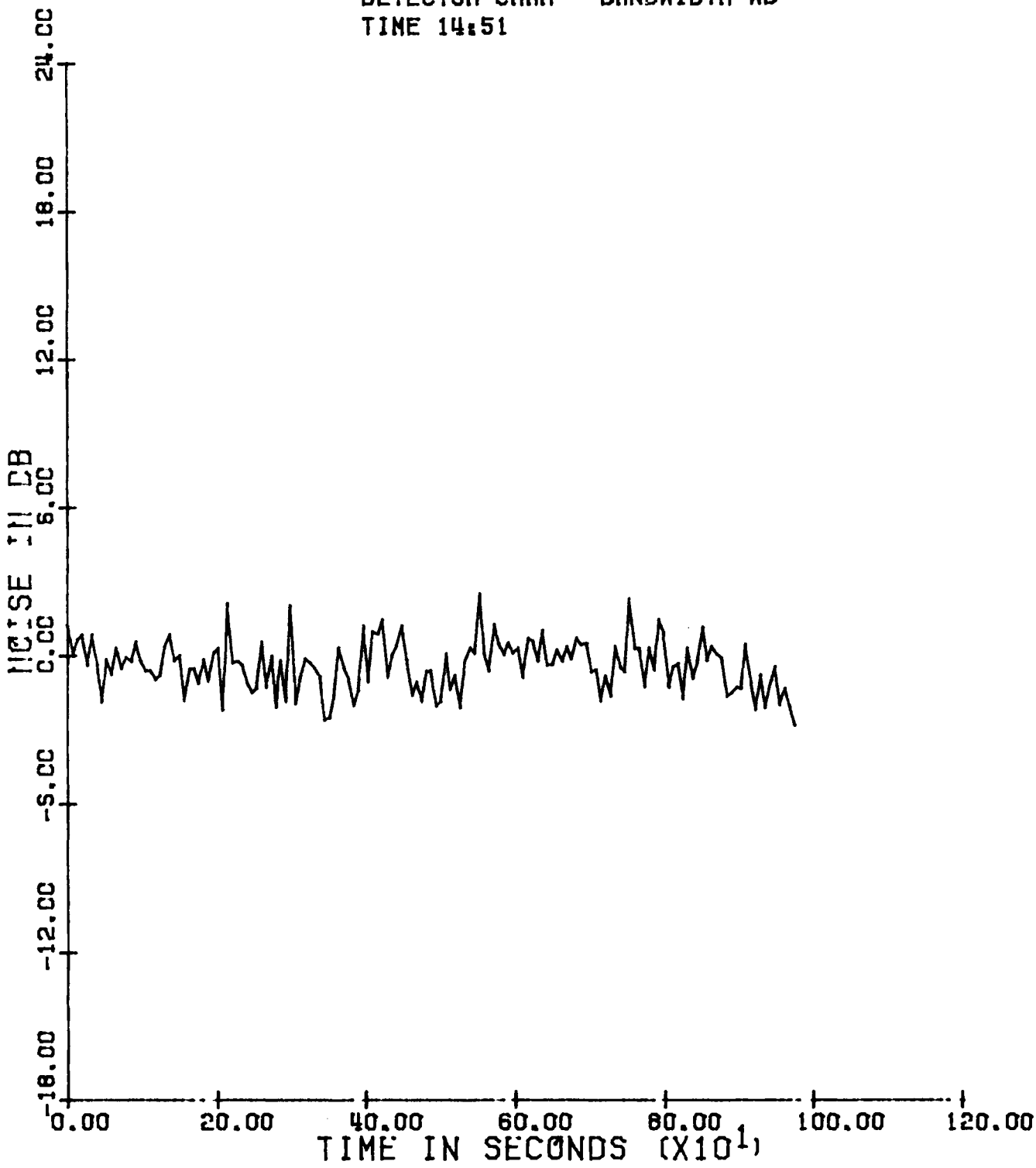

Figure 4-19.

FILE NAME BIAS FLMAR18C
DATE 18-MAR-82 BIASED DISCHARGER
RUN 3 DAYTON GRANGER
DETECTOR CARR BANDWIDTH WB
TIME 14:51

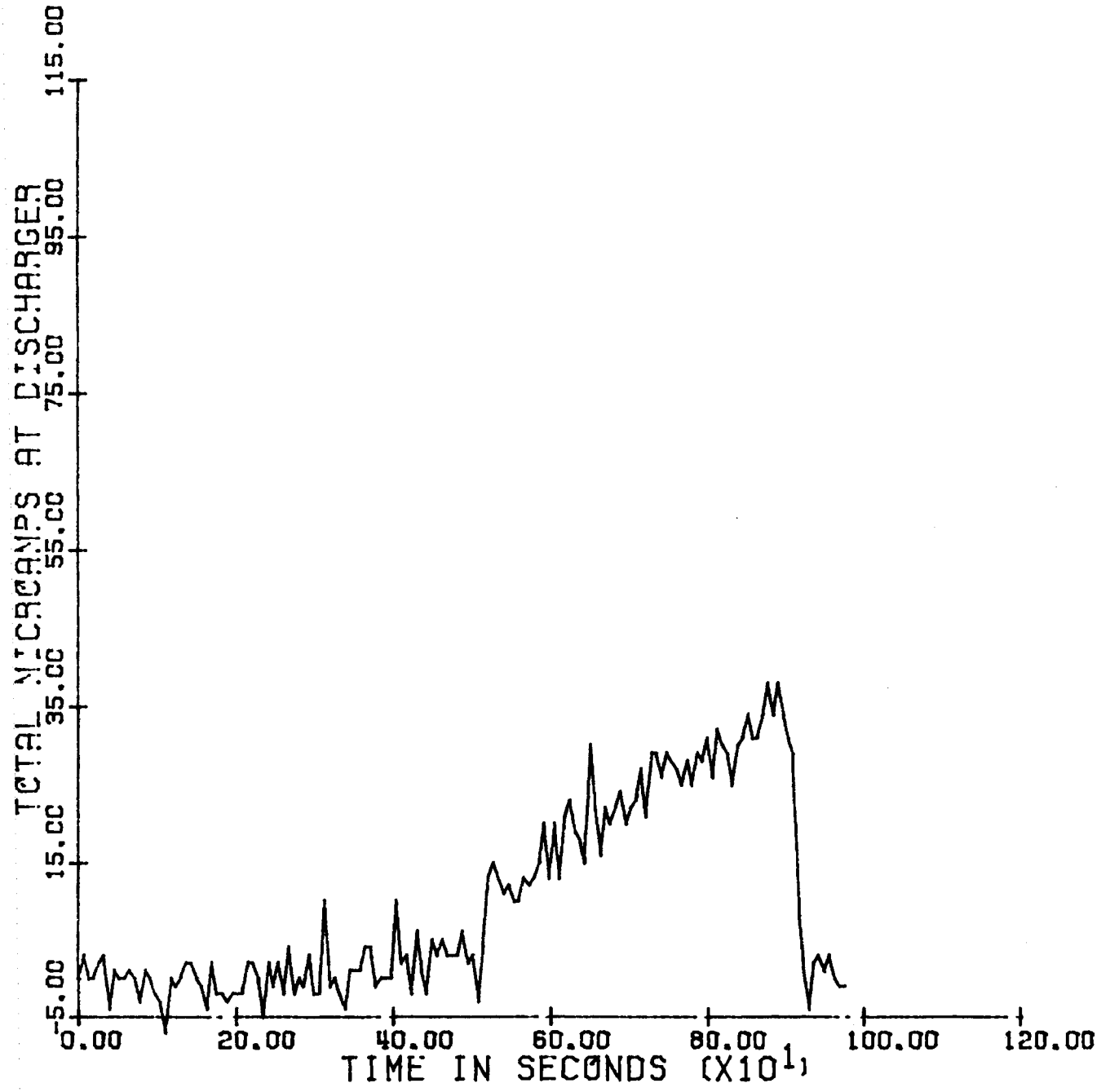

Figure 4-20.

FILE NAME BIAS FLMAR18C
DATE 18-MAR-82 BIASED DISCHARGER FLIGHT
RUN 3 DAYTON-GRANGER
DETECTOR CARR BANDWIDTH WB
TIME 14:51

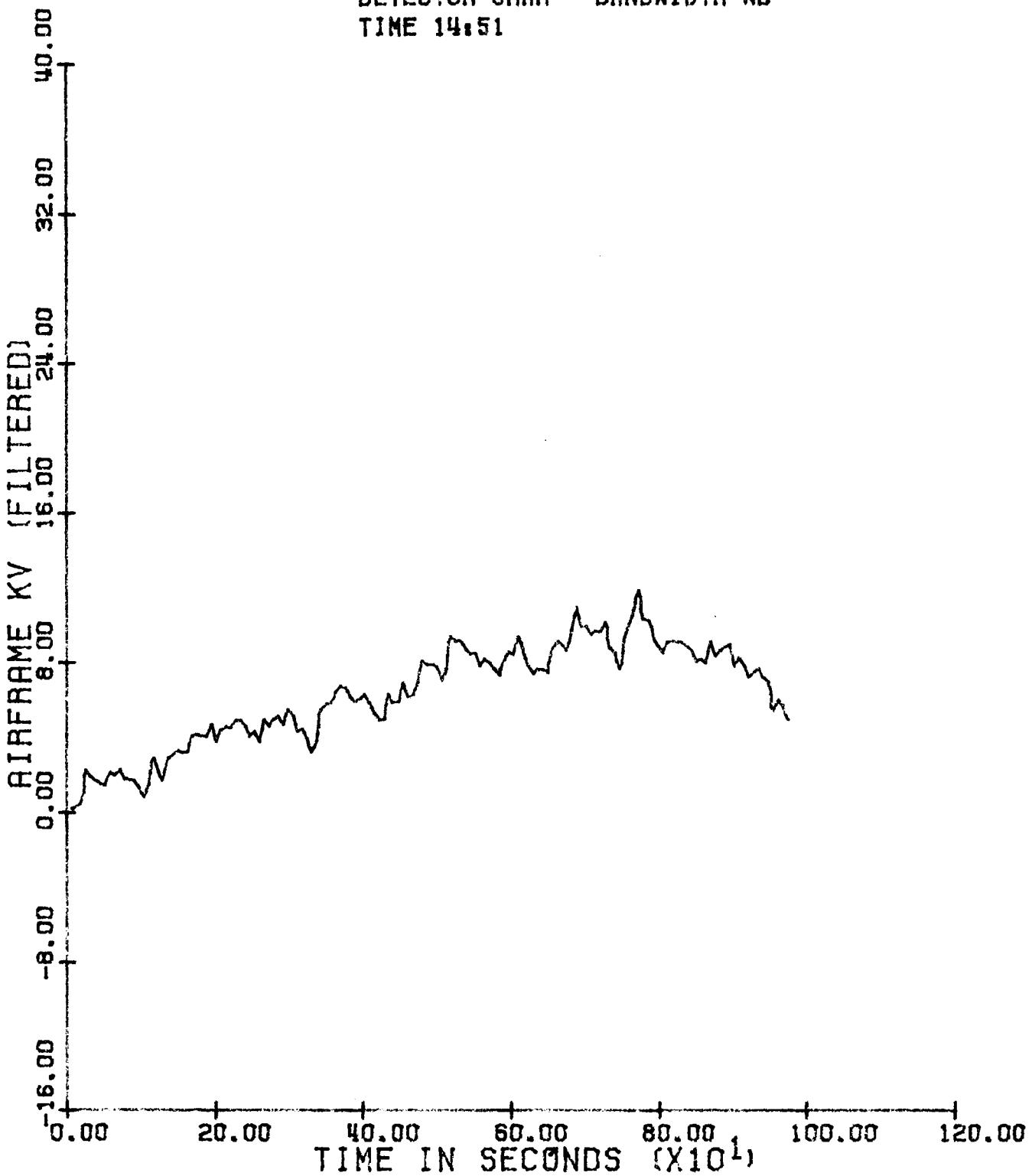

voltage rise of approximately 6 KV is allowed as compared to the 10 KV rise allowed by the Dayton-Granger dischargers Figure 4-20.

3. Biased-Discharger Flights Using TCO Manufacturing DD1 Dischargers. The flight tests of the TCO Manufacturing DD1 dischargers were conducted on March 2, March 19 and March 29, 1982. The March 2 flight was along the standard flight path; the flight on March 19 was a short data collection flight to Port Columbus airport from Albany. The last flight on March 29 was essentially along the standard route except that the flight continued to Parkersburg instead of returning to Albany after passing Henderson VOR. Three data runs were conducted on both March 2 and March 29. Only one data run was performed on the flight of March 19.

Figures 4-21 and 4-22 are the plots of noise vs. current and airframe KV vs. current for the TCO Manufacturing DD1 static-wick dischargers. These plots were taken from the data collected on the March 29 flight. The rest of the plots are presented in Volume II. The DD1 dischargers are identical to the ESD-3 dischargers used in the ground p-static tests except that the mounting base is different.

A comment about the output plots for this data is in order. The plots of noise vs. current and noise vs. time (Figures 4-21 to 4-23) for these data collection runs indicate, occasionally, noise levels significantly lower than the ambient noise levels. This is due to the frequency selection band switch in the EMC-25 interference analyzer. During the flight it was discovered that the noise level appeared to decrease but reselecting the band selector knob restored the noise output level to the values expected. This problem was believed to be due to the vibration of the aircraft. The plots where this problem is found will be indicated on the plot.

Examining Figure 4-21 indicates that the noise levels of the TCO manufacturing DD1 static-wick dischargers were similar to the results obtained with the Dayton-Granger 16375. There was no significant increase in the noise level for the charging currents off the airplane. Figures 4-23 to 4-25 are the plots of noise, current and airframe potential, respectively, for the TCO-DD1 dischargers. One obvious comparison to the Dayton-Granger dischargers was that for a given biased-discharger potential the TCO-DD1 dischargers allowed more current flow off the aircraft. The average airframe potential with the TCO-DD1 dischargers rose only 3-4 KV as compared to a rise with the Dayton-Granger 16375 dischargers of approximately 10 KV. One of the reasons for this behavior was attributed to the lower corona threshold of the TCO-DD1 as compared to the Dayton-Granger. This can be seen by comparing the time that the airframe begins to discharge current. On the Granger dischargers this occurs at about 450 seconds (Figure 4-19) which, based on Figure 4-15, was where the biased-discharger potential was being increased to 35 KV. In Figure 4-24 it can be seen that this same point on the DD1 plot occurs at 190 seconds which corresponded to the point where the biased-discharger potential was being increased to 15 KV.

Figure 4-21.

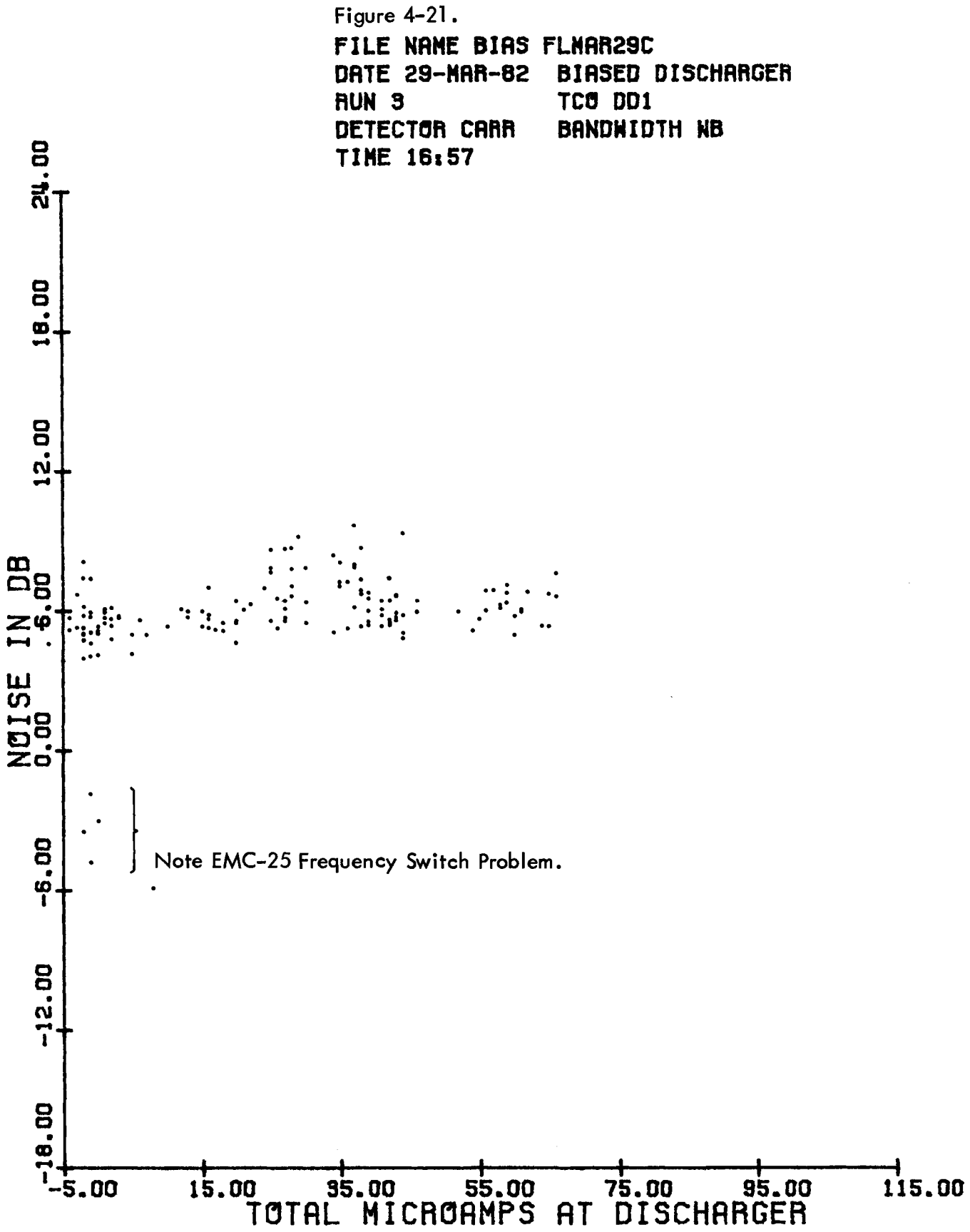
FILE NAME BIAS FLMAR29C
DATE 29-MAR-82 BIASED DISCHARGER
RUN 3 TCO DD1
DETECTOR CARR BANDWIDTH WB
TIME 16:57
NOISE IN DB
24.00
18.00
12.00
6.00
0.00
-6.00
-12.00
-18.00
-5.00
15.00
35.00
55.00
75.00
95.00
115.00
TOTAL MICROAMPS AT DISCHARGER
Note EMC-25 Frequency Switch Problem.

Figure 4-22.

FILE NAME BIAS FLMAR29C
DATE 29-MAR-82 BIASED DISCHARGER
RUN 3 TCO DD1
DETECTOR CARR BANDWIDTH WB
TIME 16:57

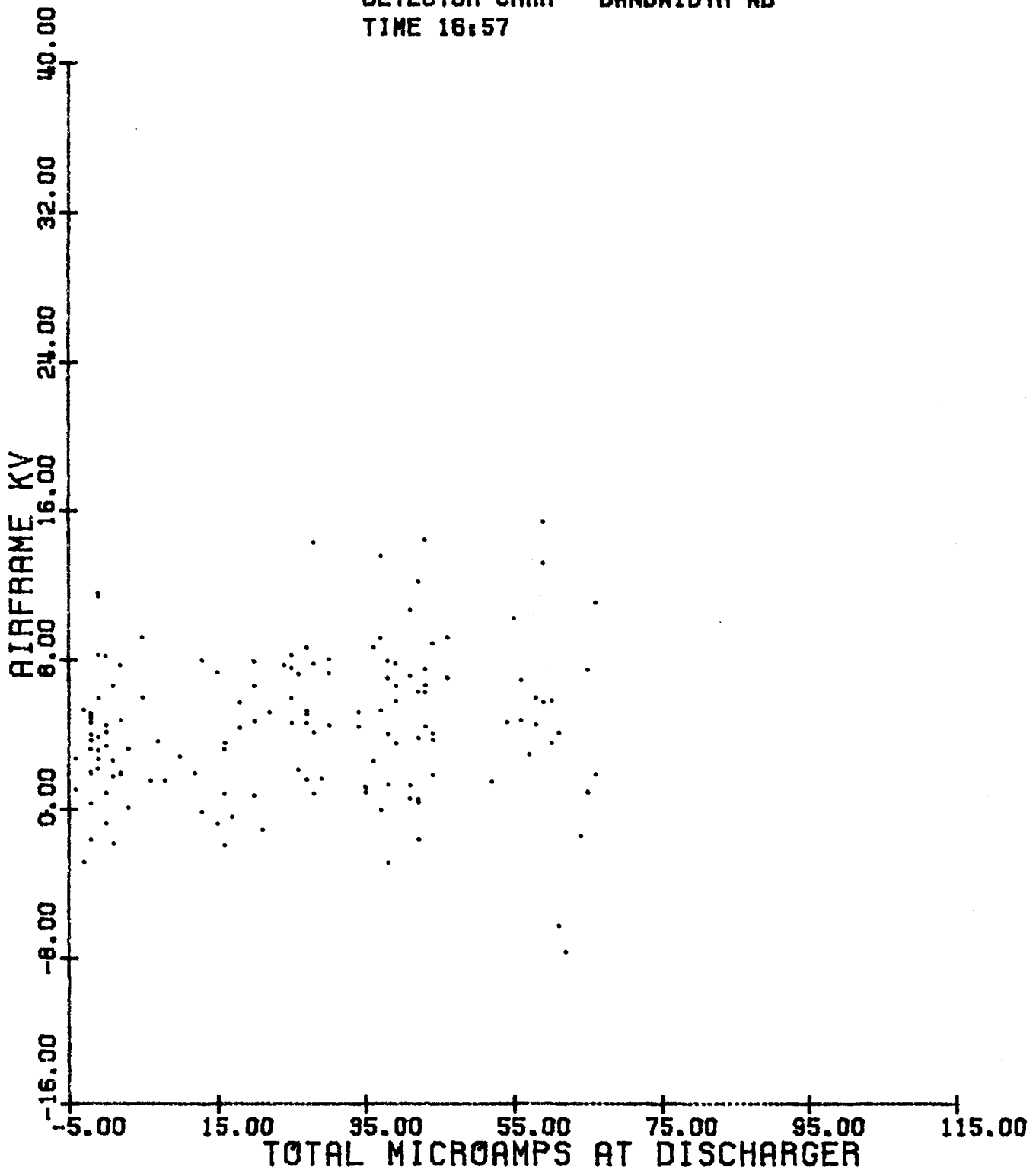

Figure 4-23.

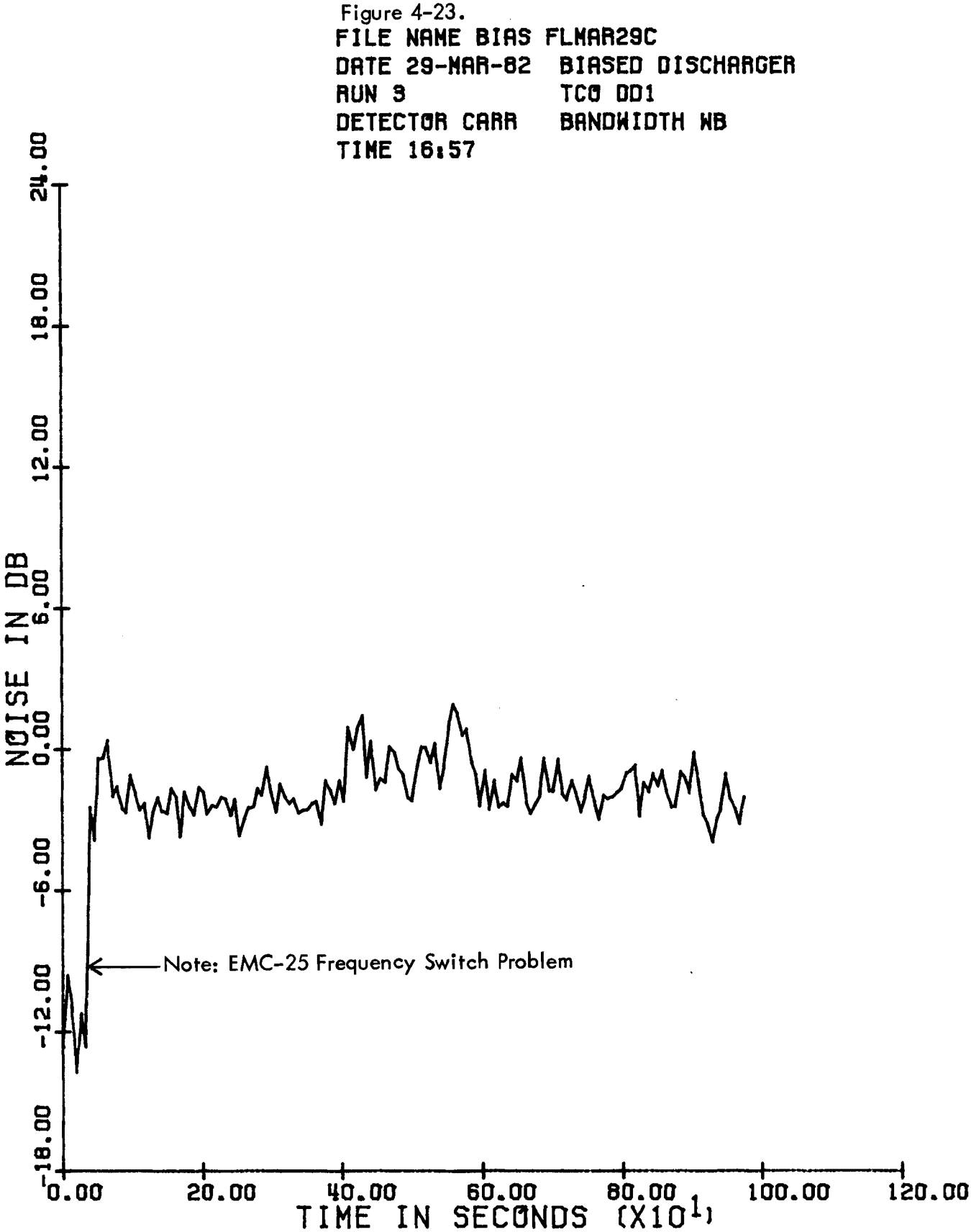
FILE NAME BIAS FLMAR29C
DATE 29-MAR-82 BIASED DISCHARGER
RUN 3 TCØ DD1
DETECTØR CARR BANDWIDTH WB
TIME 16:57
NØISE IN DB
24.00
18.00
12.00
6.00
0.00
-6.00
-12.00
-18.00
0.00
20.00
40.00
60.00
80.00
100.00
120.00
TIME IN SECØNDS (X10¹)
Note: EMC-25 Frequency Switch Problem

Figure 4-24.

FILE NAME BIAS FLMAR29C
DATE 29-MAR-82 BIASED DISCHARGER
RUN 9 TCO DD1
DETECTOR CARR BANDWIDTH WB
TIME 16:57

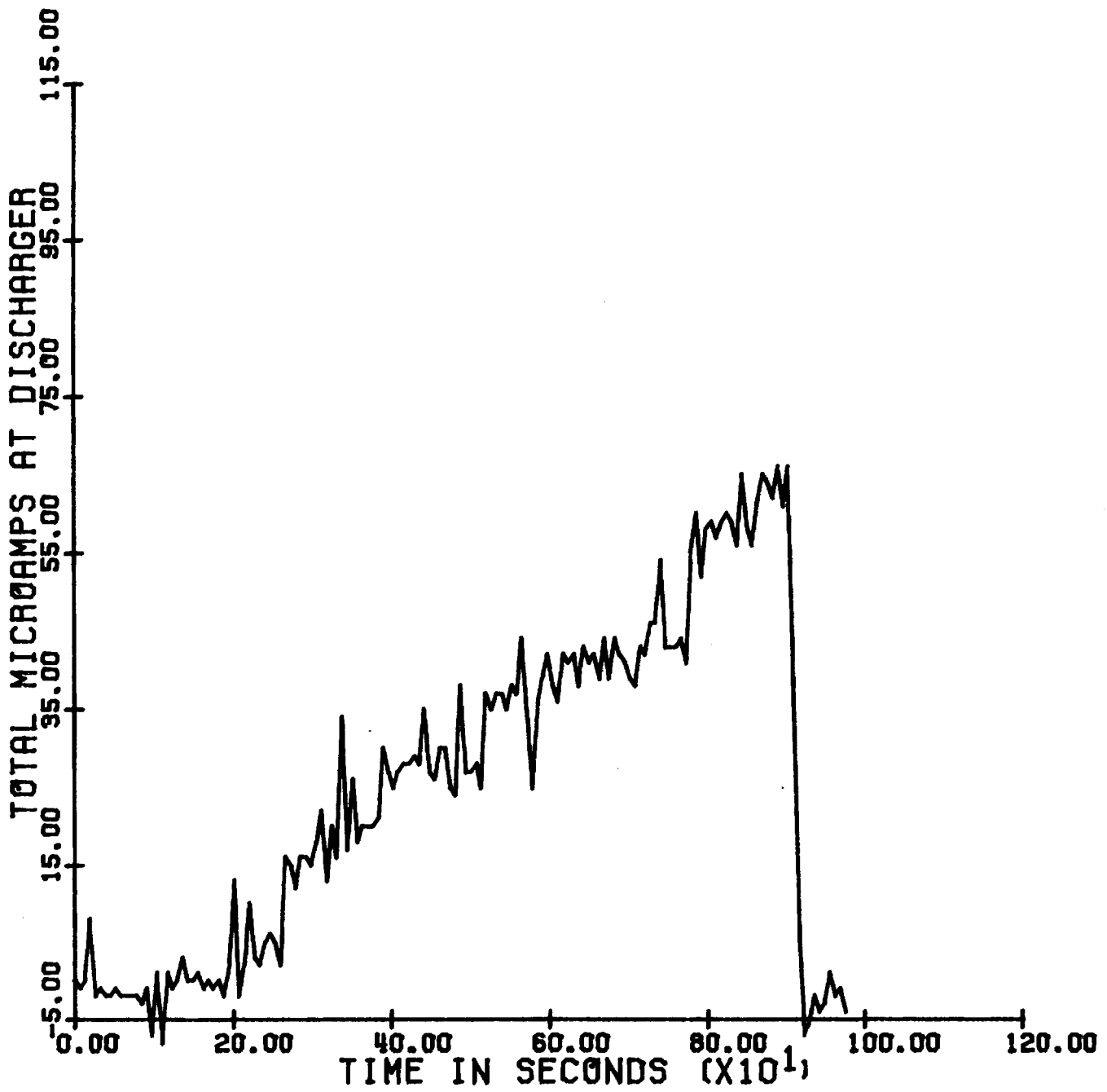

Figure 4-25.

FILE NAME BIAS FLMAR29C
DATE 29-MAR-82 BIASED DISCHARGER
RUN 3 TC0 DD1
DETECTOR CARR BANDWIDTH WB
TIME 16:57

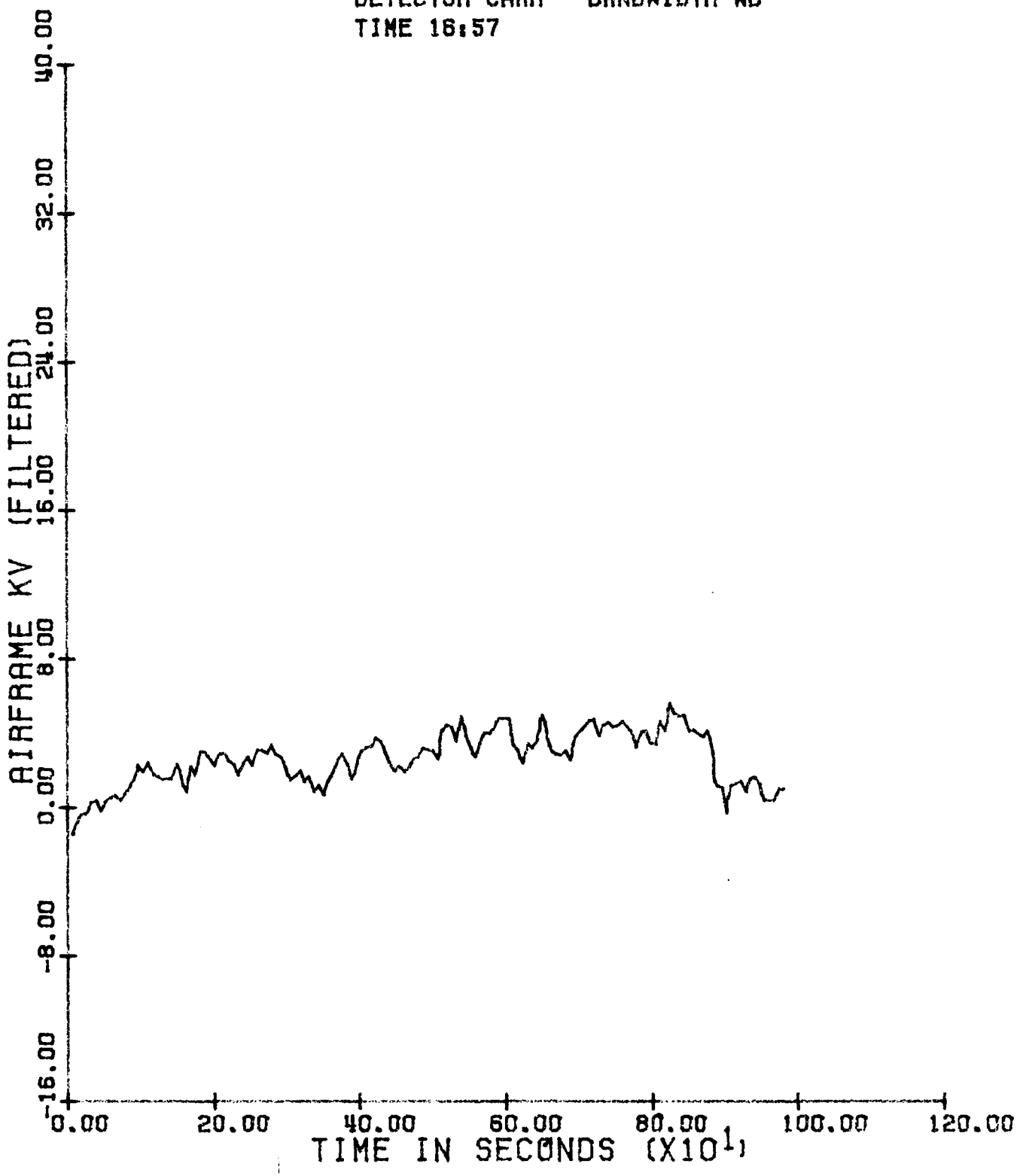

Overall, the performance of the Dayton-Granger and the TCO Manufacturing dischargers were similar with both types providing an improvement in the noise generated by corona discharge due to a p-static charge buildup on the aircraft.

4. Natural Charging Flight Test. The last flight test performed using the p-static data collection software was a flight conducted on March 11, 1982. This flight was conducted along the same route as the other standard data collection flights except that this flight was conducted in moderate to heavy rain and in the vicinity of thunderstorm activity. The aircraft was equipped with the Dayton-Granger 16375 dischargers, and the biased-discharger was not operating. The aircraft charging is soley due to p-static and crossed field effects due to the proximity of the thunderstorm activity.

Figure 4-26 is the plot of the ground track as recorded during the flight from the output of the TI-9900 Loran-C receiver. The numbers next to points on the ground track were the time in seconds that had elapsed since the discharger current measurements were begun. These numbers allow correlation between the ground track and the plots of noise, current and airframe KV vs. time in Figures 4-27 to 4-31, respectively. Figure 4-27 is a very interesting plot of the distribution of the data points of noise vs. discharger current for this flight. Values to the right of zero on the microamp scale indicate positive-point corona, and values to the left are negative-point corona. As can be seen, the slopes and characteristics of the noise levels vs. current are different for the different corona point types. From the ground p-static testing, it was shown that positive-point corona produced greater noise levels than negative-point corona which is indicated very clearly in this plot with natural charging currents. In order to obtain more information on this, additional testing in actual charging conditions is necessary.

Referring to Figure 4-26, the Loran-C ground track, there are two places where the ground track is not plotted. During these times, the TI-9900 receiver could not receive the necessary stations to output the ground track. The receiver lost track at 1380 seconds into the run and then was back to tracking again at 1680 seconds. The signal-to-noise was very poor and the receiver completly lost lock on the stations and had to begin to reacquire the stations again. At this time the aircraft was passing through an area of heavy rain with some lightning around the aircraft. P-static could be heard in the audio of the VHF communications receiver. A few minutes after the receiver began to provide navigation outputs, the aircraft flew into an area between layers. After passing the Henderson VOR, the aircraft again entered another area of rain with an increase in the p-static currents off the aircraft causing a decrease in the signal-to-noise numbers displayed on the TI-9900 receiver display. Again at 2280 seconds into the data collection run, the TI-9900 receiver lost track on the received stations necessary for navigation outputs. The receiver again acquired track of the stations at 2400 seconds into the run. About 5 miles later, the aircraft flew into clear air for the rest of the flight to the NDB and finally landing at the university airport. It can be seen by

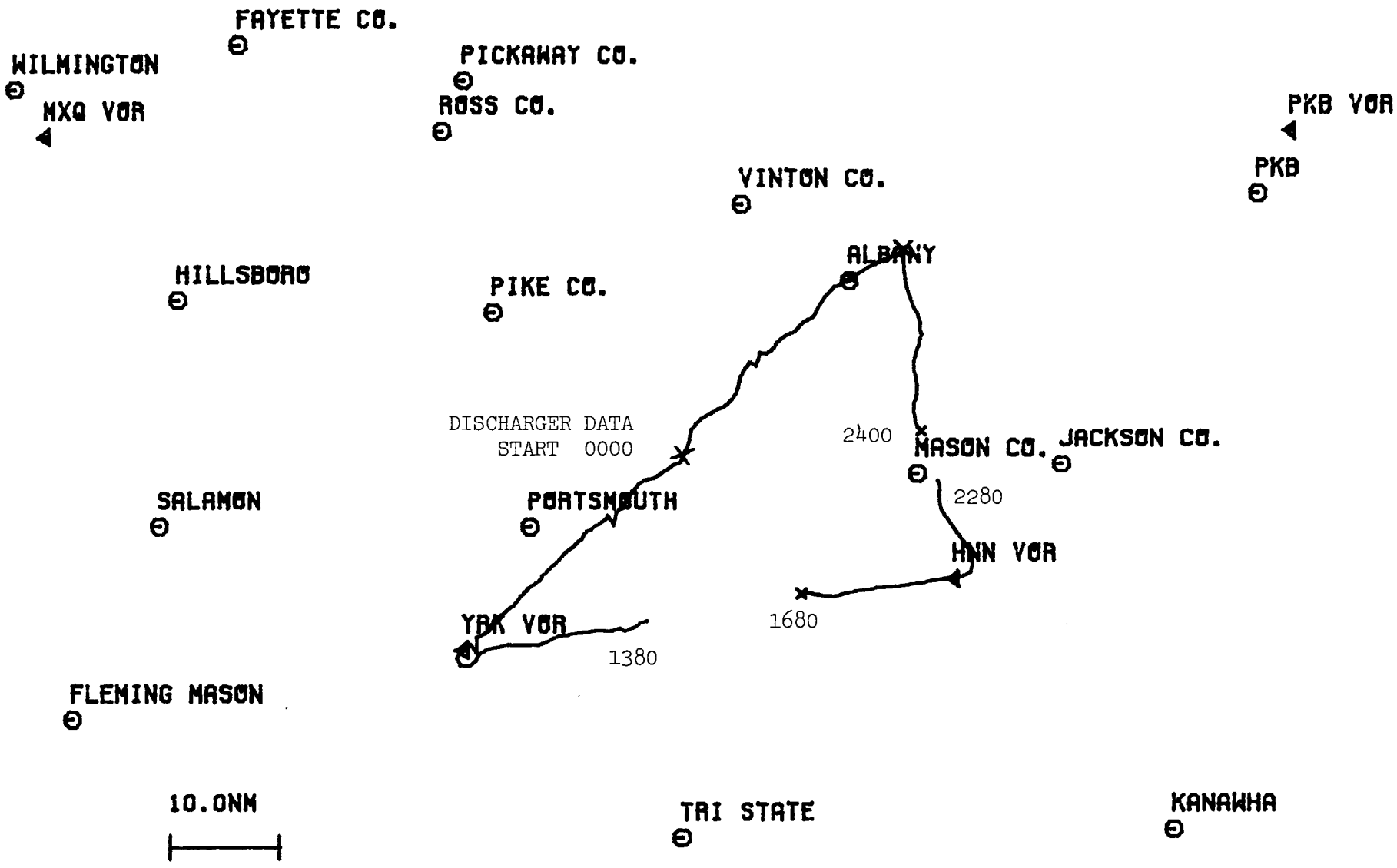

Figure 4-26. Discharger Flight Test Granger, March 11, 1982, UNI to YRK to HNN to UNI NDB to UNI Rain and CB Buildups.

Figure 4-27.

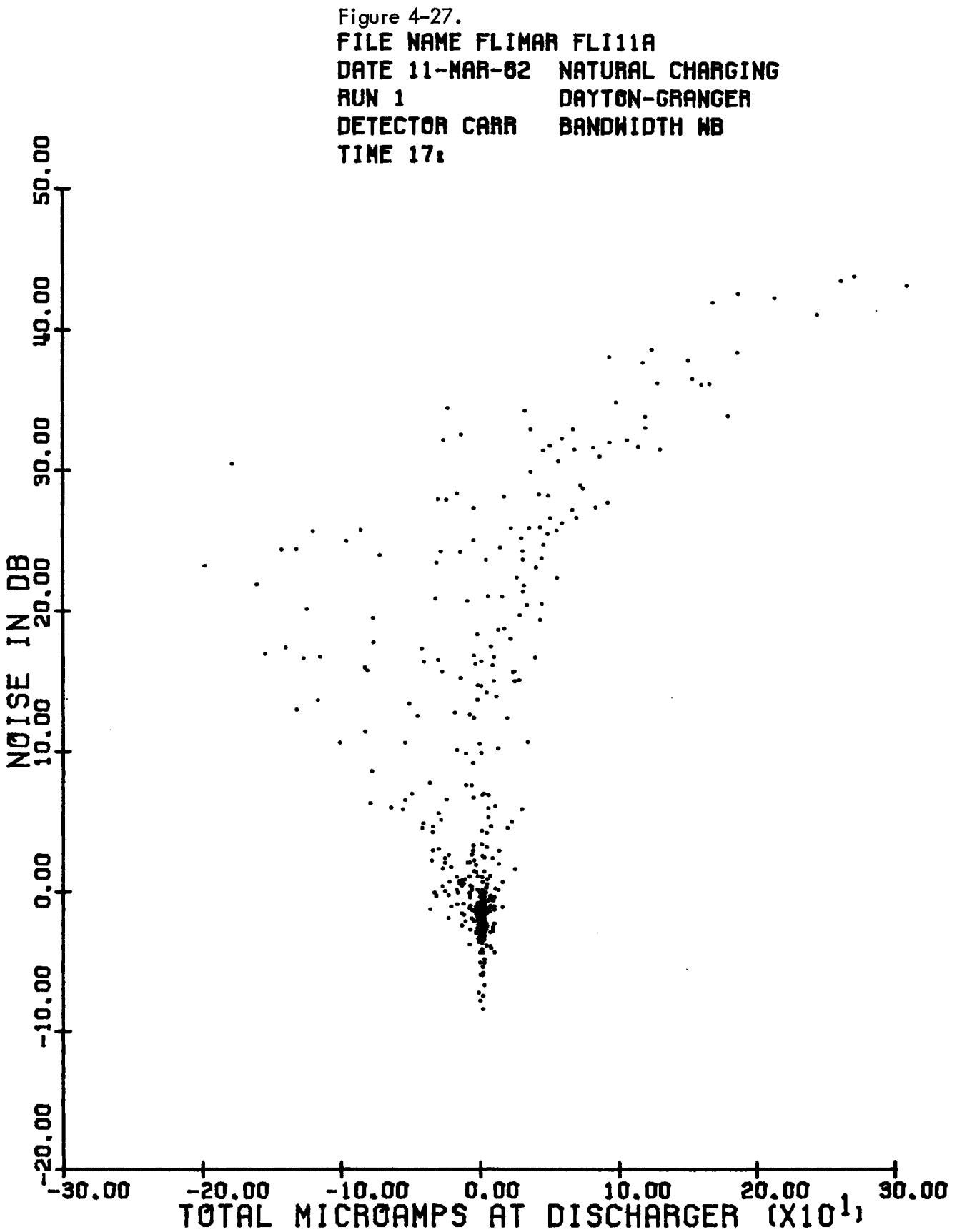
FILE NAME FLIMAR FLI11A
DATE 11-MAR-82 NATURAL CHARGING
RUN 1 DAYTON-GRANGER
DETECTOR CARR BANDWIDTH WB
TIME 17:
NOISE IN DB
50.00
40.00
30.00
20.00
10.00
0.00
-10.00
-20.00
-30.00
-20.00
-10.00
0.00
10.00
20.00
30.00
TOTAL MICROAMPS AT DISCHARGER (X10¹)

Figure 4-28.

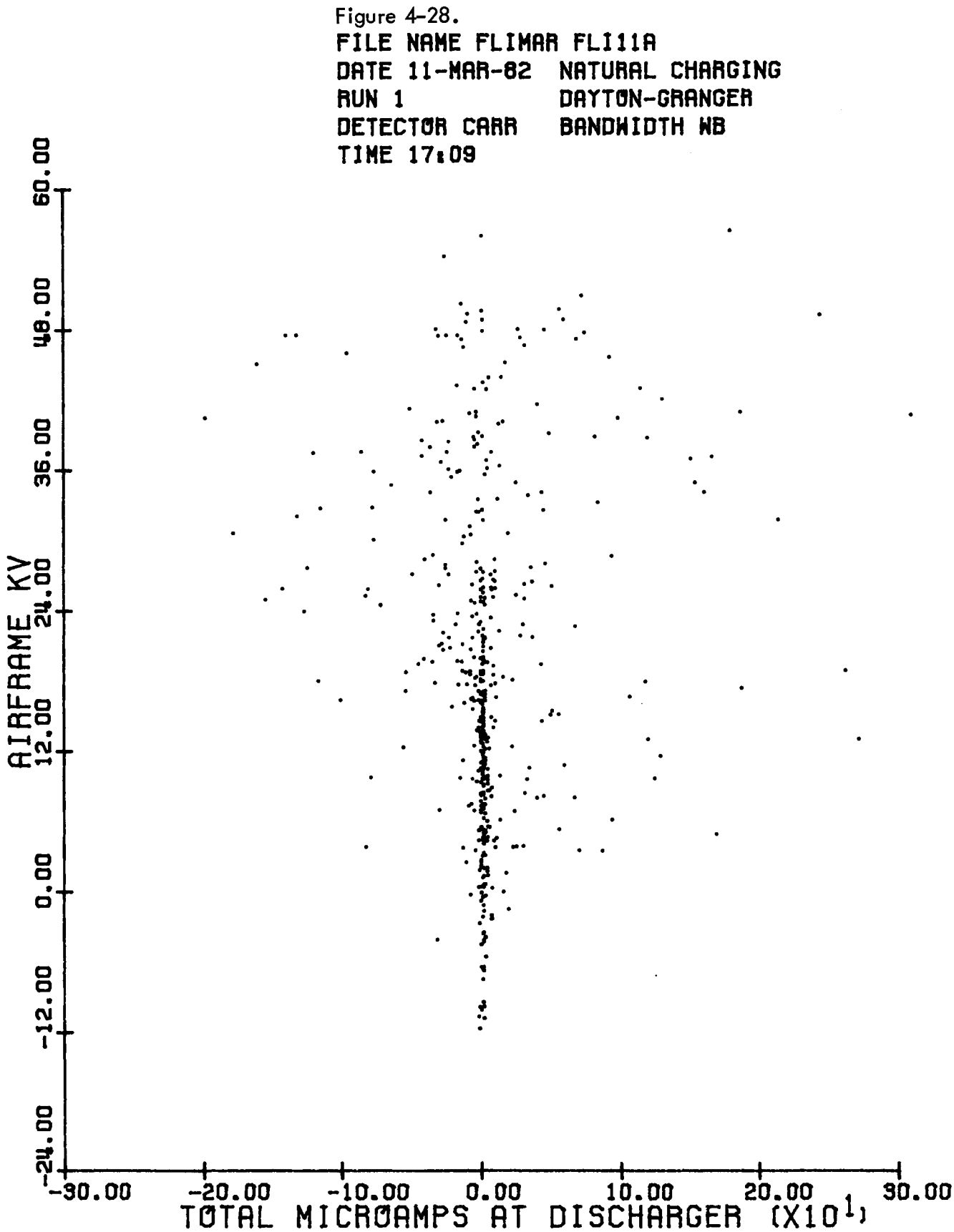
FILE NAME FLIMAR FLI11A
DATE 11-MAR-82 NATURAL CHARGING
RUN 1 DAYTON-GRANGER
DETECTOR CARR BANDWIDTH WB
TIME 17:09
AIRFRAME KV
60.00
48.00
36.00
24.00
12.00
0.00
-12.00
-24.00
-30.00
-20.00
-10.00
0.00
10.00
20.00
30.00
TOTAL MICROAMPS AT DISCHARGER (X10¹)

Figure 4-29.
FILE NAME FLIMAR FLI11A
DATE 11-MAR-82 NATURAL CHARGING
RUN 1 DAYTON-GRANGER
DETECTOR CARR BANDWIDTH WB
TIME 17:

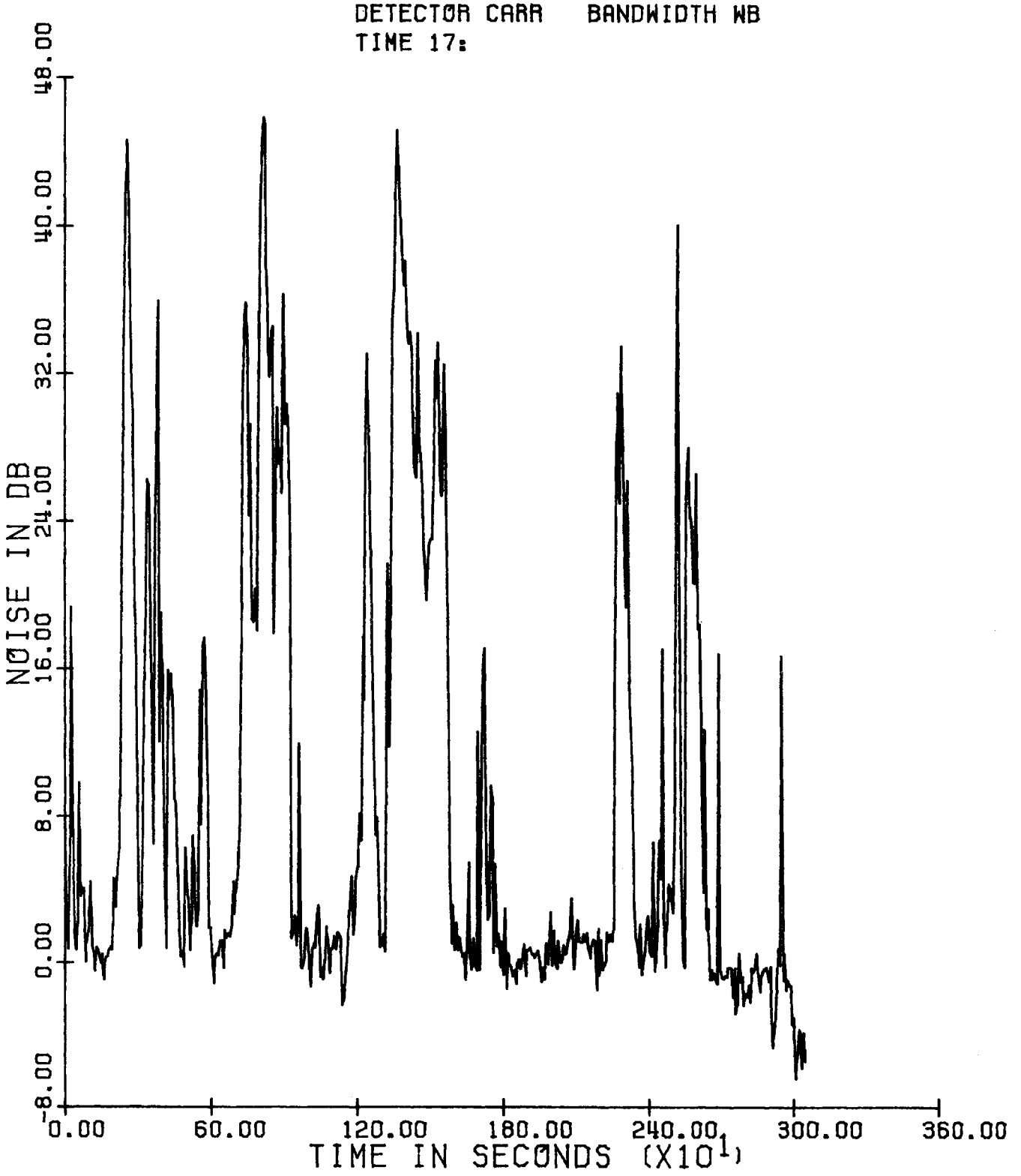

Figure 4-30.
FILE NAME FLIMAR FLI11A
DATE 11-MAR-82 NATURAL CHARGING
RUN 1 DAYTON-GRANGER
DETECTOR CARR BANDWIDTH WB
TIME 17:

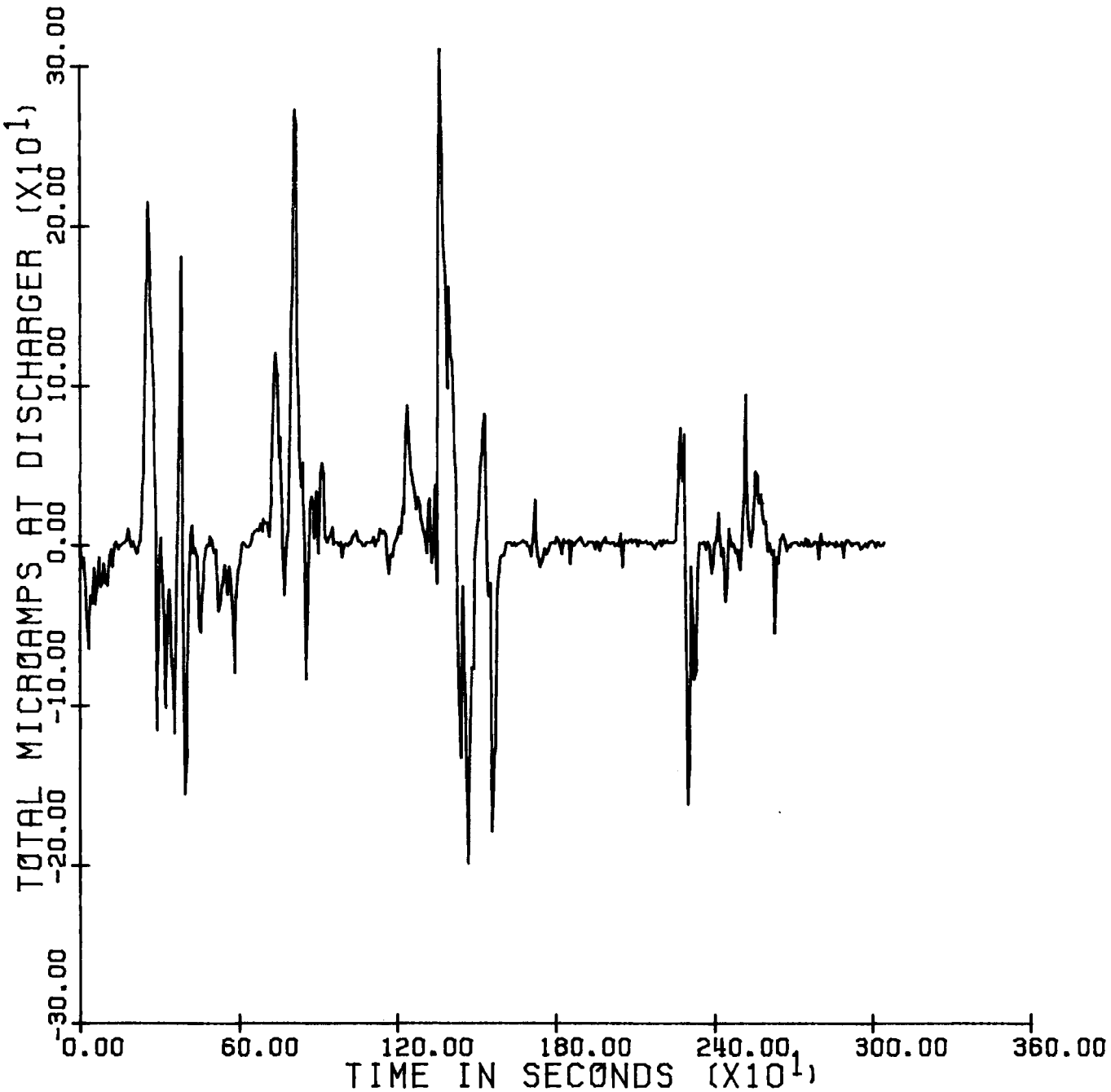

Figure 4-31.

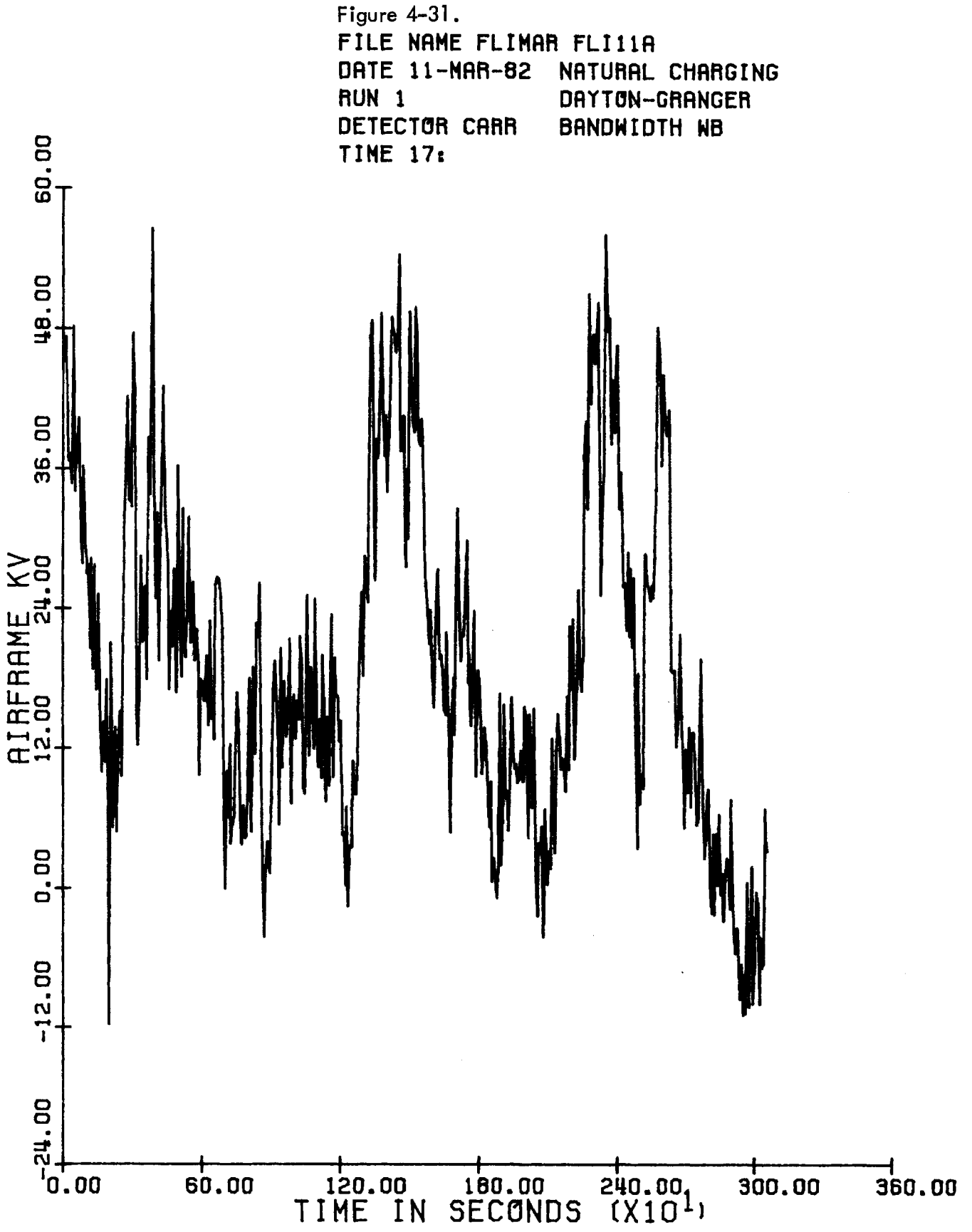
FILE NAME FLIMAR FLI11A
DATE 11-MAR-82 NATURAL CHARGING
RUN 1 DAYTON-GRANGER
DETECTOR CARR BANDWIDTH WB
TIME 17:
AIRFRAME KV
60.00
48.00
36.00
24.00
12.00
0.00
-12.00
-24.00
0.00
60.00
120.00
180.00
240.00
300.00
360.00
TIME IN SECONDS (X10¹)

observing Figures 4-29 to 4-31 the effects of the noise, discharger currents and airframe potential vs. time as the flight progressed. Especially, note the large bipolar swing in the discharger current in the vicinity of 1500 seconds. It was believed that this was due to flight through areas of charge centers relating to electrical activity in the thunderstorms. The thunderstorm activity encountered in this flight are quite typical of the type of activity that might be encountered in a flight deviating around a large area of thunderstorms.

One point that needs to be made regarding the poor noise reduction performance of this flight was that at about 1625 seconds into the discharger data collection run both the Dayton-Granger dischargers on the right elevator were lost off the aircraft. This would definitely contribute to the increased noise especially in the type of charging experienced during this flight. Therefore, it is strongly suggested that definite conclusions based on this data is inappropiate due to the problems mentioned above. Additional actual flight test data is necessary to evaluate these results.

D. Summary of P-Static Flight Tests.

In summary, the data presented here suggests that noise reduction benefits are achievable when using well-designed static-wick dischargers on aircraft to reduce the locally generated noise due to the corona discharge caused by p-static charging of the aircraft in flight. The flights conducted using the biased-discharger to develop a charge on the aircraft did not duplicate the current levels attainable in the ground p-static tests. Nevertheless, it was demonstrated that noise reductions are afforded even at these low levels. Much has been learned in making these measurements which will allow more efficent data collection in the future.

V. GROUND LIGHTNING SIMULATION TESTING

A. Lightning Simulation.

1. Test Procedure. The ground lightning simulation testing was performed at Wright-Patterson Air Force Base in Dayton, Ohio. This testing was performed using the facilities of the Atmospheric Electricity and Hazards Group at WPAFB. Figure 5-1 is a diagram of the test set up for the lightning simulation testing. The lightning fields simulator was set up to produce the fields necessary to simulate lightning strokes with a distance of 10 to 40 nm to the aircraft with these strokes occurring at azimuth angles around the aircraft every 30 degrees. The lightning simulator consisted of a high voltage power supply that would discharge into an arc in a relaxation oscillator mode. The capacitors were charged until the voltage on the air gap flashed over and the capacitors were discharged through a pulse shaping resistor that provided damping for any ringing of the current pulse. The current pulse was measured on a storage oscilloscope using a current transformer placed on one of the supply lines to the air gap, Figure 5-2. After the capacitors discharged, the supply began to charge the capacitors until the spark gap flashed over again. The time between flashes was approximately 12 seconds. Figure 5-3 is a computer plot of the current pulse based on the equivalent circuit of Figure 5-2 and the recorded parameters.

In order to determine the simulated lightning distance to the aircraft, a 3M Ryan StormScope Model 7A was used in the aircraft. Figure 5-4 is a photograph of the lightning simulator in relation to the aircraft. The StormScope antenna, Trimble Loran-C antenna and the long wire antenna used for the TI-9900 Loran-C receivers are noted on the photograph. Figure 5-5 is a closer view of the enclosed airgap used in the lightning simulator. The simulator was turned on and the distance from the aircraft center was established at about 20 meters and the StormScope was observed to have discharges plotted anywhere from 10 nm to 40 nm from the aircraft. Figure 5-6 is a photograph of the StormScope display with the simulator placed at the 240-degree azimuth relative to the nose of the aircraft. The range of the StormScope was set at 40 nm, and, as can be seen, the discharge points lie essentially on the 240-degree azimuth line of the StormScope display. The azimuth of the simulator around the aircraft was set by using the drift sight installed in the aircraft.

The equipment installed in the aircraft for data collection consisted of the following: the Heath H-89 Digital computer using an assembly program to receive asynchronously the serial output data from the Trimble and TI-9900 Loran-C receiver and dump them to the Byte Bucket Digital Cassette recorder. The TI-9900 receiver produces about 200 characters every 14.7 seconds and the Trimble also produces about 200 characters but the frequency of this entire record was about every 90 seconds. Data were taken with the simulator operating for approximately 3-5 minutes at each of 12 azimuth positions spaced 30 degrees around the aircraft. A control data set was taken with the lightning simulator off to determine the characteristics of the position outputs of the Loran-C receivers without any

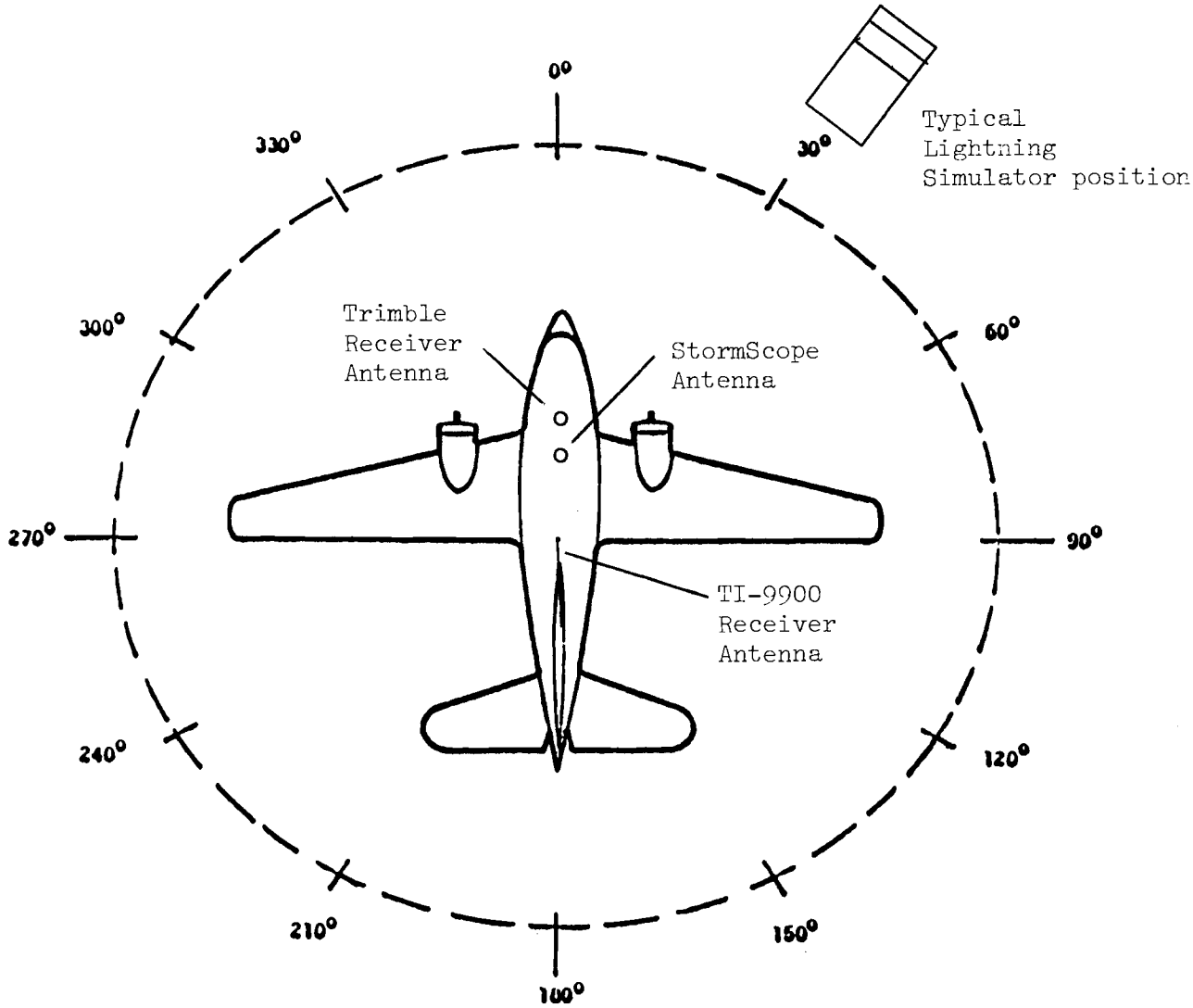

Figure 5-1. Typical Lightning Simulator Position Around N7AP.

Figure 5-2. T/SSI TEST LOG

Test No. 1 Task 30-04 Date 22 Sept 81

Test Item DC-3 (Ohio University)

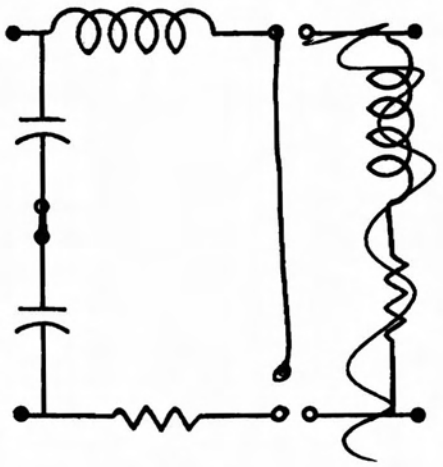

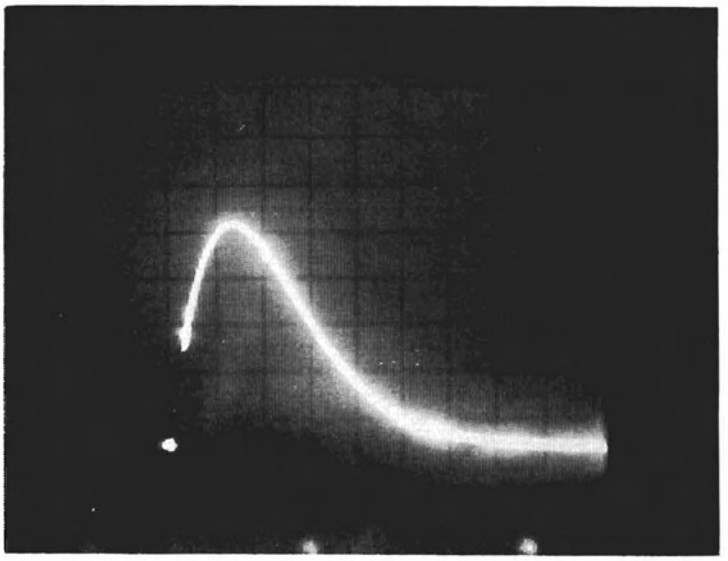

V_c= 30K C_t = 15 μf

V_p= ____ L_t ≅ 5 μh

I_p= 3KA R_d= 5 Ω

R_L= ____

Scale Factors

CT	10:1

Vert. 64 V /Div.

Horiz. 2 μS /Div.

Remarks Spark gap at 62 ft at 0° to A/C

Instrumentation HP 1744A & scope camera - Pearson 110A CT

Test Supervisor JS Contract F33601-79-D0065

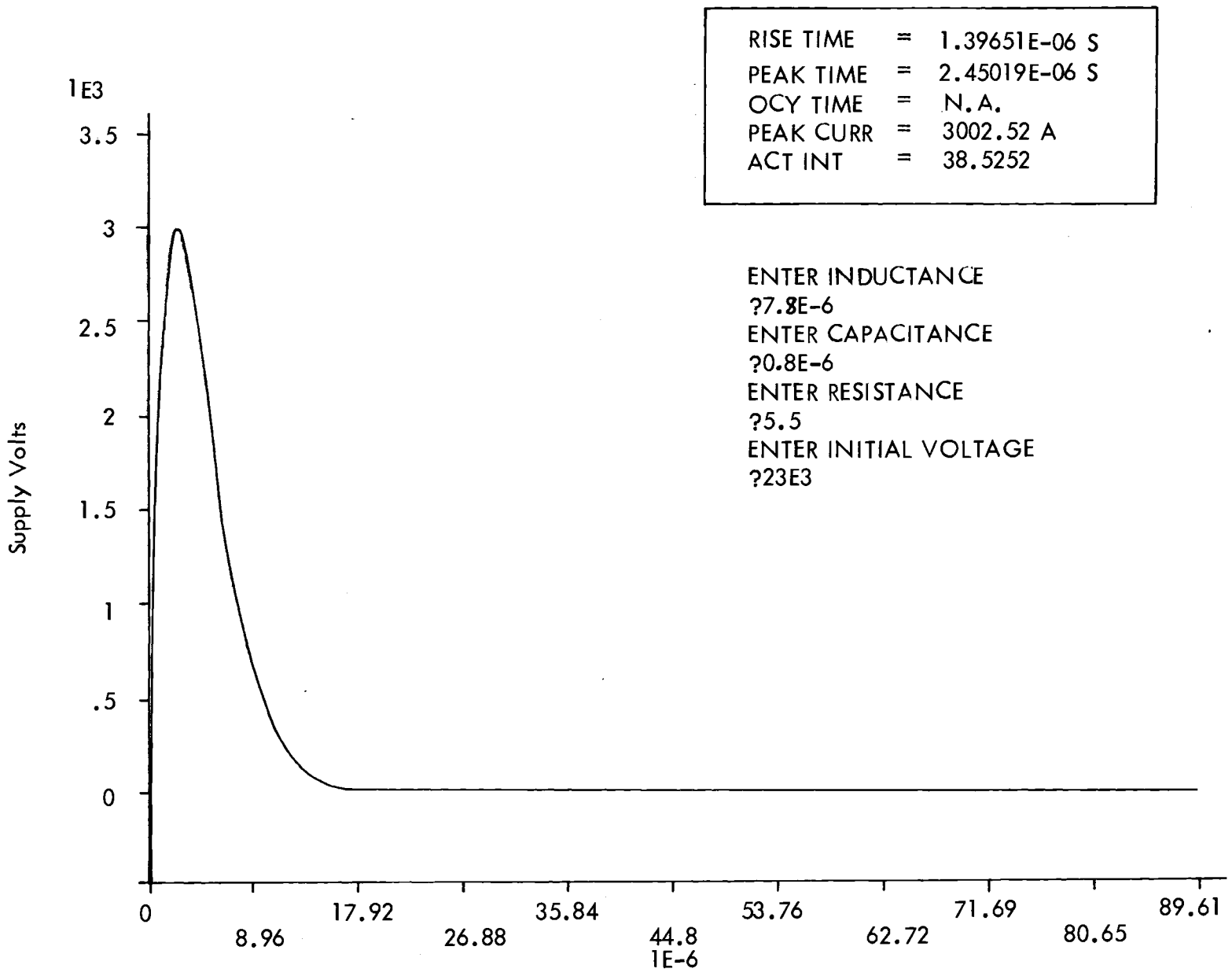

Figure 5-3. Computer Generated Plot of Current Pulse of Simulator.

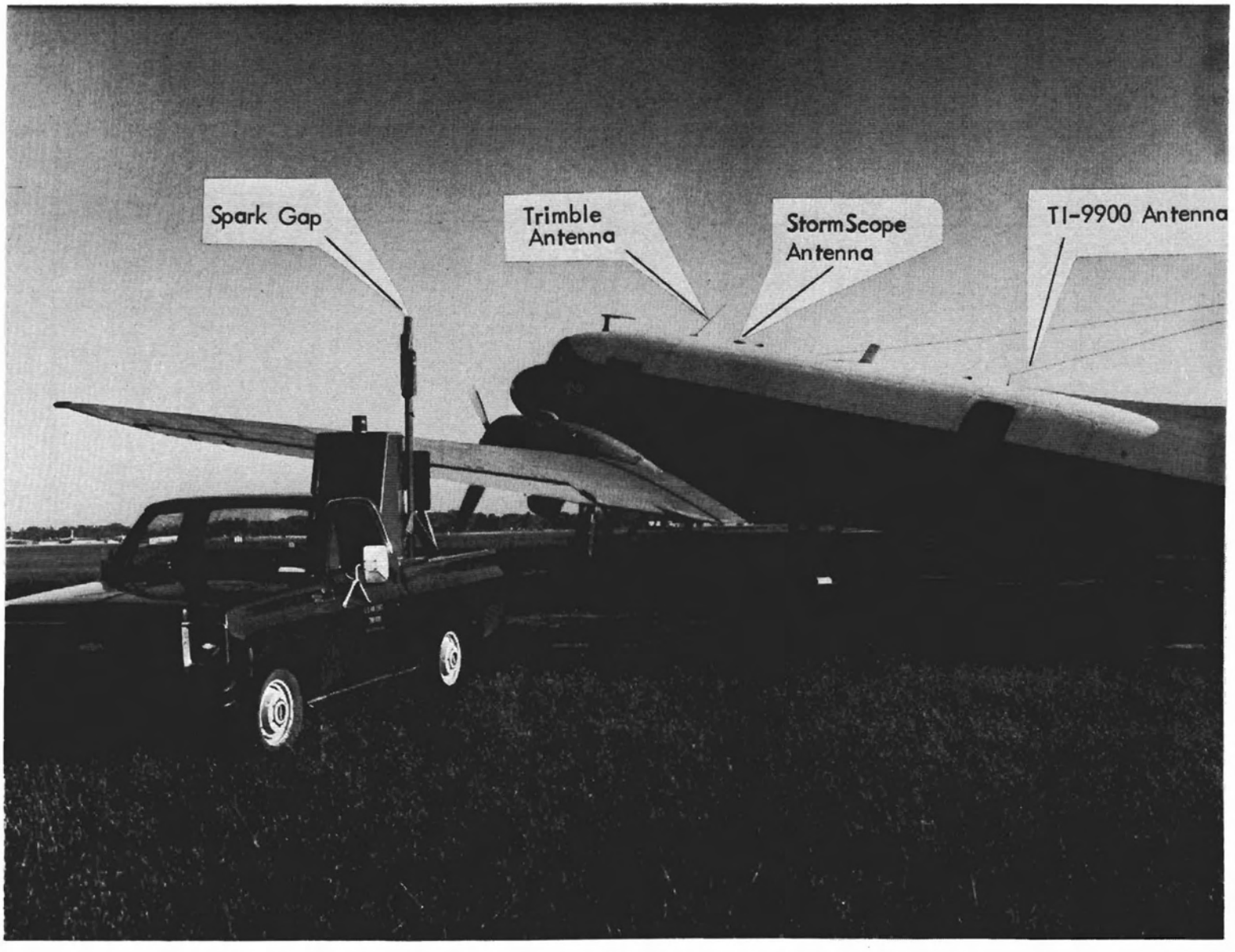

Figure 5-4. Typical Position of Lightning Simulator Around Aircraft.

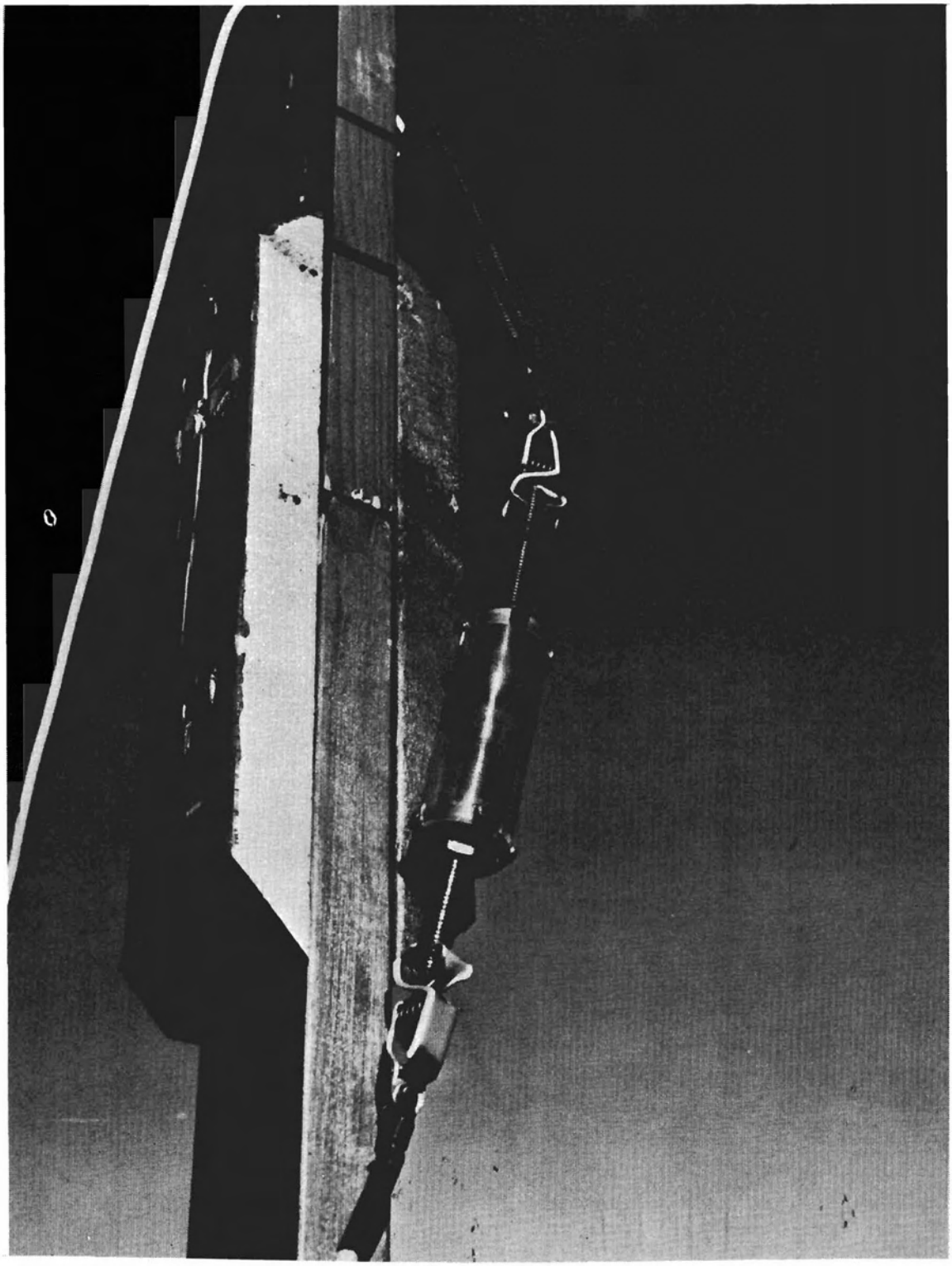

Figure 5-5. Close-Up View of Spark Gap of Lightning Simulator.

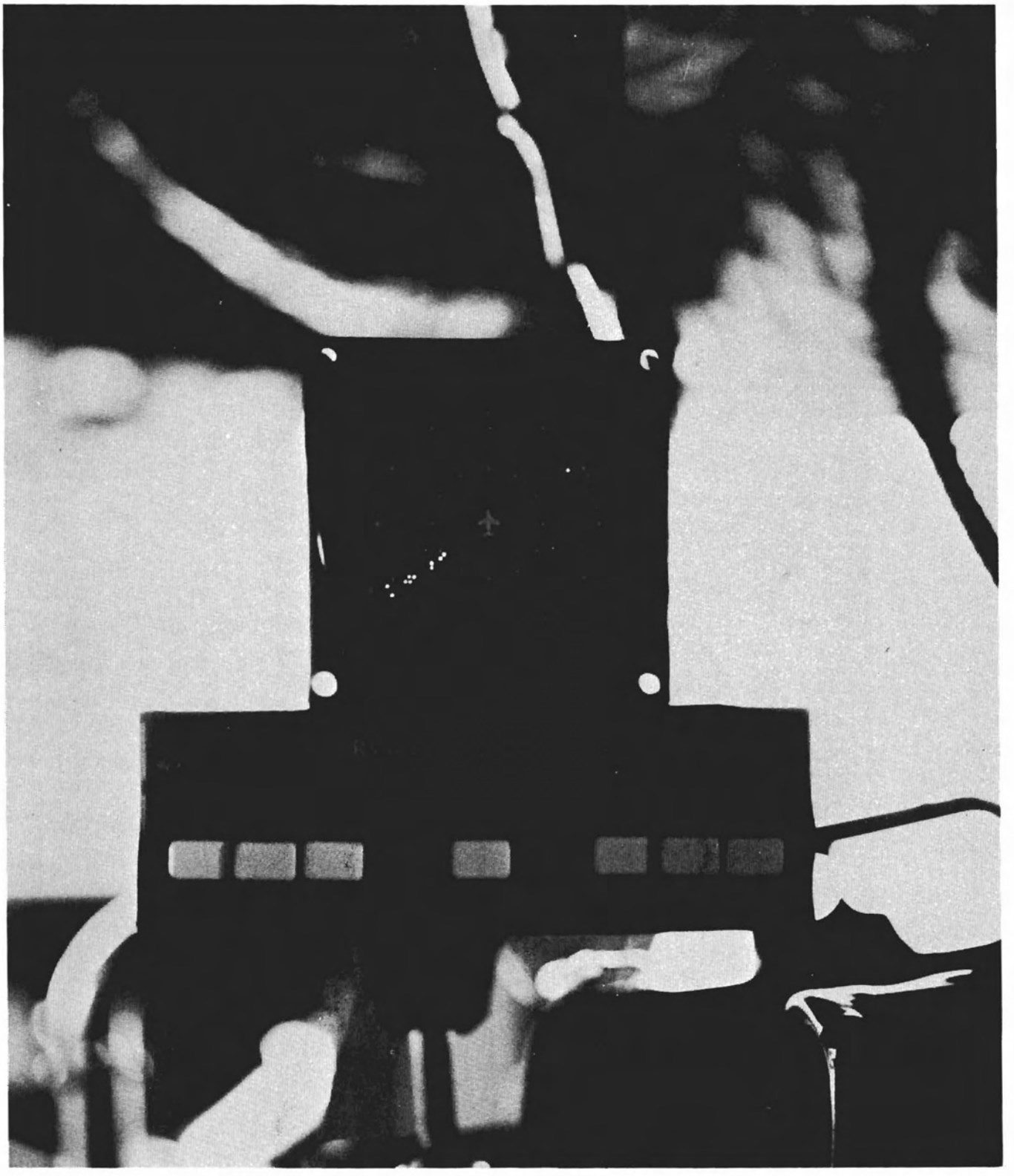

Figure 5-6. Display of StormScope for 240° Azimuth Testing.

lightning stroke activity. Therefore, there was a total of 24 measurements made in the ground lightning simulations which involved 12 azimuth positions; one data set without the simulator operating and one with the simulator operating at each azimuth.

2. Ground Lightning Simulation Test Results. The ground lightning simulation test results were very consistently good. Figures 5-7 to 5-14 are graphic output for the tests every 90 degrees of azimuth. All of the graphic output for all 12 azimuth positions are presented in Volume II. The data presented here represents data taken with both receivers tracking the 9960 GRI of the Loran-C north-east chain. The station pairs selected for the position output data are the Seneca, N.Y. - Carolina Beach, N.C. (M-Y) and Seneca, N.Y. (M-Z) pairs which produce an optimum position determination in the area of WPAFB. Each square in the figures represents 0.05 nm either side of the position determined as the average of all the output position data for that azimuth. The X in the middle of the box represents this average position. The circles represent the plots of the output data. Note many of the points are overstrikes indicating the same output position. A position of 0.05 nm represents a deviation of approximately 93 meters or 304 ft. In most cases, it is difficult to see any increase in the deviations for the lightning simulation case and the ambient noise measurements. For the data output of the Trimble receiver there was less than 3 output data points which will not allow the calculation of a standard deviation; this is noted on the graphic output that apply. Note that both receivers produced, on the average, almost identical output position data. The only deviation was in the north-south position direction of ±0.02 degree which in this area relate to a position error of ±122 ft. There were a few cases of east-west deviation but this was very small. This was based on comparing the average position output of the TI-9900 with the Trimble Model 10A average position output.

Since the frequency of the simulated lightning strokes was very slow, the probability of producing significant position output errors was quite low. The repetition frequency of the lightning strokes was limited by the charging current available in the high voltage power supply used in the lightning simulator. Also, the production of rapid return stroke lightning simulation was not provided as this simulation facility was not available.

In general, based on the information collected during these tests, it can be concluded that for light spheric activity within 40 nm of the Loran-C receiver no significant errors have been detected. Further information could be obtained by operating the Loran-C receivers in a fixed ground installation while recording occurrence of spheric activity along with the Loran-C receiver position output data. This would provide a stroke rate vs. position output error qualitative measure of performance.

B. Antenna Static Field Testing.

1. Test Procedure. The idea behind the antenna static field testing was to induce a high static field on the Loran-C receiver antenna

Figure 5-7.

TI9900 RECEIVER TEST
WPAFB DAYTON, OHIO
.1 NM SQUARES
AZIMUTH= 000

AMBIENT

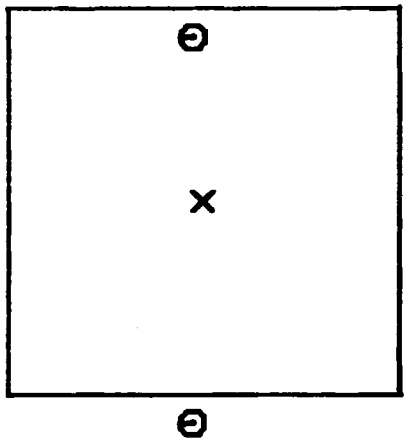

LIGHTNING

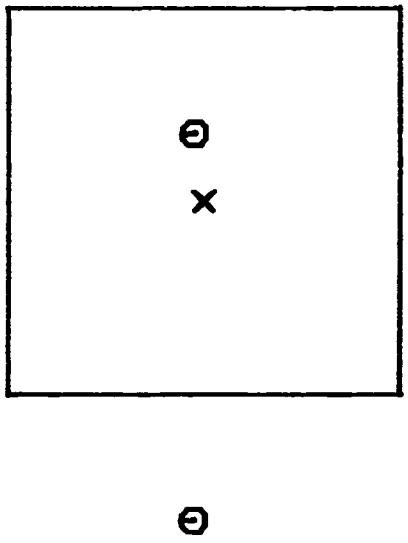

.05 NM

NUMBER OF POINTS 12		
CENTER	39	49.76 N
	84	2.20 W
S2 =	.00003	NM
S =	.00583	NM

NUMBER OF POINTS 12		
CENTER	39	49.78 N
	84	2.20 W
S2 =	.00002	NM
S =	.00440	NM

Figure 5-8.

TRIMBLE RECEIVER TEST
WPAFB DAYTON, OHIO
.1 NM SQUARES
AZIMUTH= 000

AMBIENT

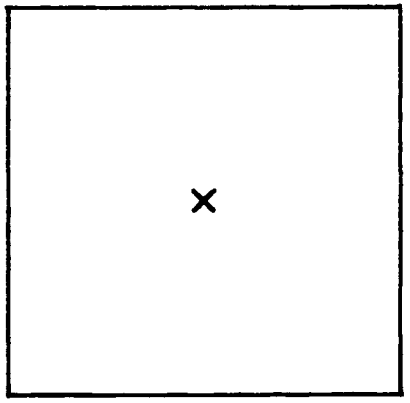

LIGHTNING

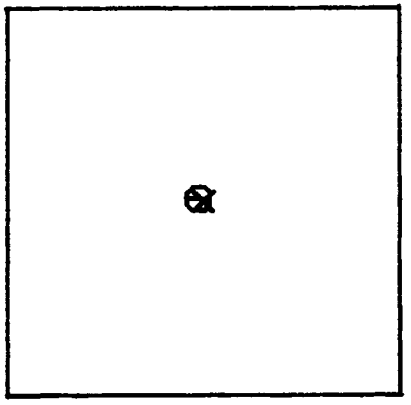

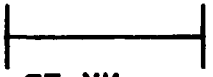

.05 NM

NUMBER OF POINTS 2
CENTER 39 49.78 N
84 2.20 W
S AND S2 NOT AVAILABLE

NUMBER OF POINTS 1
CENTER 39 49.78 N
84 2.20 W
S AND S2 NOT AVAILABLE

Figure 5-9.

TI9900 RECEIVER TEST
WPAFB DAYTON, OHIO
.1 NM SQUARES
AZIMUTH= 090

AMBIENT

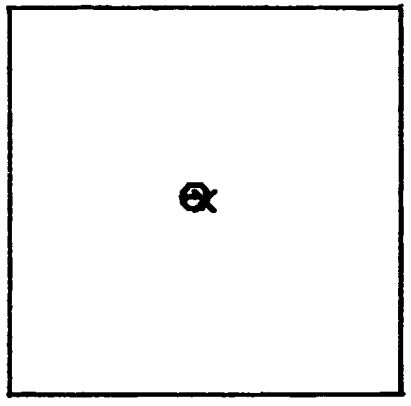

LIGHTNING

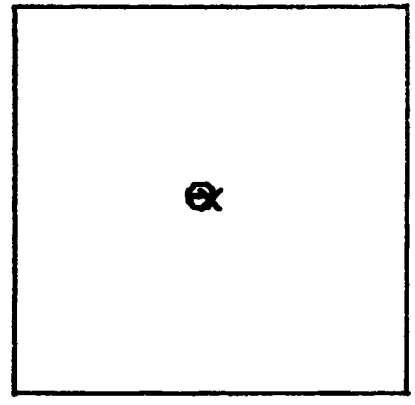

NUMBER OF POINTS 12		
CENTER	39	49.80 N
	84	2.20 W
S2 =	.00000	NM
S =	.00001	NM

NUMBER OF POINTS 12		
CENTER	39	49.80 N
	84	2.20 W
S2 =	.00000	NM
S =	.00001	NM

Figure 5-10.

TRIMBLE RECEIVER TEST
WPAFB DAYTON, OHIO
.1 NM SQUARES
AZIMUTH= 090

AMBIENT

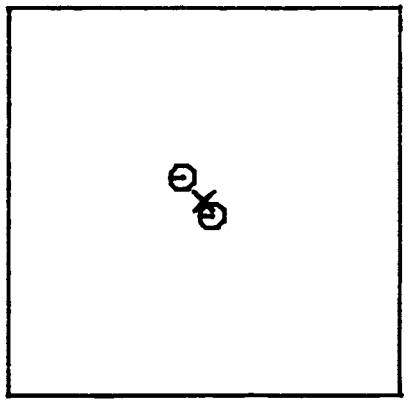

LIGHTNING

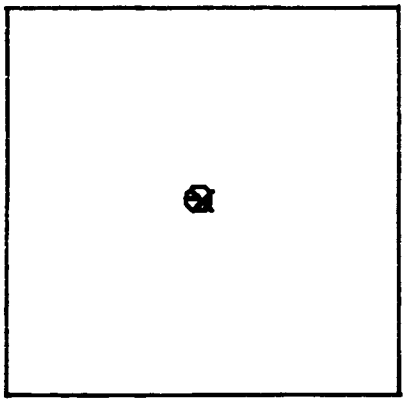

.05 NM

NUMBER OF POINTS 2
CENTER 39 49.80 N
84 2.20 W
S AND S2 NOT AVAILABLE

NUMBER OF POINTS 1
CENTER 39 49.80 N
84 2.20 W
S AND S2 NOT AVAILABLE

Figure 5-11.

TI9900 RECEIVER TEST
WPAFB DAYTON, OHIO
.1 NM SQUARES
AZIMUTH= 180

AMBIENT

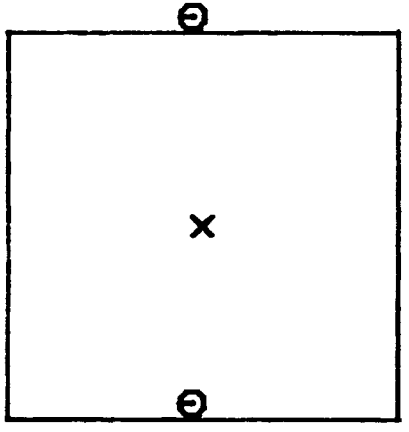

LIGHTNING

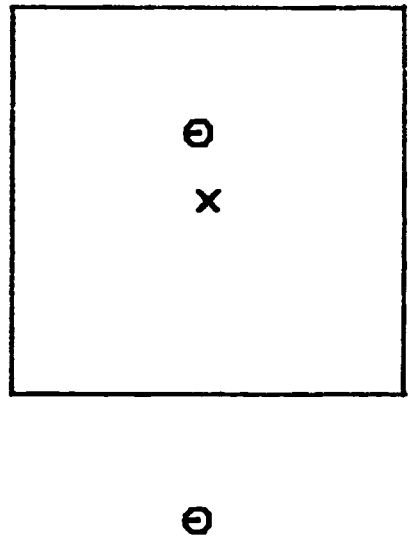

.05 NM

NUMBER OF POINTS 13
CENTER 39 49.75 N
84 2.20 W
S2 = .00003 NM
S = .00587 NM

NUMBER OF POINTS 12
CENTER 39 49.78 N
84 2.20 W
S2 = .00002 NM
S = .00440 NM

Figure 5-12.

TRIMBLE RECEIVER TEST
WPAFB DAYTON, OHIO
.1 NM SQUARES
AZIMUTH= 180

AMBIENT

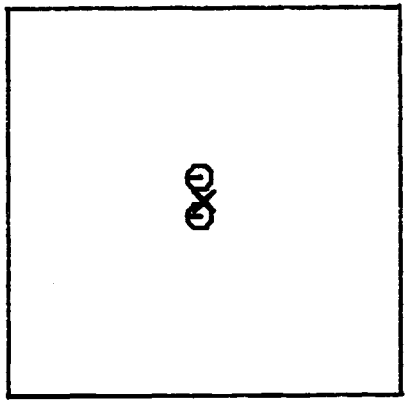

LIGHTNING

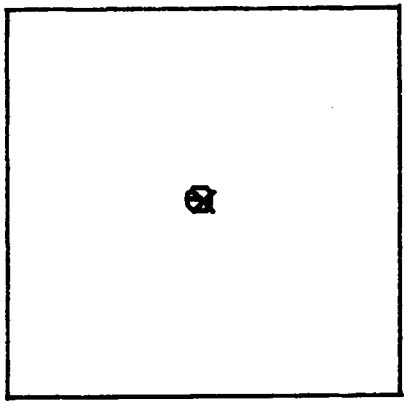

.05 NM

NUMBER OF POINTS 2
CENTER 39 48.78 N
84 2.20 W
S AND S2 NOT AVAILABLE

NUMBER OF POINTS 1
CENTER 39 48.78 N
84 2.20 W
S AND S2 NOT AVAILABLE

Figure 5-13.

TI9900 RECEIVER TEST
WPAFB DAYTON, OHIO
.1 NM SQUARES
AZIMUTH= 270

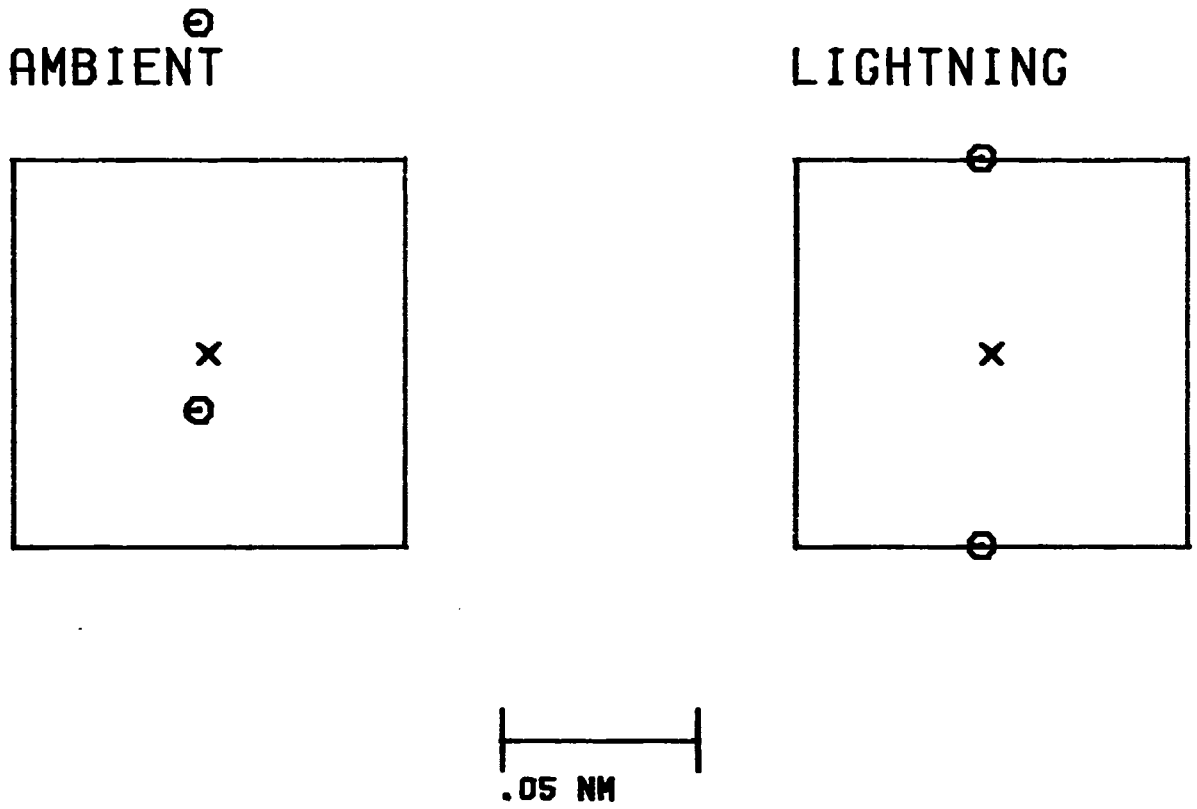

NUMBER OF POINTS 13		
CENTER	39	49.71 N
	84	2.20 W
S2 =	.00002	NM
S =	.00425	NM

NUMBER OF POINTS 12		
CENTER	39	49.75 N
	84	2.20 W
S2 =	.00003	NM
S =	.00591	NM

Figure 5-14.

TRIMBLE RECEIVER TEST
WPAFB DAYTON, OHIO
.1 NM SQUARES
AZIMUTH= 270

AMBIENT

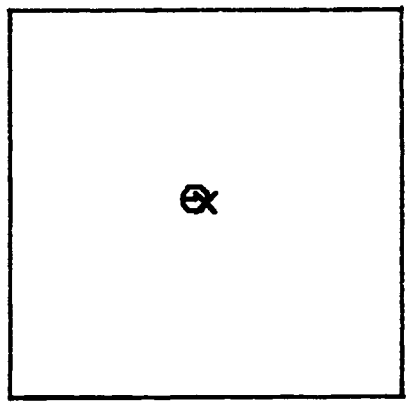

NUMBER OF POINTS 2
CENTER 39 49.75 N
84 2.20 W
S AND S2 NOT AVAILABLE

LIGHTNING

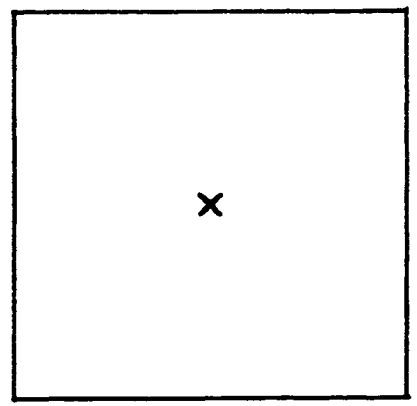

.05 NM

NUMBER OF POINTS 2
CENTER 39 49.75 N
84 2.20 W
S AND S2 NOT AVAILABLE

to see if this produces any significant position errors. There were two antennas, one for each of the Loran-C receivers. One is a long-wire antenna and the other is a small whip antenna approximately 30 inches in length. The Trimble Model 10A antenna is a custom-made antenna provided for our testing by Trimble Navigation. This antenna consists of an antenna base made of Derlyn plastic with a fiberglass whip antenna and a metal conductor placed in the whip, Figure 5-15. The preamplifier was built into the base and calibrated at the factory to provide essentially identical performance as the recommended 8-foot whip typically used in marine Loran-C applications. The antenna used with the TI-9900 Loran-C receiver is a long wire that is connected from the top of the aircraft above the door, to near the top of the rudder, Figure 5-16. The capacitance of this antenna is approximately 45 pf at 100 KHz, which is sufficent to operate the receiver according to the designers at Texas Instruments.

To induce the static electric field, a set of parallel aluminium plates were placed equally on either side of the antenna. See Figure 5-17, a photo of the Trimble 10-A antenna with the static field generator in place. One side of the pair of plates was connected to the airframe ground and the other plate was connected to the high voltage supply. The field was increased 10 KV/meter from 0 KV to 100 KV/meter. This relates to a voltage across the plates of between 1.0 Kv and 10.0 Kv. The plates were separated by 10.0 cm. to provide easy field calculation neglecting the effects of fringing at the edges of the parallel plates.

Almost the entire antenna was immersed in the static field for the Trimble receiver, while only a small portion of the TI-9900 antenna was immersed in the field due to constraints on the physical size of the parallel plates.

The data collection equipment used with this testing was the same as that used in the ground lightning simulation testing described above. The method of testing was to take data on the output of each of the receivers on the Heath H-89 digital computer for between 3 and 5 minutes at each power supply output voltage. The data started with the HV power supply at 0 volts and then increased 1000 volts every 3-5 minutes until 10 Kv was reached. With a 10 cm spacing on the parallel plates, this resulted in fields from 0 to 100 KV/meter which are representive of the electric fields encountered during flights near thunderstorms. The ambient field data output of the receivers was taken with the voltage on the plates at 0 volts. This was used as a control to determine the baseline of the output data for the static field tests.

2. Static Electric Field Test Results. The results of the static fields on the antennas is presented in a similar manner as in the ground lightning simulation testing. Figures 5-18 to 5-25 are the output plots for electric fields of 10, 20, 50 and 100 KV/meter with Figure 5-26 being a summary of the results plotted as standard deviation vs. static electric field intensity. The summary plot indicates a trend toward a position output bias. Even with the TI-9900 receiver, which shows the highest values of standard deviation, this was still a position error of

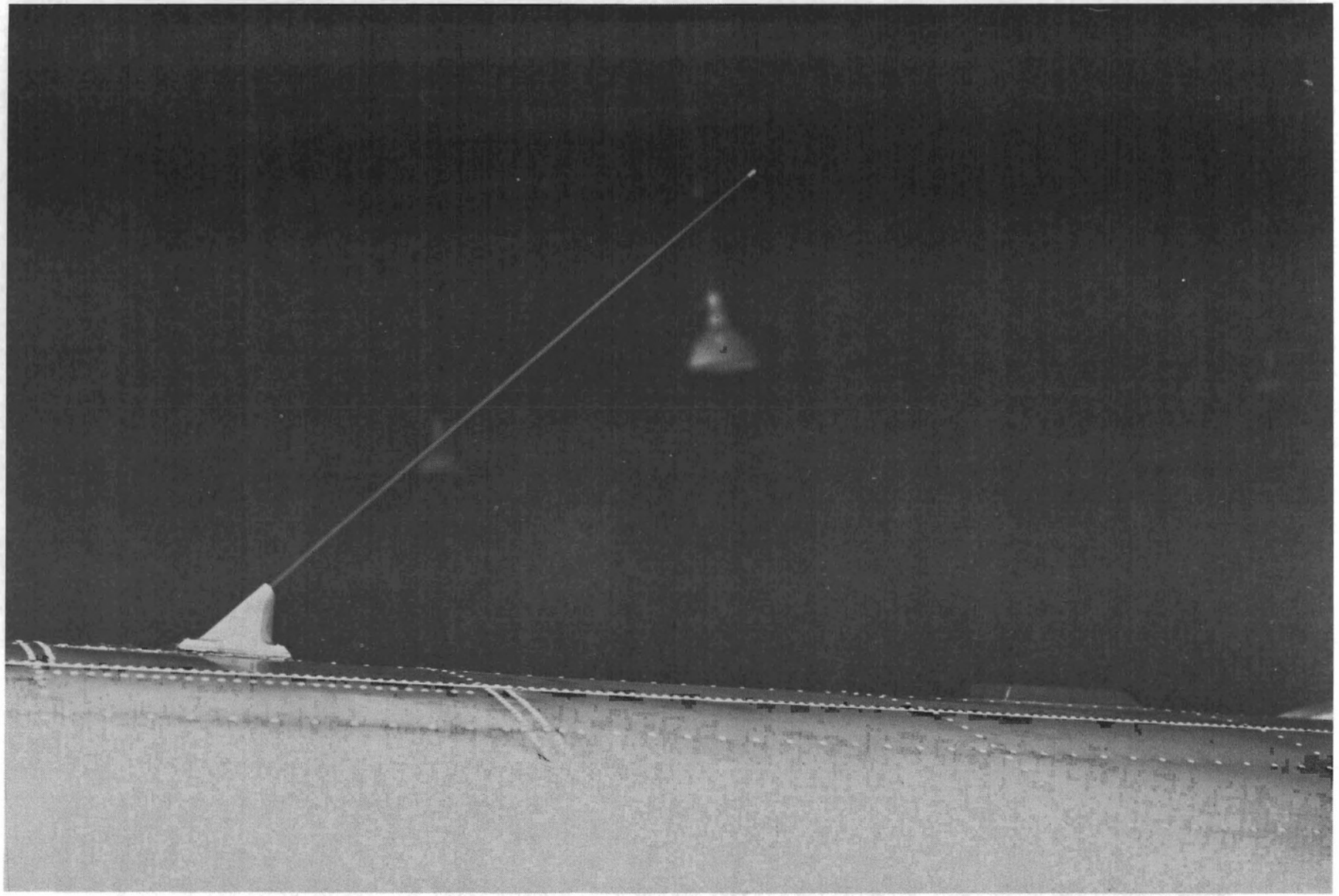

Figure 5-15. Trimble Loran-C Antenna and StormScope Antenna.

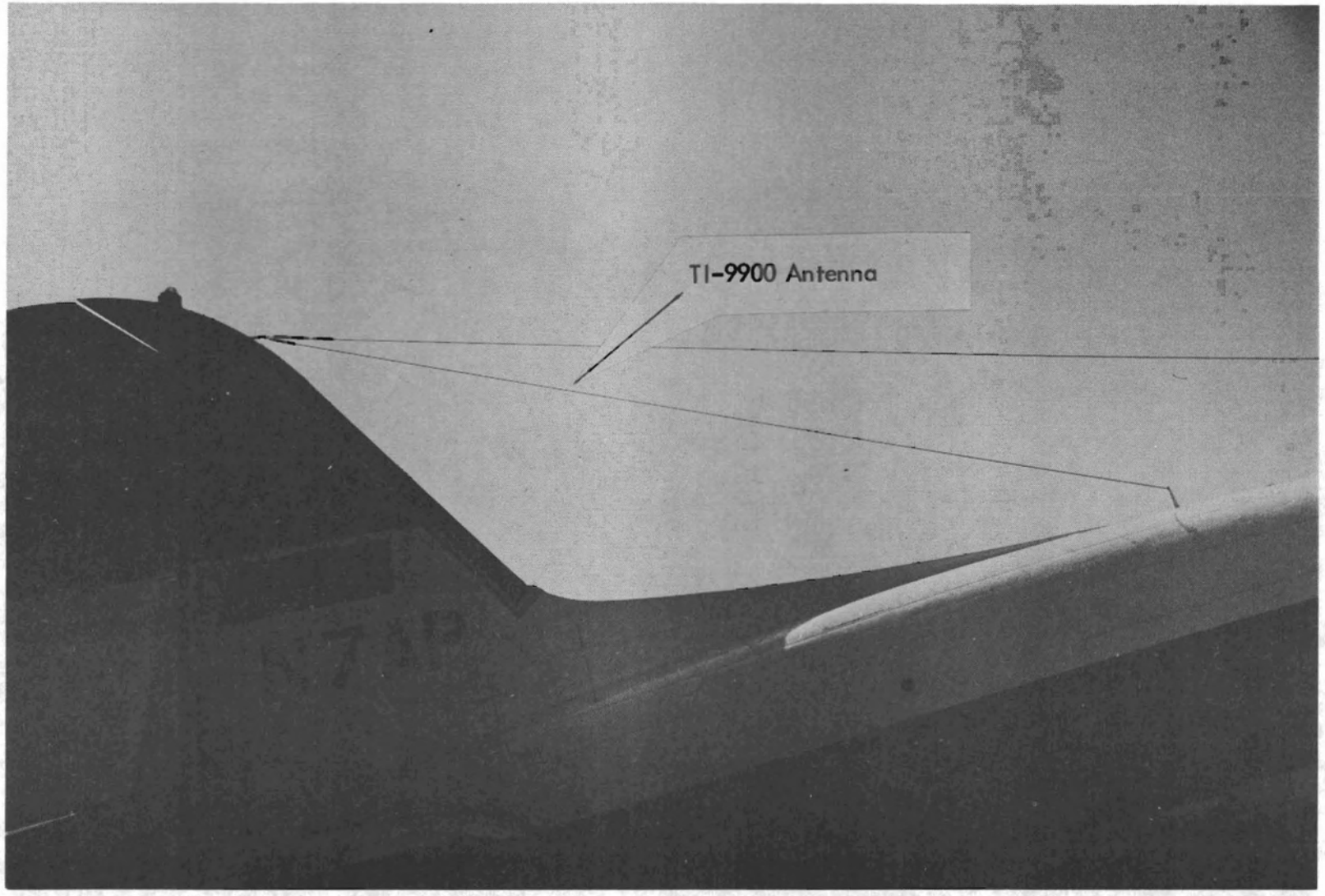

Figure 5-16. TI-9900 Loran-C Antenna.

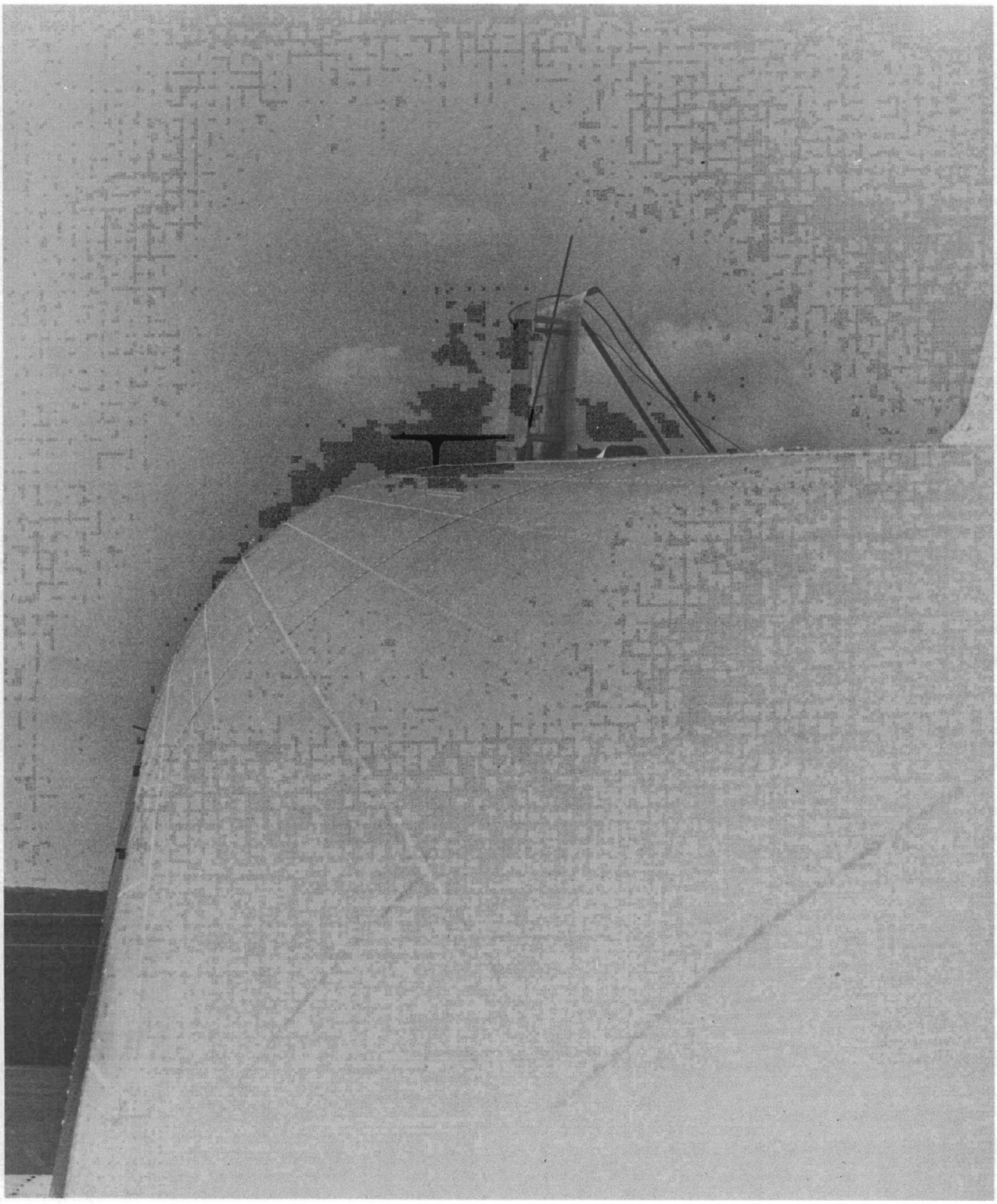

Figure 5-17. Static Field Fixture Around Trimble Loran-C Antenna.

Figure 5-18.

TI9900 RECEIVER APPLIED STATIC FIELD TEST
WPAFB DAYTON, OHIO
.1 NM SQUARES
10 KV/METER

AMBIENT

STATIC FIELD

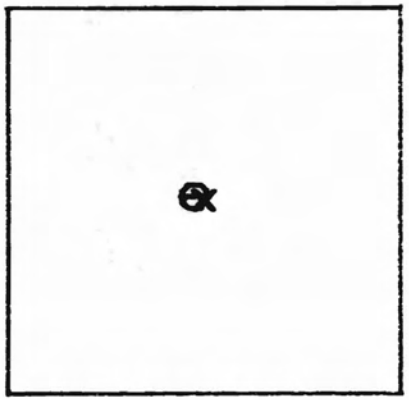

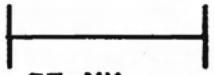

.05 NM

NUMBER OF POINTS 7
CENTER 39 48.80 N
64 2.20 W
S2 = .00000 NM
S = .00001 NM

NUMBER OF POINTS 7
CENTER 39 48.80 N
64 2.20 W
S2 = .00000 NM
S = .00001 NM

Figure 5-19.

TRIMBLE RECEIVER APPLIED STATIC FIELD TEST
WPAFB DAYTON, OHIO
.1 NM SQUARES
10 KV/METER

AMBIENT

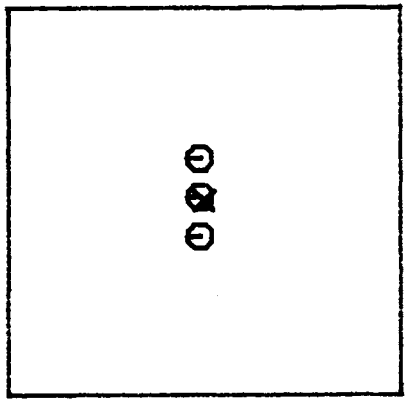

STATIC FIELD

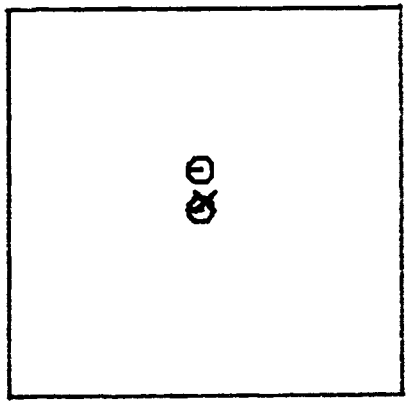

.05 NM

NUMBER OF POINTS 3
CENTER 39 49.58 N
84 1.95 W
S2 = .00000 NM
S = .00113 NM

NUMBER OF POINTS 4
CENTER 39 49.57 N
84 1.95 W
S2 = .00000 NM
S = .00057 NM

Figure 5-20.

TI9900 RECEIVER APPLIED STATIC FIELD TEST
WPAFB DAYTON, OHIO
.1 NM SQUARES
20 KV/METER

AMBIENT

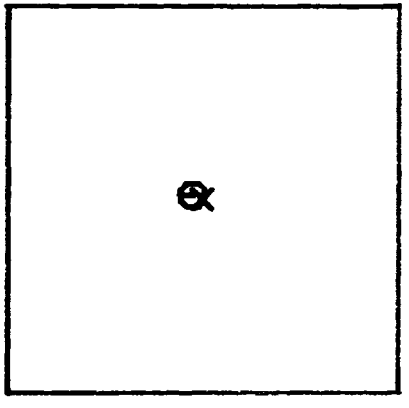

STATIC FIELD

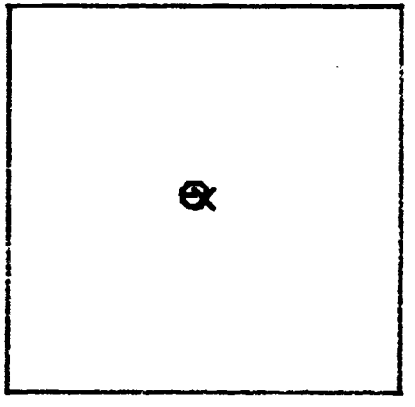

.05 NM

NUMBER OF POINTS 7		
CENTER	39	49.80 N
	84	2.20 W
S2 =	.00000	NM
S =	.00001	NM

NUMBER OF POINTS 7		
CENTER	39	49.80 N
	84	2.20 W
S2 =	.00000	NM
S =	.00001	NM

Figure 5-21

TRIMBLE RECEIVER APPLIED STATIC FIELD TEST
WPAFB DAYTON, OHIO
.1 NM SQUARES
20 KV/METER

AMBIENT

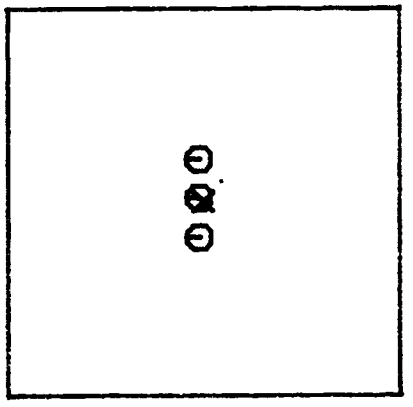

STATIC FIELD

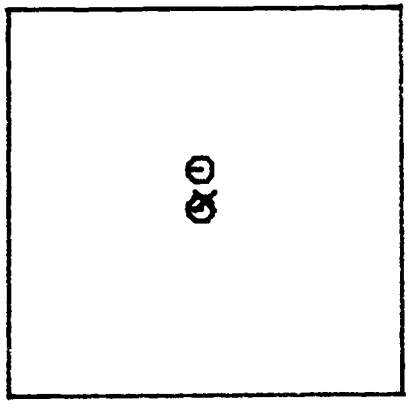

.05 NM

NUMBER OF POINTS 3		
CENTER	39	49.58 N
	84	1.95 W
S2 =	.00000	NM
S =	.00113	NM

NUMBER OF POINTS 4		
CENTER	39	49.57 N
	84	1.95 W
S2 =	.00000	NM
S =	.00057	NM

Figure 5-22.

TI9900 RECEIVER APPLIED STATIC FIELD TEST
WPAFB DAYTON, OHIO
.1 NM SQUARES
50 KV/METER

AMBIENT

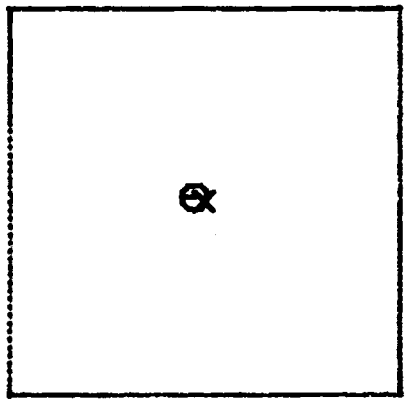

STATIC FIELD

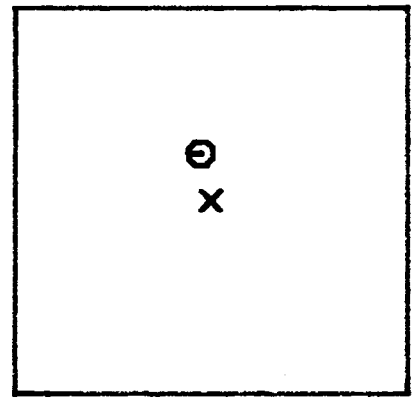

NUMBER OF POINTS 7
CENTER 39 49.80 N
84 2.20 W
S2 = .00000 NM
S = .00001 NM

NUMBER OF POINTS 9
CENTER 39 49.78 N
84 2.20 W
S2 = .00001 NM
S = .00377 NM

Figure 5-23.

TRIMBLE RECEIVER APPLIED STATIC FIELD TEST
WPAFB DAYTON, OHIO
.1 NM SQUARES
50 KV/METER

AMBIENT

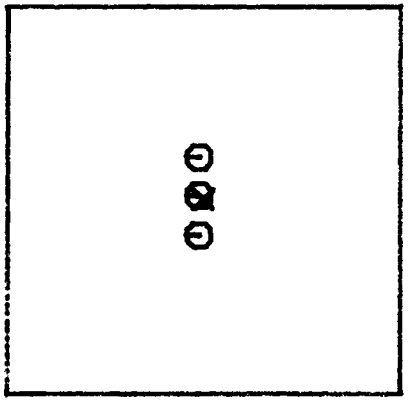

STATIC FIELD

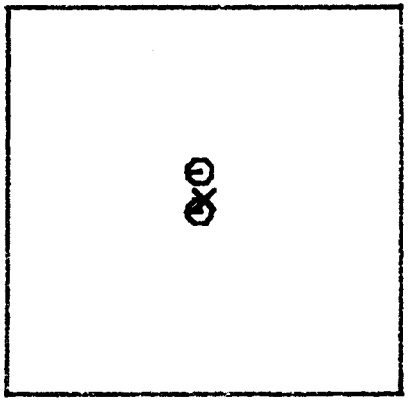

NUMBER OF POINTS 3		
CENTER	39	49.58 N
	84	1.95 W
S2 =	.00000	NM
S =	.00113	NM

NUMBER OF POINTS 3		
CENTER	39	49.58 N
	84	1.95 W
S2 =	.00000	NM
S =	.00065	NM

Figure 5-24.

TI9900 RECEIVER APPLIED STATIC FIELD TEST
WPAFB DAYTON, OHIO
.1 NM SQUARES
100 KV/METER

AMBIENT

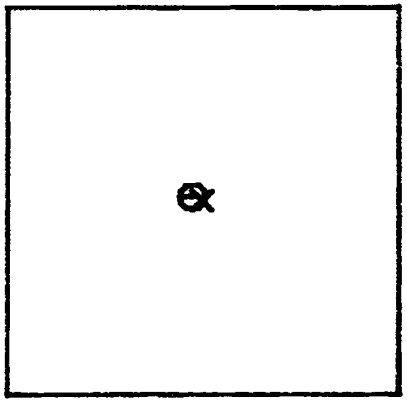

STATIC FIELD

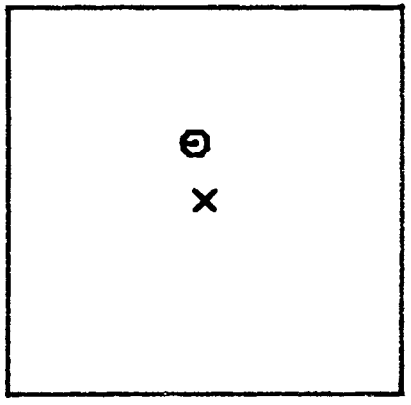

NUMBER OF POINTS 7		
CENTER	39	49.80 N
	84	2.20 W
S2 =	.00000	NM
S =	.00001	NM

NUMBER OF POINTS 7		
CENTER	39	49.78 N
	84	2.20 W
S2 =	.00002	NM
S =	.00428	NM

Figure 5-25.

TRIMBLE RECEIVER APPLIED STATIC FIELD TEST
WPAFB DAYTON, OHIO
.1 NM SQUARES
100 KV/METER

AMBIENT

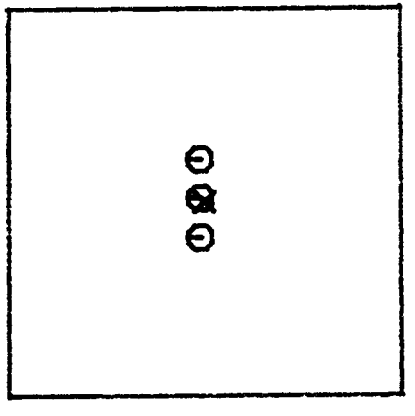

STATIC FIELD

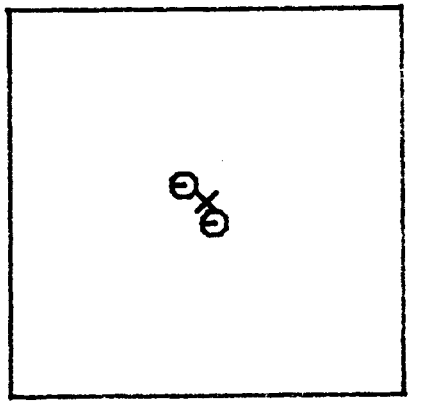

.05 NM

NUMBER OF POINTS 3		
CENTER	39	49.58 N
	84	1.95 W
S2 =	.00000	NM
S =	.00113	NM

NUMBER OF POINTS 3		
CENTER	39	49.59 N
	84	1.96 W
S2 =	.00000	NM
S =	.00099	NM

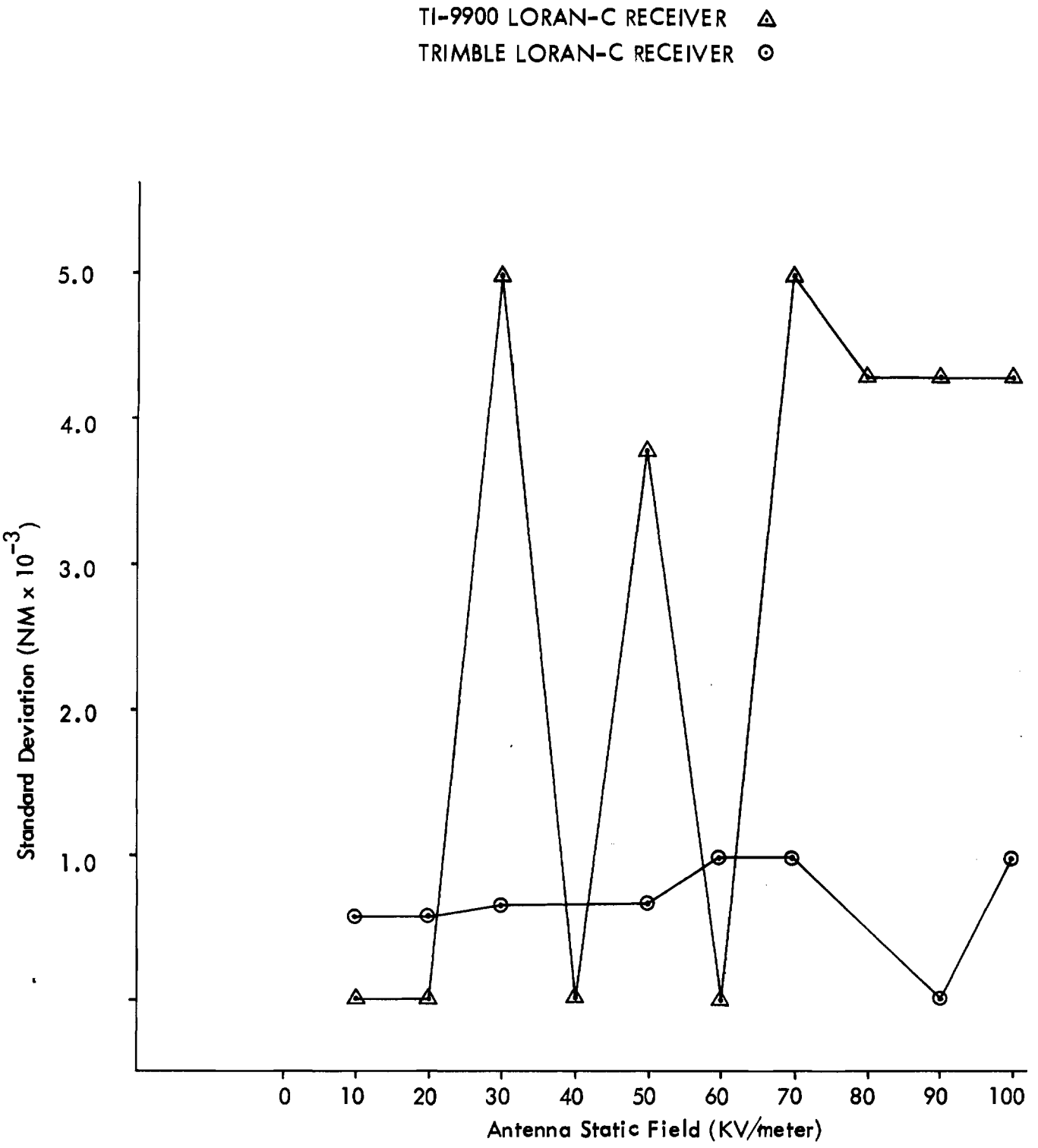

Figure 5-26. Static Field Testing.
WPAFB Dayton, Ohio September 1981.

30 ft. The 100 KV/meter electric field intensity is a very high value that would indicate a good possibility of lightning near the aircraft. The static field antenna measurements were one way of evaluating the dynamic performance of the antenna preamplifier because the high static fields can cause failures in the preamp if it was not properly designed. Also, the high static field can cause a decrease in the dynamic range of the receiver if the preamp is DC coupled to the antenna. If the aircraft becomes charged due to p-static, the static electric fields due to this charging will produce a static electric field around the antenna. This static electric field will generally not be as strong as the fields produced near thunderstorm activity.

One point to note about the position output data from the Trimble receiver is the deviation in position of the receiver in the static field test as compared with the receiver output position determined in the lightning simulation testing (Figures 5-8 and 5-19). The size of the parallel plates was almost the same size as the height of the Trimble antenna. This shielding of the Trimble antenna was believed to cause the discrepancy in the Trimble receiver's ability to determine the true position. The signal-to-noise values determined by the Trimble receiver were smaller with the parallel plates than without the parallel plates which tends to support the fact that the receiver was seeing a shielding effect due to the presence of the parallel plates. This does not invalidate the data taken here because we were really only interested in the relative position errors which we were still able to measure. This effect was not observed in the TI-9900 because the parallel plates were small compared to the length of the antenna.

C. Summary of Ground Lightning and Static Field Tests.

In summary, the results of the ground lightning simulation testing of the Loran-C receivers has not produced significant results that conclusively point either way regarding the performance of the receivers in thunderstorm conditions. One problem was the inability of the lightning simulation equipment to produce a high repetition rate for the lightning strokes to contaminate significantly the received Loran-C signal. More flight testing near thunderstorm conditions will likely produce more relevant data.

The antenna static field measurements proved to be a very useful test which indicated that the preamplifier designs used in these receivers were adequate to handle the magnitude of static electric fields that might be encountered in the vicinity of lightning activity. This test was useful also because it allowed separating the effects of the static electric field with any other noise caused by natural charging on the airframe due to p-static or any noise due to lightning stroke activity.

VI. FLIGHT TESTS IN THUNDERSTORM CONDITIONS

1. Test Procedure. A combination of several means were used to position the aircraft near the thunderstorm activity for these tests. On the ground telephone calls to Flight Service and the National Weather Service radar facility at the Port Columbus Airport, along with observations of the StormScope in the aircraft, provided valuable information on the positions of the thunderstorm activity. The personnel at the Weather Service office were very helpful in providing copies of the radar scope overlays for use in determining, after the flights, where the principle rain activity was occurring.

In flight the StormScope and the weather radar on board the aircraft aided in locating the thunderstorm activity that was needed. Communications with Flight Service and ATC Center personnel were also helpful, although they were quite confused due to our continued requests to fly into the weather activity shown on their radar scopes.

The data collection equipment used during this series of flights consists of the following: the TI-9900 Loran-C receiver, Trimble Model 10A Loran-C receiver, the Heath H-89 digital computer with software, and handwritten notes taken during the flights. The serial output of the TI-9900 and Trimble 10A were recorded using the same merge software used in the ground lightning testing and output to the Byte Bucket Digital Cassette recorder. No discharger current or noise data were recorded as the quality of the output position of the receivers were the primary data of interest.

The TI-9900 has an output voltage that can drive a course deviation indicator. For these flights, the pilots were provided with a CDI with an indicator sensitivity of ±0.5 nm either side of course to track to the waypoints. This CDI was available for the pilots on flights after September 8, 1981.

There was a total of five flights made during this series of tests. Three of the flights were made in thunderstorm conditions and the other two were made in clear weather to determine the performance of the receiver without any thunderstorm activity in the area.

2. Thunderstorm Flight Test Results. Figures 6-1 and 6-2 are plots of the proposed flight paths for the flights in thunderstorm conditions conducted on August 29, 1981. The flight was performed in two legs; the first leg involved initially leaving UNI and proceeding directly to Midwest (MXQ) VOR to Appleton (APE) VOR landing at Port Columbus Airport. Approximately 35 nm from Ohio University (UNI), the MXQ VOR failed and the flight then diverted to Springfield (SGH) VOR and then Port Columbus via vectors to the approach. After visiting the National Weather Service Radar Facility and obtaining more information on the position of the weather, the return trip was started. This leg involved Port Columbus (CMH) directly to Zanesville (ZZV) VOR directly to UNI NDB and then directly to UNI. Figures 6-3 to 6-6 are the actual ground tracks for this flight for each of the Loran-C receivers. These figures have noted the

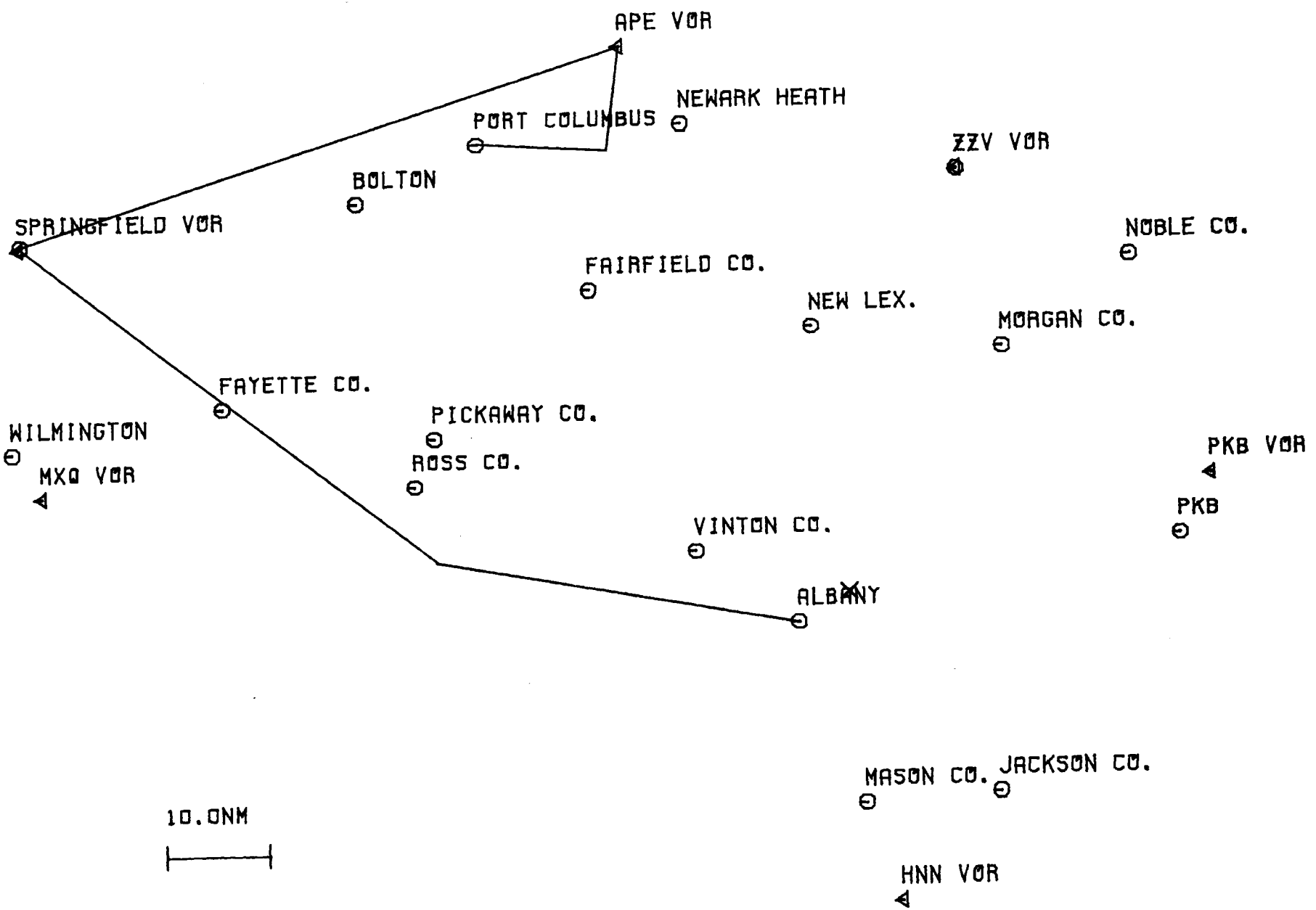

Figure 6-1. Flight Plan Route, August 29, 1981, UNI Towards SGH VOR To APE VOR Then Approach to Port Col, Thunderstorm Activity.

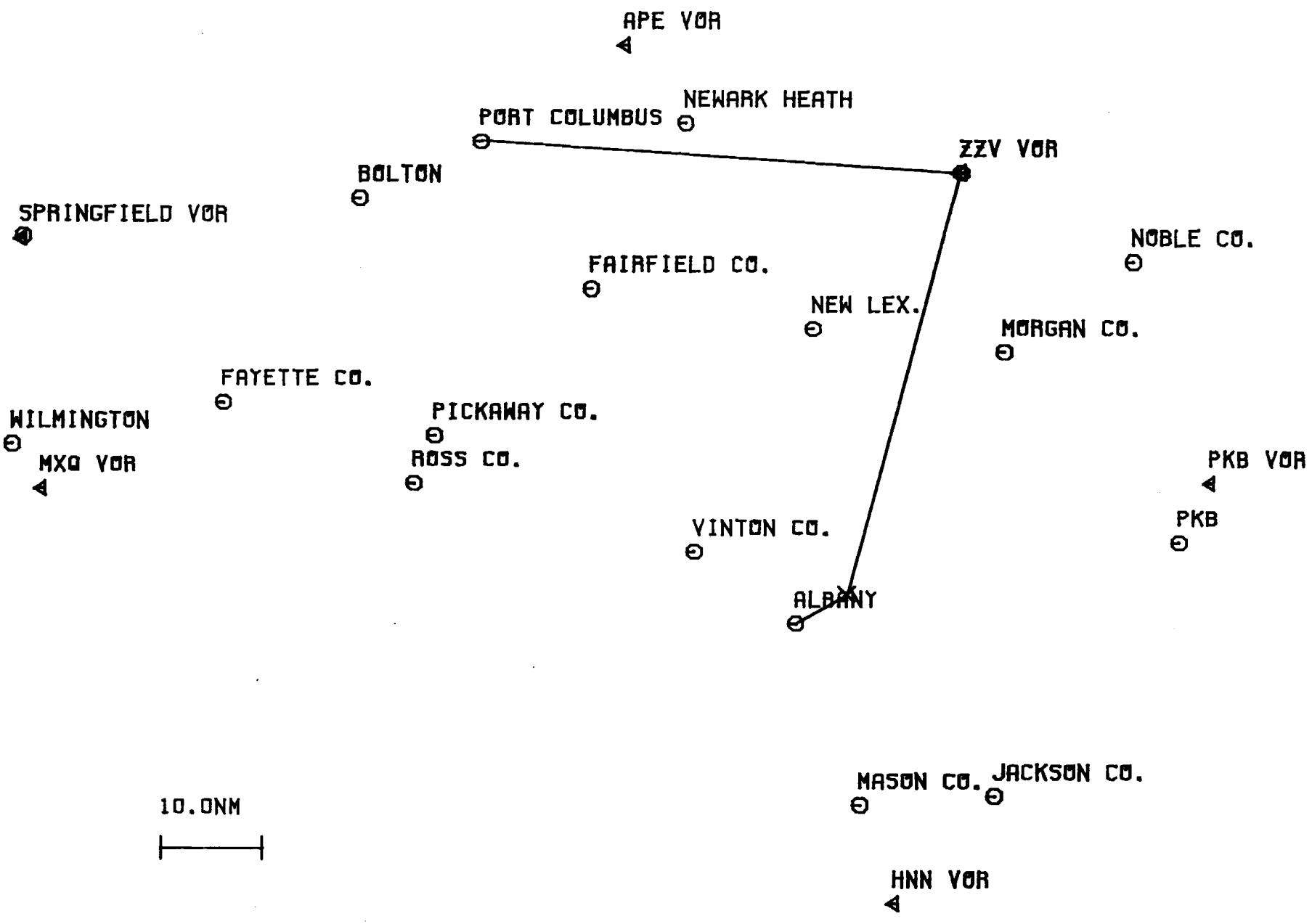

Figure 6-2. Flight Plan Route, August 29, 1981, Port Columbus to ZZV VOR to UNI NDB to UNI, Thunderstorm Activity.

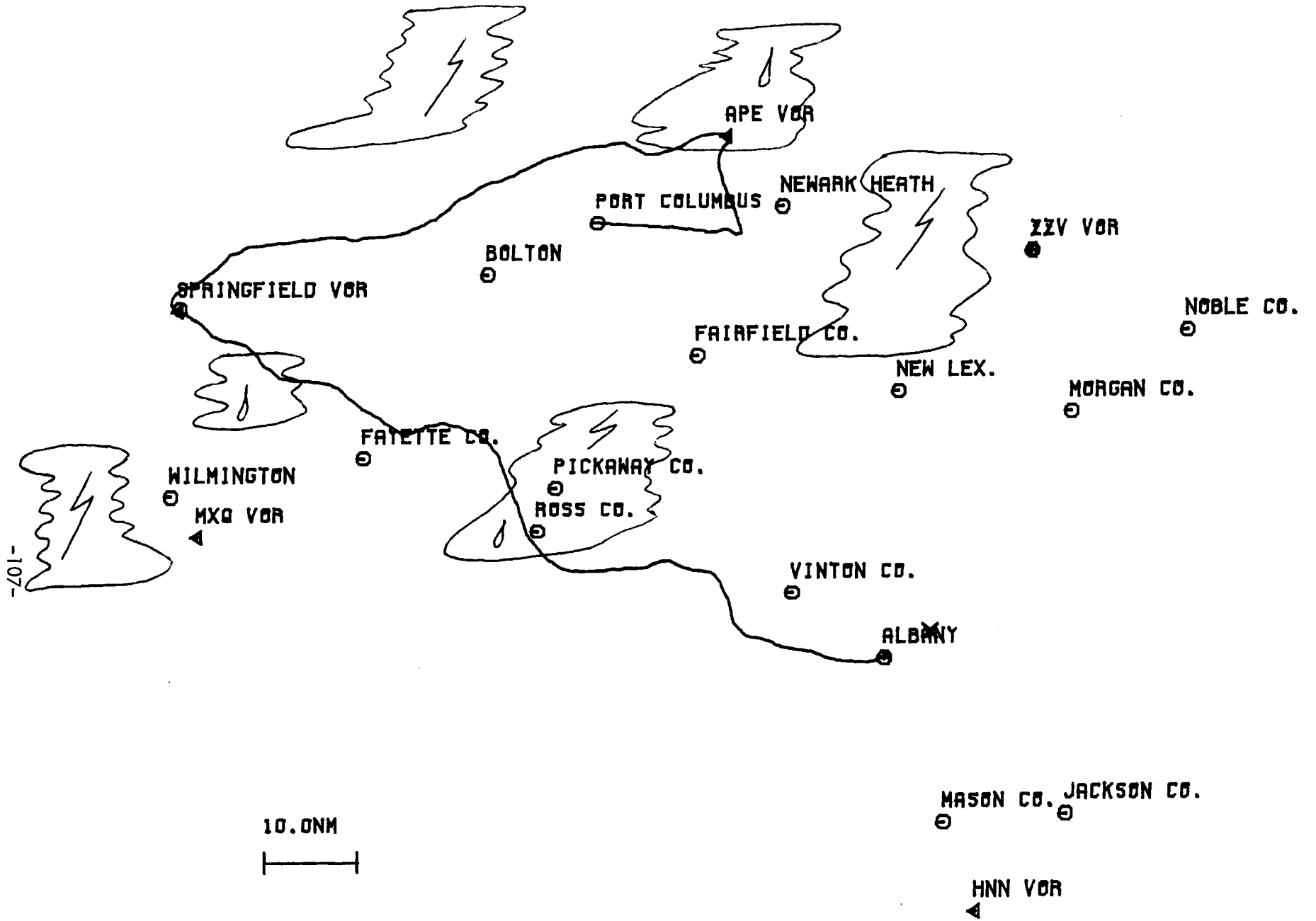

Figure 6-3. Flight Test TI9900 Receiver, August 29, 1981, UNI Towards SGH VOR To APE To Port Columbus, Thunderstorm Activity.

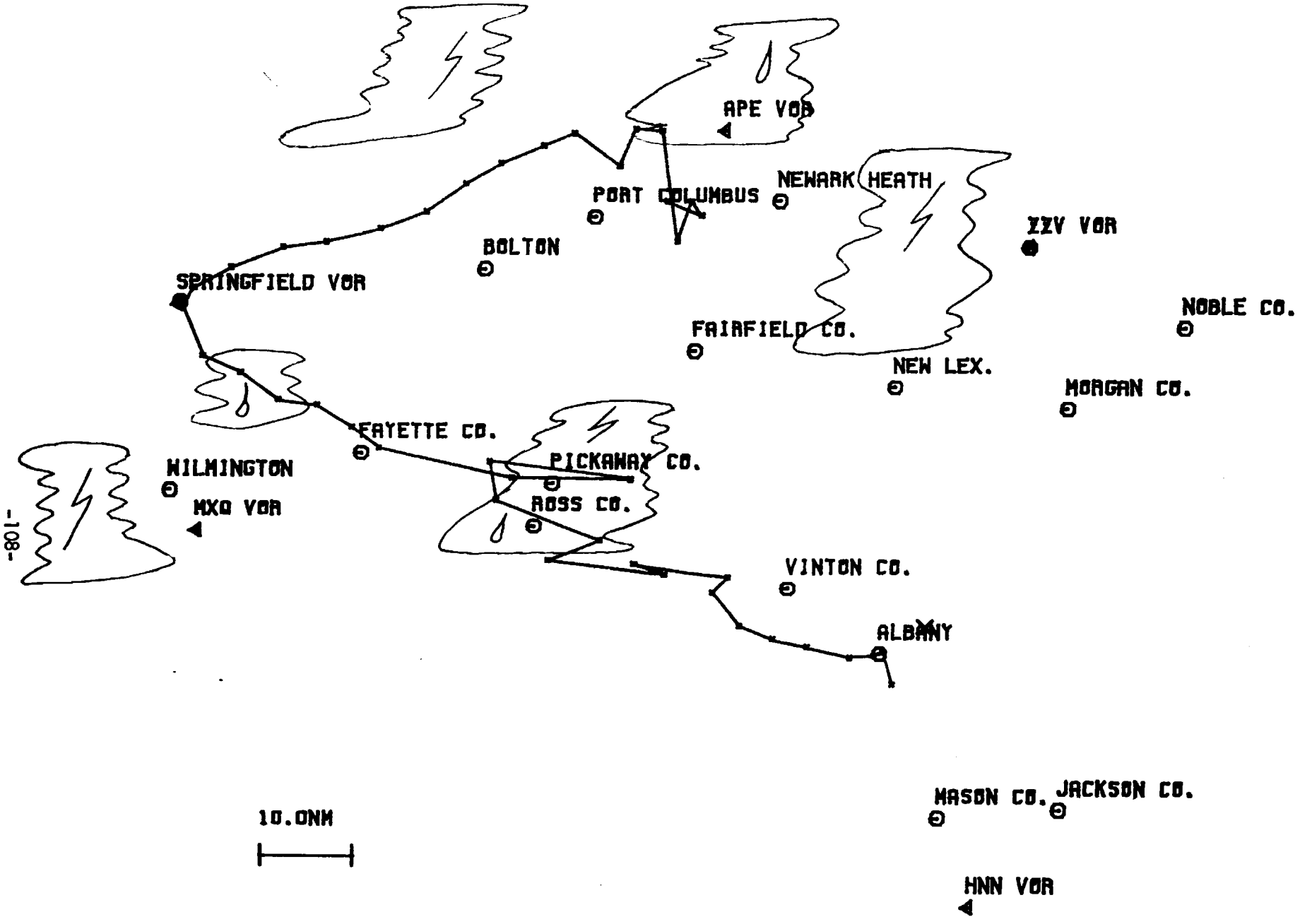

Figure 6-4. Flight Test Trimble Receiver, August 29, 1981, UNI To MXQ Divert to SGH to APE Landing at Port Columbus, Thunderstorm Activity.

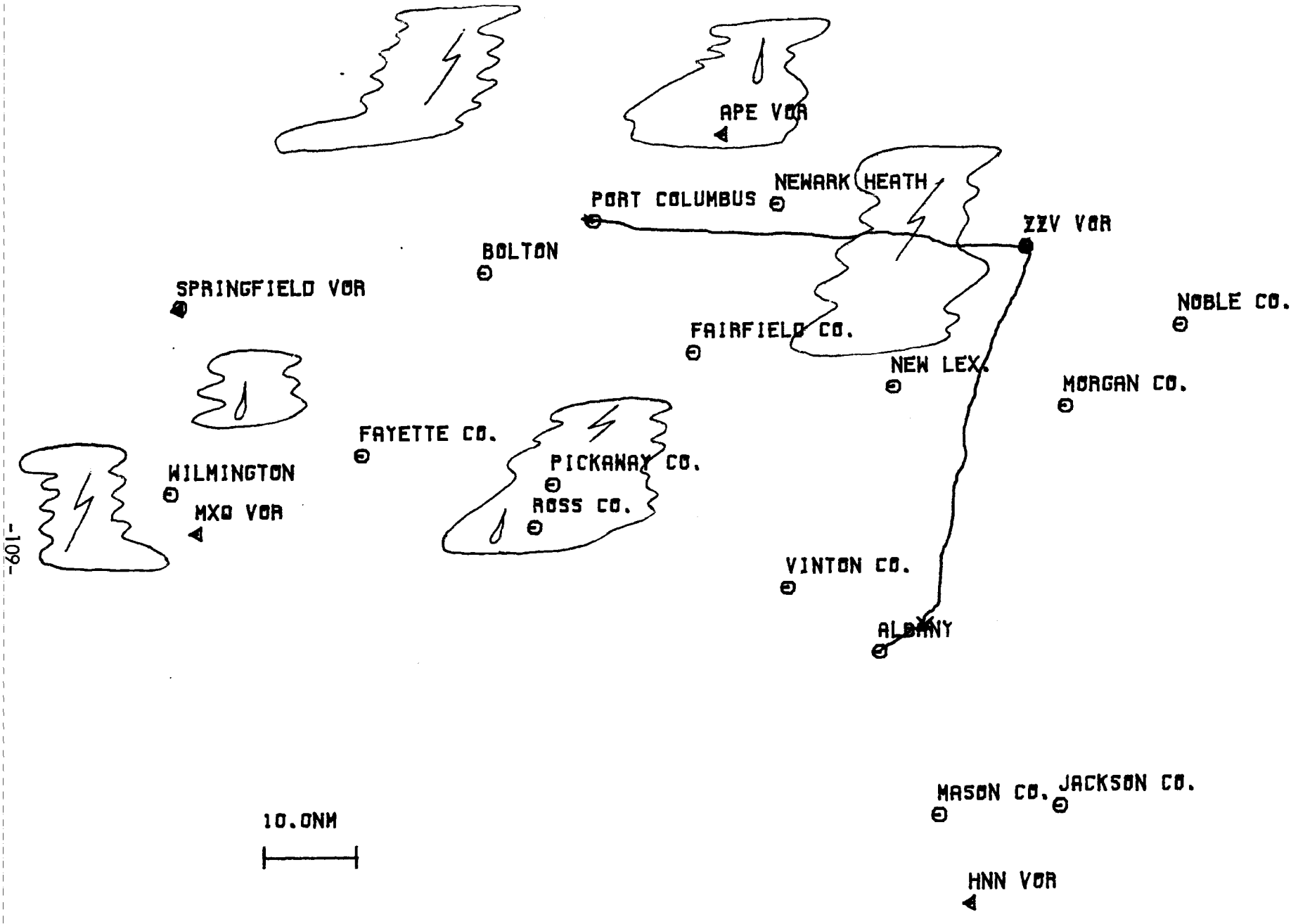

Figure 6-5. Flight Test TI9900 Receiver, August 29, 1981, Port Columbus to ZZV VOR to UNI NDB to UNI, Thunderstorm Activity.

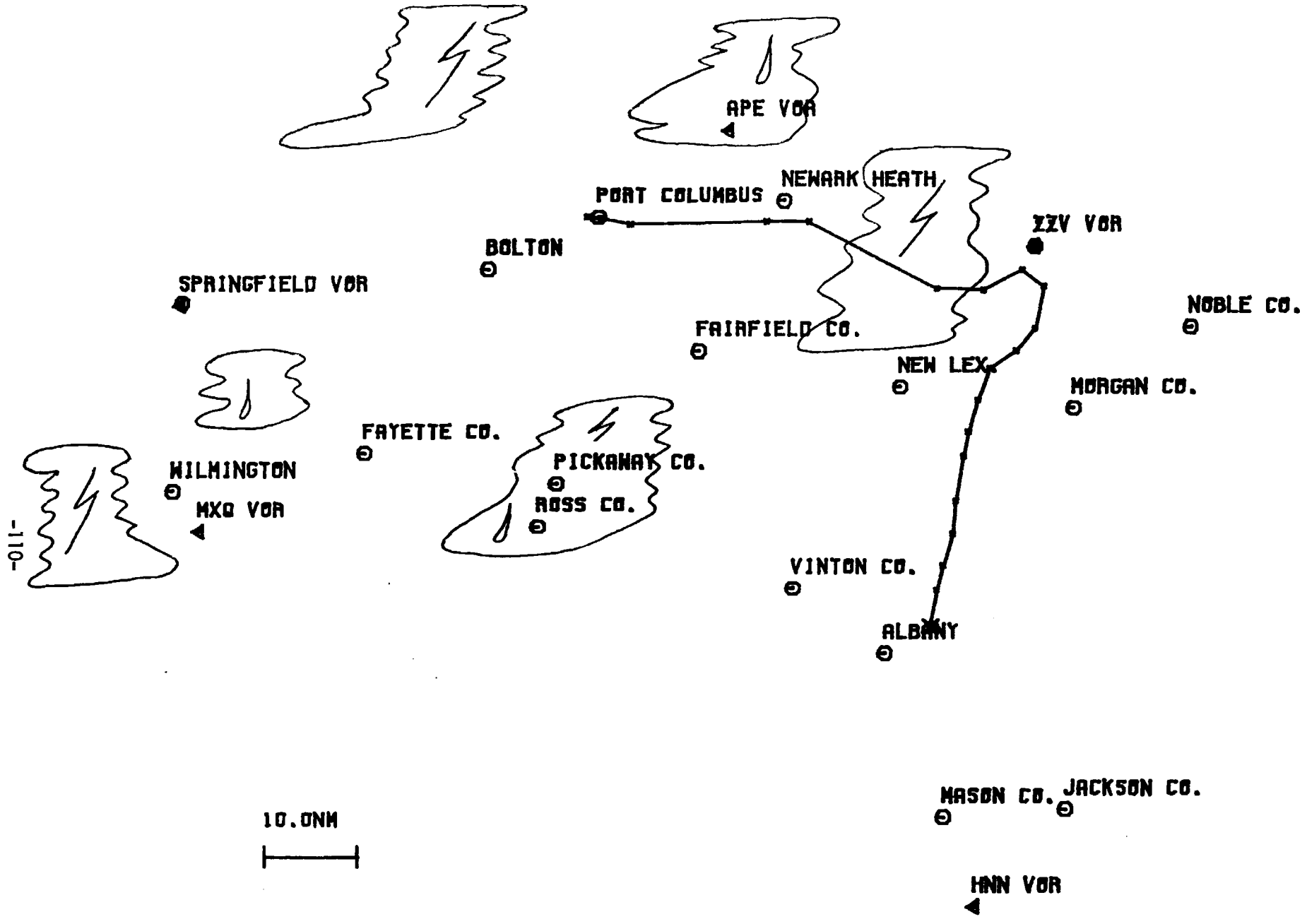

Figure 6-6. Flight Test Trimble Receiver, August 29, 1981, Port Columbus to ZZV to UNI NDB to UNI, Thunderstorm Activity.

thunderstorm and rain activity as noted by the radar and notes taken during the flight, Figure 6-7. The plots of the TI-9900 receiver indicate that the continuity of the ground track is good and that the receiver apparently had no problem with reception of the Loran-C stations with the lightning activity in the area. In monitoring the receiver during the flight, the signal-to-noise levels were quite acceptable with approximately 5 to 6 db variation in the signal-to-noise levels.

The Trimble receiver appeared to have a little more difficulty but this was believed to be due more to the slow update rate and signal tracking algorithm rather than the atmospheric noise during the flight. The Trimble receiver also indicated adequate signal-to-noise values so that it was not having problems receiving the Loran-C stations.

Overall, the results were impressive as the ground tracks plotted indicated good accuracy. The coordinates for the ground fixes were obtained from IFR facilities directories or were determined from latitude and longitude measurements made off VFR sectional charts. The ground tracks plotted indicate that the Loran C was definitely able to provide good enroute navigation information.

Figure 6-8 is the plot of the proposed flight path for the test conducted August 31, 1981 in thunderstorm conditions. The proposed flight path begins at UNI airport directly to Midwest VOR directly to Appleton VOR directly to the UNI NDB and then directly to UNI airport. Takeoff time for this flight was 3:16 P.M. Figures 6-9 to 6-11 are radar scope overlays of the weather approximately every hour starting just before takeoff time. This information along with notes taken during the flight regarding rain and lightning activity is shown on Figures 6-12 and 6-13, the ground tracks of the Trimble and TI-9900 receivers. The receivers indicated during the flight that the signal-to-noise of the Loran-C was adequate for tracking. The aircraft charging was also monitored during the flight with currents less than 100 micro-amps indicated. This flight was conducted at 6000 ft. MSL. At the Appleton VOR the aircraft was flying through an area of moderate rain. The StormScope indicated electrical activity essentially in all directions at ranges as low as 10 nm. There was lightning in clouds in the vicinity of Midwest VOR. The southern deviation on the leg between UNI and MXQ was to approach what appeared to be a thunderstorm build-up in that area. Figure 6-13 indicates this deviation very accurately for both receivers.

The final flight in thunderstorm conditions was conducted on October 1, 1981. The 1½ hour flight was conducted in the heaviest weather yet encountered in this test program. A fast moving cold front moved through Ohio setting off level 3 and 4 thunderstorm activity. Level 3 thunderstorm activity consists of possible severe turbulence and lightning with level 4 described as severe turbulence likely with ligntning. During this flight a prototype of a weather radar uplink receiver was installed in the aircraft [3]. This receiver was part of an evaluation of a weather radar uplink system, conducted by Ohio University, which uplinks to the aircraft, the Port Columbus National Weather Service WSR-74C weather radar information on

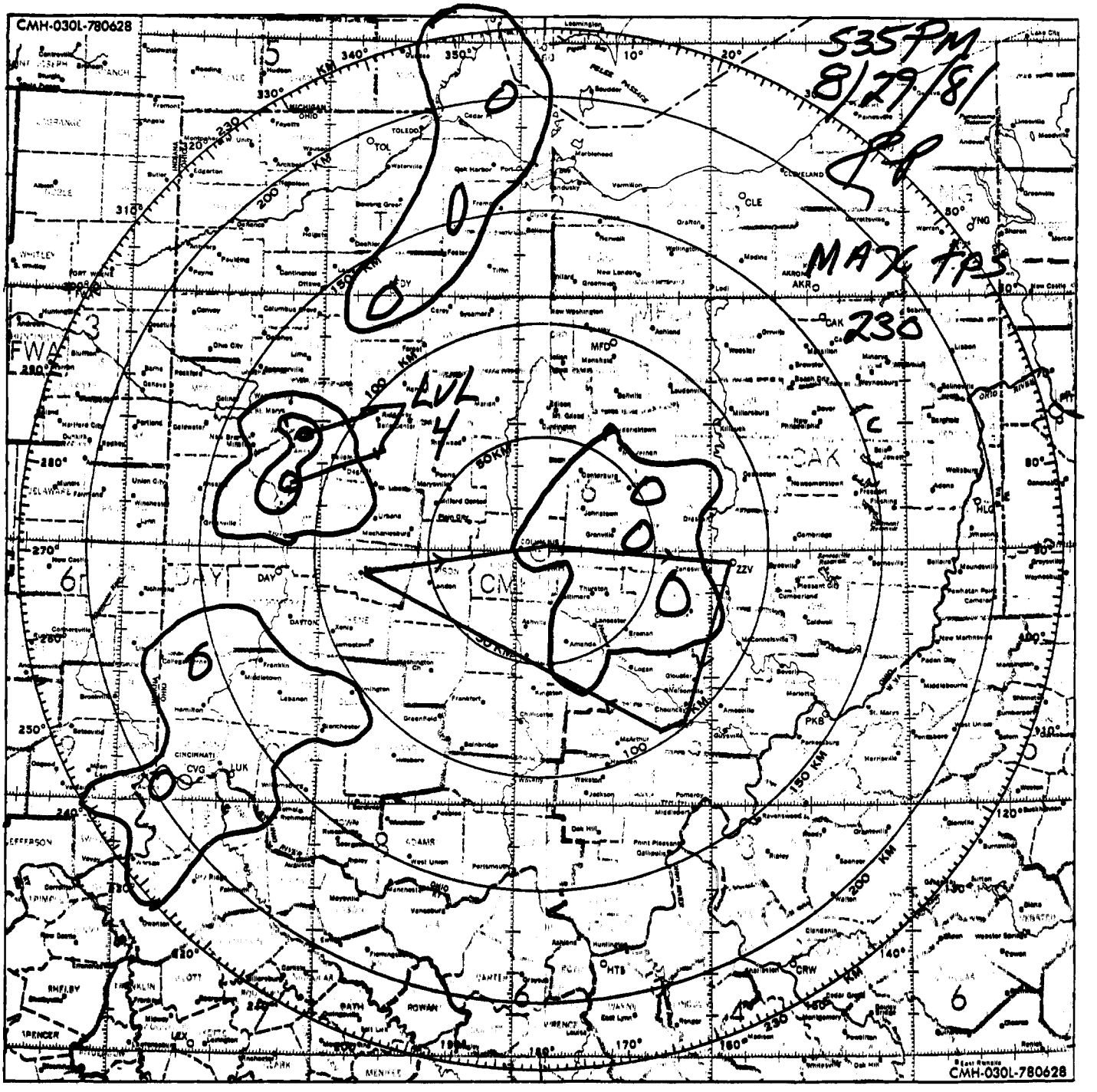

Figure 6-7. Radar Overlay for Flight of August 29, 1981.

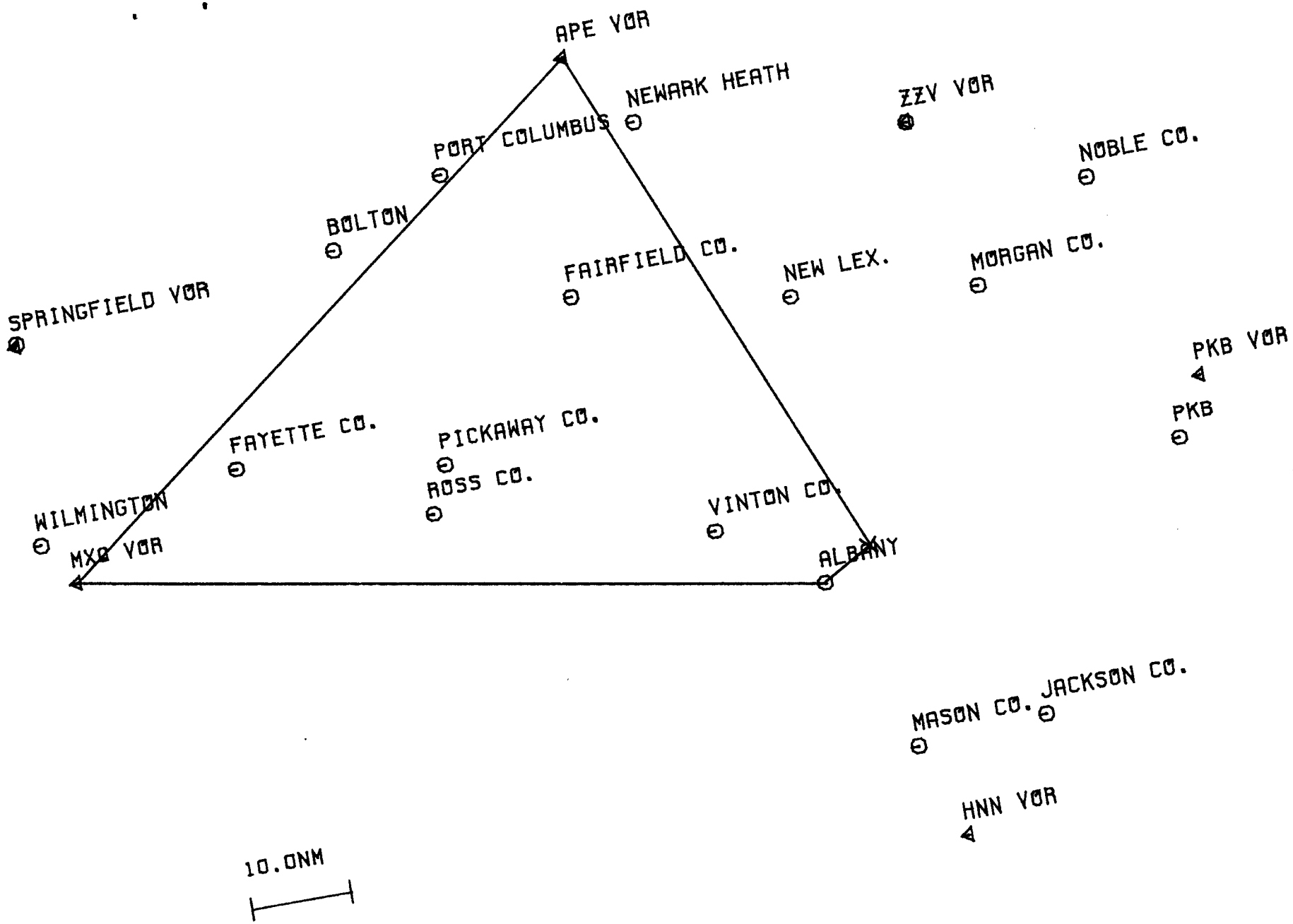

Figure 6-8.
FLIGHT PLAN ROUTE
AUGUST 31,1981
UNI TO MXQ TO APE TO UNI NDB TO UNI
OPERATION ACTIVY

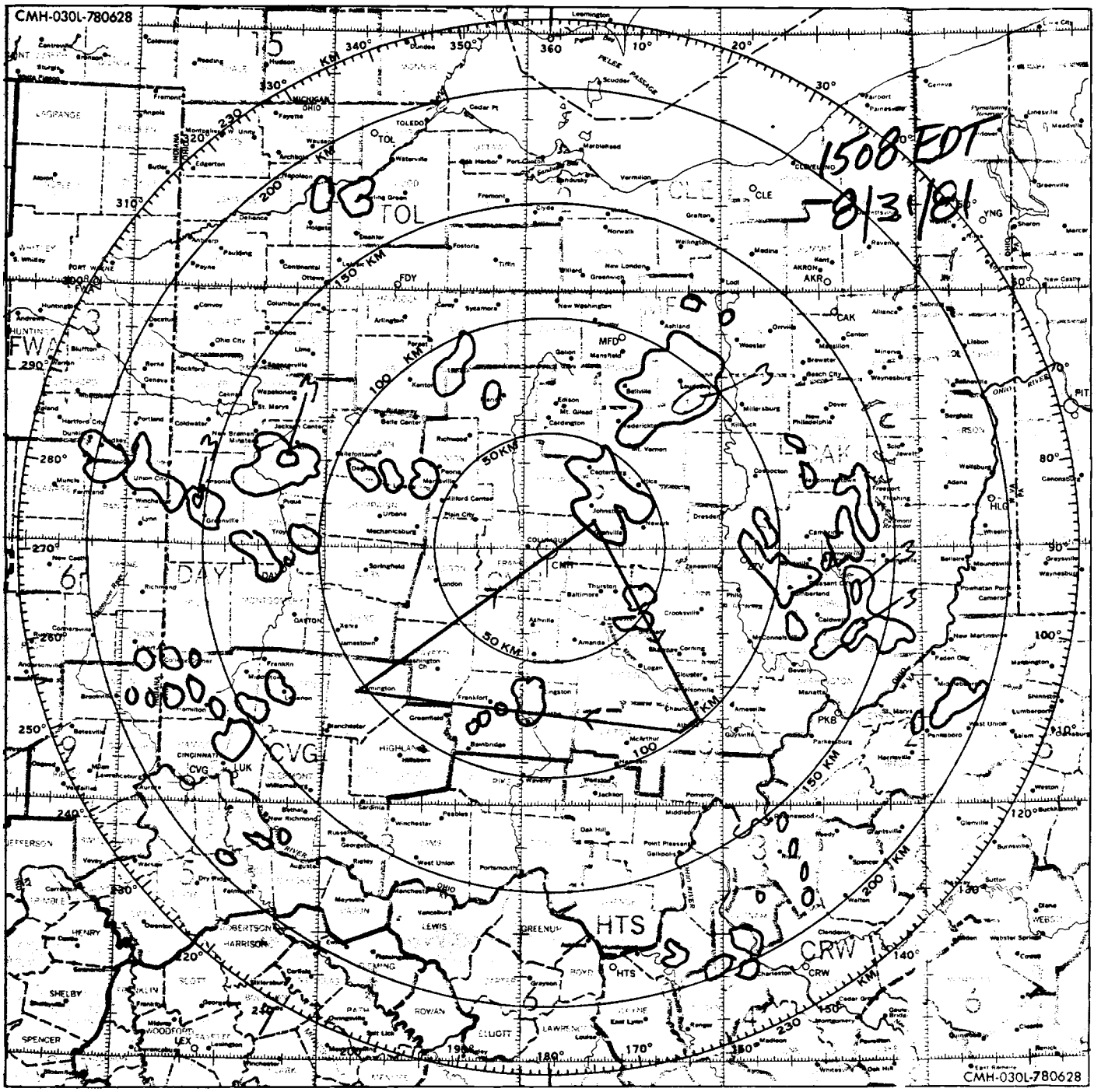

Figure 6-9. Radar Overlay August 31, 1981 - 15:08 P.M.

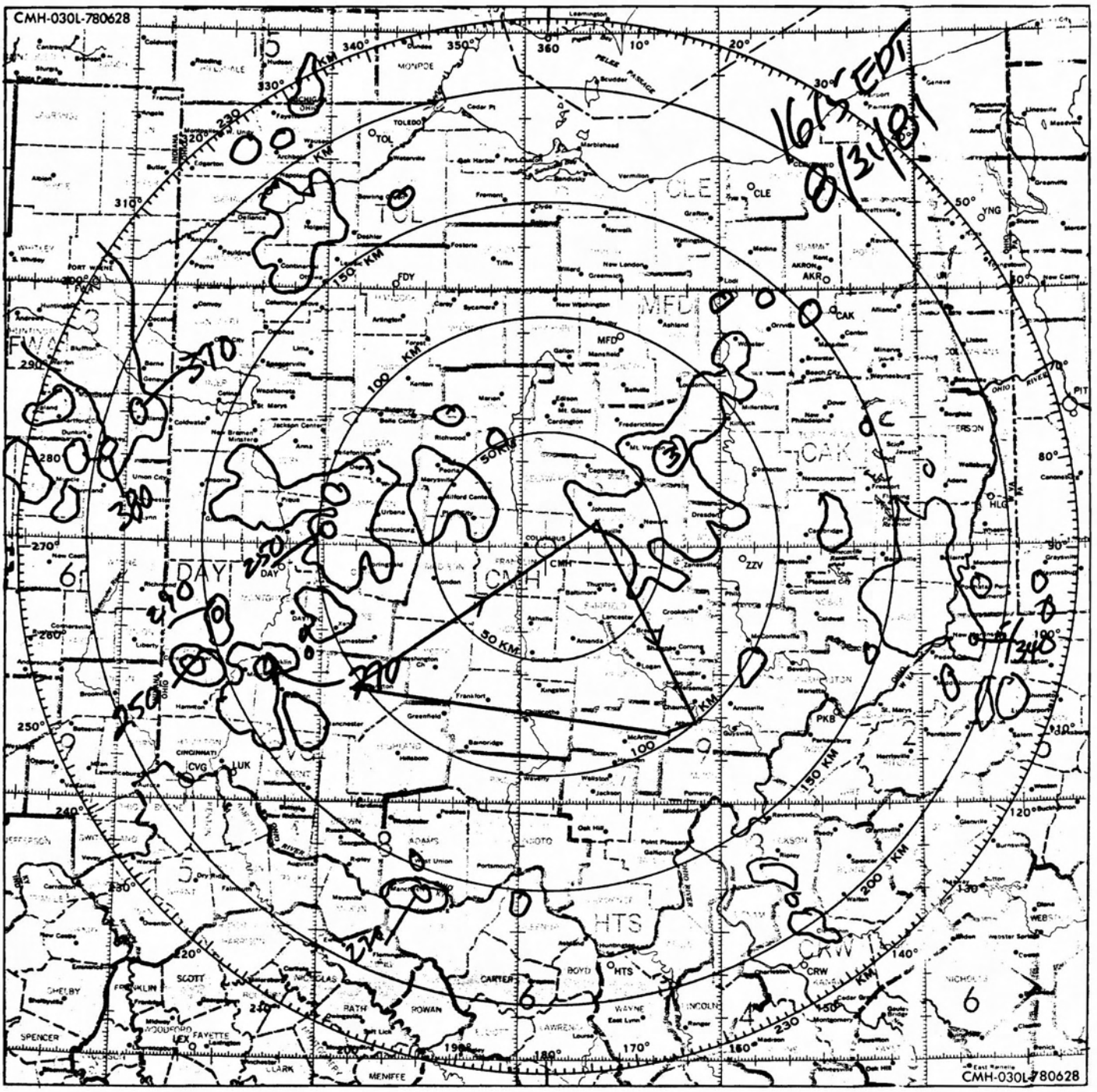

Figure 6-10. Radar Overlay August 31, 1981 - 16:15 P.M.

Figure 6-11. Radar Overlay August 31, 1981 - 17:15 P.M.

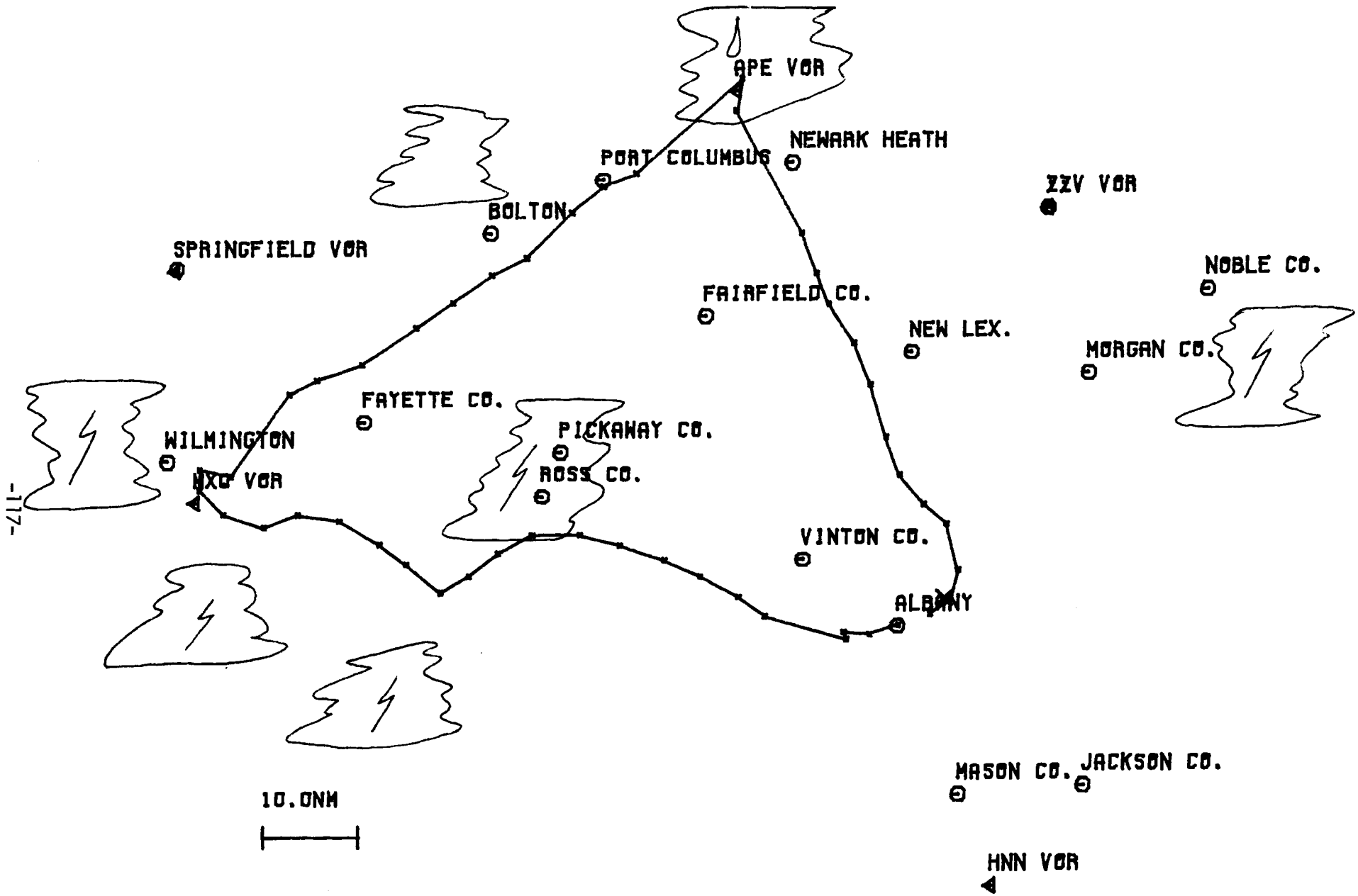

Figure 6-12. Flight Test of the Trimble Receiver, August 31, 1981, UNI to MXQ to APE to UNI NDB to UNI, Thunderstorm Activity.

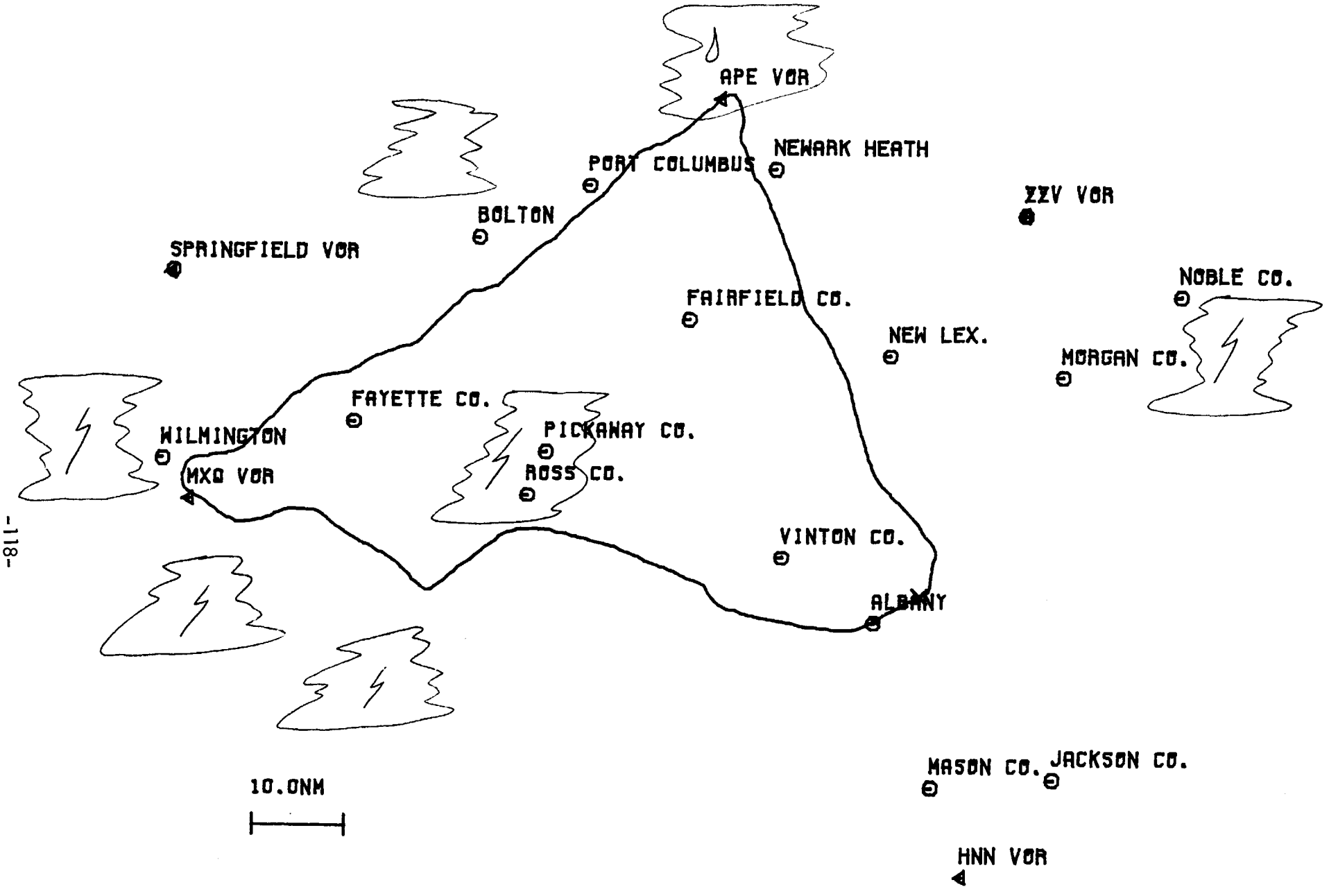

Figure 6-13. Flight Test T19900 Receiver, August 31, 1981, UNI to MXQ to APE to UNI NDB to UNI, Thunderstorm Activity.

an audio subcarrier of the Zanesville VOR. Based on Flight Service Weather information the flight proceeded northeast bound. The FAA/MITRE weather radar uplink receiver in the aircraft indicated that the heaviest weather was south of the current position. Figure 6-14a is a copy of the printout of the FAA/MITRE weather radar uplink receiver output that indicates the line of thunderstorms in the area. Figure 6-14b is a plot of the ground track as recorded by hand written notes during the flight as there was a problem in recording the digital output of the TI-9900 receiver on the Byte Bucket digital cassette recorder.

The flight encountered moderate to heavy rain and light to moderate turbulence. There was lightning above and around the aircraft as the flight progressed. During the flight, the instrumentation for the p-static dischargers on the aircraft showed the aircraft transversing areas of high static fields as the polarity and magnitude varied quite dramatically. The aircraft was consistently discharging at 300 to 500 microamperes in both positive- and negative-point corona. The S/N values from the TI-9900 did vary approximately 20 db during the flight with the receiver indicating no deceptive or erratic performance. At one point in the flight, when the aircraft was encountering high p-static discharging rates with increased electrical activity above and around the aircraft, the TI-9900 did lose cycle track on the Dana and Carolina Beach stations of the 9960 GRI rate for approximately 20 seconds while track on the Seneca, N.Y. was preserved. The receiver produced no obviously incorrect data points and continued to provide a consistent position output. The S/N values for the two stations dropped to about -15 db S/N during the cycle track loss which then promptly returned to normal. The total flight time for this flight was 2.5 hours and produced no other cycle track loss. The Loran output data was used continually during the flight to position the aircraft during the test.

Figures 6-15 and 6-16 are ground track plots for flights in clear weather conditions. These flights were made to determine the ability of the receivers to provide navigation information in near ideal conditions. Figure 6-15 represents a flight on August 12, 1981 using the Trimble receiver. The flight consisted of a closed course from Henderson VOR. As can be seen in the ground track produced by this receiver, the slow update rate produces data approximately every 4.5 nm. The receiver also indicated problems in determining the aircraft position at certain times, but when this happens the receiver has always provided an indication that the displayed position was suspect. This condition was also true in all of the flights in thunderstorm conditions. The Trimble 10A receiver is an accurate receiver but it just does not provide good real time position information in an aircraft.

Figure 6-16 is the ground track for the September 24, 1981 flight in clear weather conditions of the TI-9900 Loran-C receiver. This flight was conducted during the return of N7AP to Ohio University after the ground lightning testing at WPAFB, Dayton, Ohio. This was the first flight that was conducted with the pilots using the CDI for steering correction commands from the Loran-C receiver. The flight was conducted directly to the NDB, at UNI airport using the ± 0.5 nm either side of course CDI as the

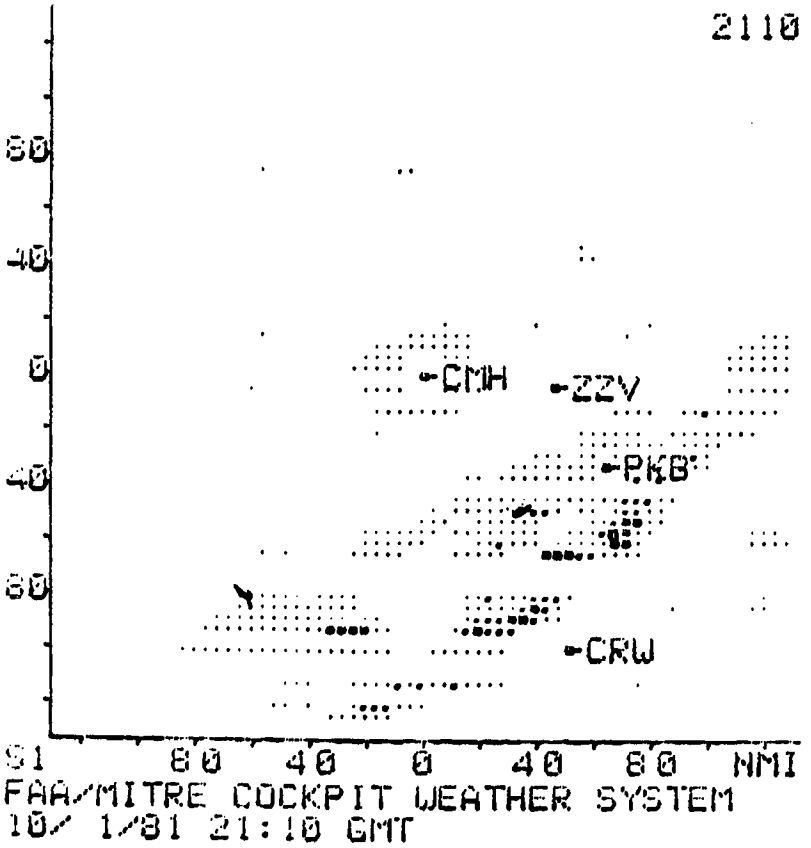

Figure 6-14a. Copy of the Printout of the FAA/ Mitre Weather Radar Uplink Receiver Output.

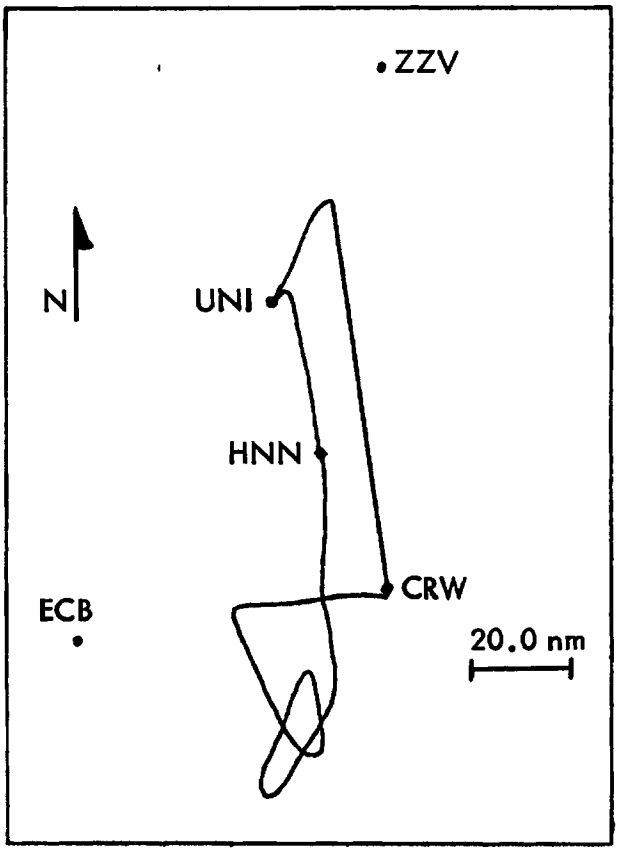

Figure 6-14b. A Plot of the Ground Track.

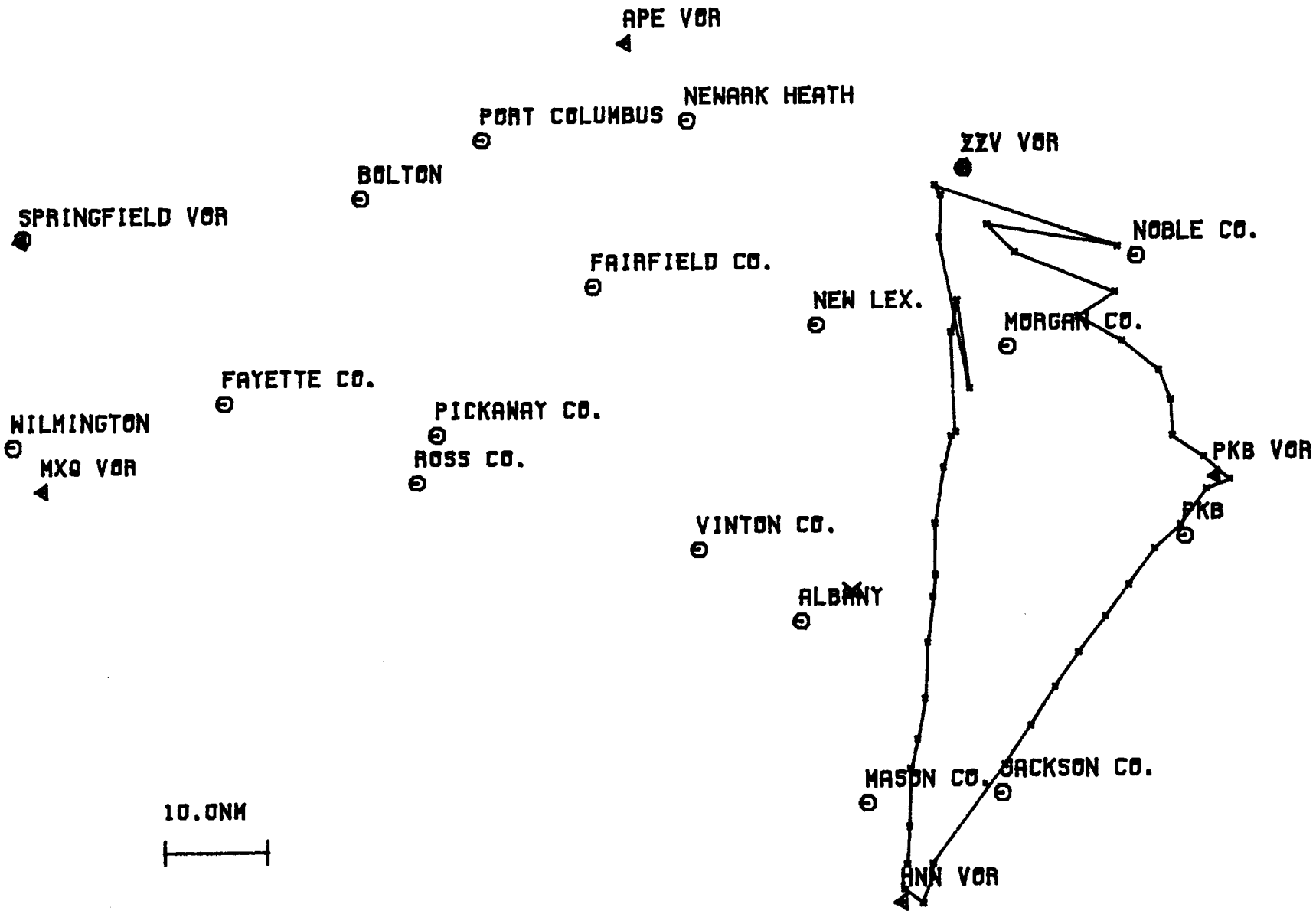

Figure 6-15. Flight Test Trimble Receiver, August 12, 1981, HNN to PKB to ZZV to HNN, No Thunderstorm Activity.

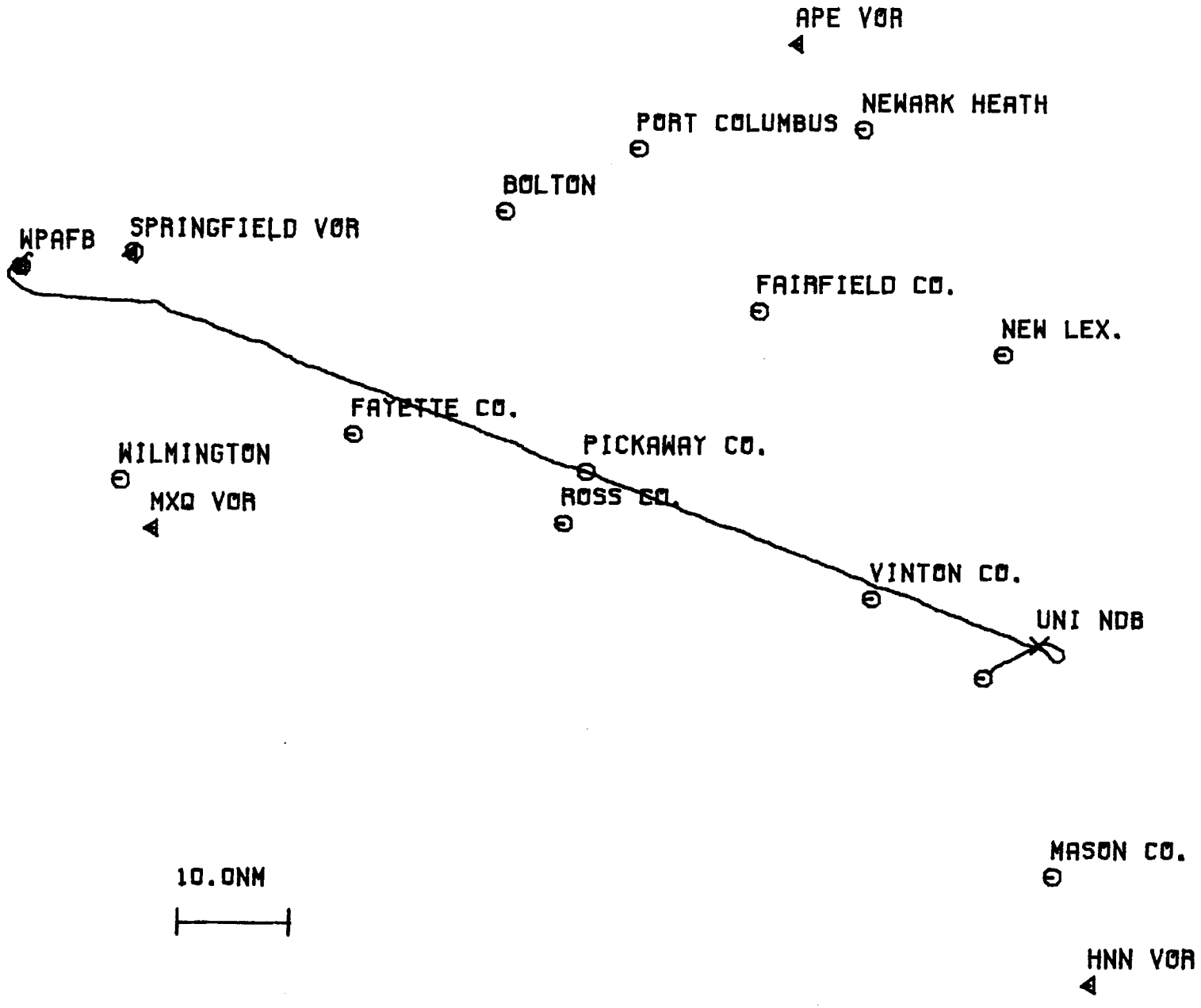

Figure 6-16. Flight Test of the TI9900 Receiver, September 24, 1981, WPAFB to UNI NDB to UNI, No Thunderstorm Activity.

primary navigation aid. The flight was conducted in VFR conditions with no thunderstorm activity. As Figure 6-16 indicates, the TI-9900 provided what appeared to be accurate course information. Also, note the ground track crossing Pickaway County airport. The aircraft did indeed cross that airport as indicated. In all tests involving the TI-9900 receiver, the quality of the plots obtained has been excellent. Comparing this plot with plots obtained during thunderstorm flights indicates that the receiver does provide real-time navigation information to the pilot.

3. Summary of Thunderstorm Flight Test Results. The flights conducted in actual thunderstorm condition indicated that the Loran-C receivers did provide adequate navigation information. Two of the flights conducted provided position accuracy of 0.1 to 0.3 nm in cross-track error for flight over known ground fixes. This information represents approximately 15-20 visual observations crossing VOR's and airports. These errors are well within the tolerance specified in AC-90-45A [4] for a two-dimensional enroute and terminal RNAV system.

Two other flights in thunderstorm conditions did provide loss of navigation information during part of the flight but further testing is required before conclusions can be made regarding these incidents.

VII. RECOMMENDATIONS

The recommendation based on the data obtained during the entire project would be to continue flight testing in thunderstorm and/or p-static charging conditions. A small data collection package weighing less than 25 pounds can be built and installed in several different types of aircraft to record several of the following parameters: aircraft discharging current, 100 KHz noise level, Loran-C signal-to-noise level, lightning stroke rate, and altitude. Another device that could assist the pilot in determining the qualitative level of p-static charging is a p-static current indicator. This device would consist of a small meter assembly to be mounted in the cockpit with an instrumented static wick mounted on a p-static hot spot on the airframe, such as the top of the rudder. The meter in the cockpit would be marked with green, yellow and red arcs that would correspond to low or normal, moderate and warning levels of charging, respectively, on the airframe. The pilot then with this device has qualitative information regarding the level of charging occurring on the aircraft and the possible effects on avionics performance.

It would be beneficial if manufacturers would provide drawings and procedures for the installation of static-wick dischargers for all IFR equipped aircraft. This would allow the aircraft owner or operator to have the aircraft equipped with efficient dischargers when a problem with p-static is discovered.

One additional noise source that was not investigated in this report is the effects of streamer currents caused by bound charge on non-conducting surfaces of the aircraft such as radomes, windscreens and fiberglass engine shrouds. Several manufacturers provide treatments for these surfaces but an evaluation of these methods is necessary to determine their effectiveness.

VIII. REFERENCES

[1] "VLF P-Static Noise Reduction in Aircraft" Volume 1, Current Knowledge, R. W. Lilley and R. W. Burhans, September 1980.

[2] "Dielectric Electronic Charge Reduction", Robert L. Truax, TCO Manufacturing Corp., Technical Paper, Business Aircraft Meeting, Wichita, Kansas, April 1981.

[3] "Evaluation of the FAA/MITRE Weather Data Device", Technical Report, OU/AEC/EER/54-1, D. G. Pullins, January, 1982.

[4] Advisory Circular, Approval of Area Navigation Systems for Use in the U.S. Nationl Airspace System, AC90-45A, DOT, FAA, Reprint, February 1980.

IX. ACKNOWLEDGEMENTS

The author would like to thank the following:

Mr. Dick Zoulek for his assistance in making the necessary installation of equipment on board N7AP for the ground and flight tests. Mr. Zoulek provided considerable effort in keeping N7AP ready to fly at short notice.

Mr. David Bernard who wrote all of the software necessary to produce the graphic output plots of the data. His assistance in this respect provided the quality results of the graphic output reflected throughout this report.

Mr. Thomas Zumwalde for his assistance in construction, modification and installation of the interface for the instrumented static-wick dischargers and the Serial Lab Products Remote I/O unit.

X. PROJECT TEAM MEMBERS AT OHIO UNIVERSITY

Dr. Richard H. McFarland	Director of Avionics Engineering Center (AEC) and Chief Pilot N7AP.
Dr. Robert W. Lilley	Associate Director, AEC
James D. Nickum	Project Engineer
Delmar G. Pullins	Copilot N7AP
Lance Dale	Copilot N7AP
Richard Zoulek	Chief Mechanic N7AP
Robert Truax	Consultant, TCO Manufacturing Co.
David Bernard	Research Intern
Thomas Zumwalde	Research Intern

DOT/FAA
RD-82/45,I

The effects of precipitation
static and lightning on the
airborne reception of LORAN-C
volume 1: analysis /
00026834